Dynamics of Liquid Crystals in a Magnetic Field: Phenomena Near Equilibrium

Giorgia Tordini

Dynamics of Liquid Crystals in a Magnetic Field:

Phenomena Near Equilibrium

Giorgia Tordini

Dynamics of Liquid Crystals in a Magnetic Field: Phenomena Near Equilibrium
G. Tordini
Thesis Radboud Universiteit Nijmegen - Illustrated
With references - With summary in Dutch
ISBN: 978-90-9029574-9
Cover: 21 aligned domains. Design by the author.

Dynamics of Liquid Crystals in a Magnetic Field: Phenomena Near Equilibrium

Proefschrift

ter verkrijging van de graad van doctor
aan de Radboud Universiteit Nijmegen
op gezag van de Rector Magnificus,
volgens besluit van het College van Decanen
in het openbaar te verdedigen op 13 mei 2016
om 10.30 uur precies

door

Giorgia Tordini

geboren op 11 april 1974
te Rome (Italië)

Promotor:
Prof. dr. P.-C.-M. Christianen
Prof. dr. J.-C. Maan

Manuscriptcommissie:
Prof. dr. Th.H.M. Rasing
Prof. dr. A. Fasolino
Dr. W. Bras (NWO, DUBBLE@ESRF, Grenoble, Frankrijk)

Het werk beschreven in dit proefschrift is uitgevoerd aan de Faculteit der Natuurwetenschappen, Wiskunde en Informatica van de Radboud Universiteit Nijmegen en maakt doel uit van het onderzoeksprogramma van de 'Stichting voor Fundamenteel Onderzoek der Materie' (FOM), die financieel gesteund wordt door de Nederlandse Organisatie voor Wetenschappelijk Onderzoek (NWO).

Most sets of values would give rise to universes that, although they might be very beautiful, would contain no one able to wonder at that beauty.

Stephen Hawking

to Emile wondering at the beauty

Preface

This thesis presents investigations on liquid crystals in high magnetic fields, a great source of beautiful images that inspired me from the first observation. Measurements, comprehension and part of writing were performed at the High Field Magnet Laboratory (HFML), with invaluable help and support of all people working there. I am grateful to all my HFML-colleagues. A special mention to my colleagues who made my experiments technically possible. Among them, Hans, Frans and Ramon. I thank Marius for initiating me to the liquid crystals world. Any measurement would not have been possible without the permanent staff of the HFML, always available for support, night and day. I would like to thank my collaborators outside the HFML: Annalisa for the interest shown in my experiments and for being a gender model, Oksana and Bastiaan for explaining some of the most mysterious results I have got, and Wim for the experience and the new ideas he brought into this work. Special thanks to my friend Bea, for having fixed my results into history, and for being my Dutch family, together with Paula, Valeria, Henar, Marta C, Cuca, Rosalyne, Celine, Mirto, Marta T., Salva, Kanar, Iglika, Eugenio, Tanja, Brecht and Odette. Thanks to all of you I enjoyed my time in Nijmegen.

Finally, a big *grazie* to Claudietto for his love, confidence and support. This thesis is devoted to Emile, our son.

Contents

Chapter 1

Introduction

1.1 Aim of this work

The work presented in this thesis on phase transition dynamics in liquid crystals has the ambition to explore regions where matter evades simple definitions, shading in nuances of existence that we call coexistence. The unique properties of liquid crystals pave the way to perform experiments at the border of two phase states, perturbing delicate equilibria [1]. In our case the key to access these extraordinary enclaves is birefringence microscopy in high magnetic fields. The fundamental relevance of the study of phase transition dynamics is linked to the need to understand and predict how matter evolves. In liquid crystals we can study, at room temperature, the formation of isolated topological defects [2], [3], [4], [5], [6] similar to those observed in magnetism [7], superconductors [8] and cosmology [9]. For instance, even after the 'Big Bang', in the cooling of the early universe, a sequence of symmetry breaking phase transitions shaped the universe as we know it now. In 1991 the astrophysicist Zurek [10] established the link between cosmology and condensed matter, proposing experiments in liquid crystals to test the theory of universe formation. By following the evolution of defects during first and second order phase transitions in liquid crystals the topological defects known as cosmic strings in Kibble theory found an experimental confirmation [11]. On the other hand, liquid crystal structures can explain various self-assembled morphologies in biology, e.g. the plant cell wall, chromosomes, nacre [12], and the wings of a butterfly [13]. The ambition of this work is to contribute to the understanding of matter in its interdisciplinary aspects.

We are not the first to show that many liquid crystalline systems can be aligned by an applied magnetic field, by cooling them from the isotropic phase to the nematic phase [14], but the results are impressive enough to stimulate curiosity on the microscopic laws that generates such a macroscopic effect. In figure 1.1 we look at the effect of magnetic field on samples of three different polymer liquid crystals and in particular on C5-30 5-[(4'cyanobipheniyl-4yl)oxy] pentylnorborn-5-ene-2,3-dicarboxylate], with polymerization degree $n = 30$. The samples are shown at room temperature before (top) and after (bottom) having been exposed to the field. The material appears opaque when no magnetic field was applied and becomes perfectly transparent if cooled through its Isotropic-Nematic phase transition in a 15 T magnetic field. The graph shows the corresponding measured birefringence (phase difference of light due to the gradient of refractive index) as the temperature decreases. The large increase of the signal takes place around the isotropic to nematic (I-N) phase transition temperature, where the alignment with the magnetic field takes place. The macroscopic change in optical properties from opaque to transparent had been previously observed at the High Field Magnet Laboratory [15], [16]. Note that applying the same field intensity in the nematic phase, without crossing the phase transition temperature, does not produce the same effect. Indeed the actual alignment is achieved exactly during the phase transition, and where we are going to investigate the actual physics of this effect with our experiments.

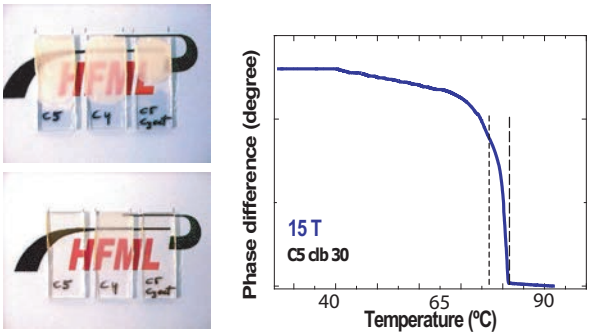

Figure 1.1: The effect of a magnetic field of 15 T on the liquid crystal polymer C5-30 is shown. The same material appears opaque (top left) when no magnetic field was applied during the isotropic to nematic phase transition and becomes perfectly transparent (bottom left) if cooled through its I-N transition in a 15 T magnetic field. Right: the corresponding measured phase difference (optical refraction) as a function of the temperature. Note that in our experiment the temperature is decreased and optical signal is detected from right to left in the graph. The rapid increase of optical refraction around the I-N phase transition corresponds to the alignment induced by the magnetic field. The dashed lines indicates the metastable region where the I-N takes place.

1.2 Structure of this work

Liquid crystals constitute a peculiar phase of matter that combines properties like fluidity, as in liquids, and long range periodic order (the order occurs over a distance that is much greater than the intermolecular distance), as in solids. They form an ideal model system for our investigations since their behaviour can easily be studied: phase transitions appear near room temperature and are optically accessible thanks to the intrinsic birefringence of the liquid crystal (=LC) molecules. Moreover, at the phase transition LCs react to external fields of moderate intensities. Nevertheless, the basic behaviour is relevant for a research goal with multidisciplinary implications. Many elements of spontaneous symmetry breaking typical of phase transitions can be studied in high detail in our octylcyanobiphenyl − 8CB− model system. The versatility of liquid crystals and their many different applications are explored in more detail in Chapter 2. The phase states of our model system 8CB are described by following the decrease of the temperature and the multiple effects of a magnetic field on the liquid crystal molecules that are exposed to it. The experimental technique of birefringence microscopy in a magnetic field, which allows us to see in full colors the amazing evolution of the liquid crystalline structure through its phase transitions, is introduced in Chapter 3. In Chapter 4 the effects of magnetic manipulation of 8CB at the Isotropic -Nematic transition is discussed. In Chapter 5 we investigate the realignment of the smectic-A phase induced by the magnetic field after a rotation of the model system with respect to the magnetic field. The reorientation is studied as a function of the rotation angle, the temperature and the magnetic field strength. In Chapter 6 we describe and explain the formation of surface patterns in high magnetic field at the interface between the smectic-A phase and the substrate. Moreover, by changing the system orientation, we observe the reorientation of the defects pattern in a high magnetic field.

References

[1] P. G. de Gennes and J. Prost, *The Physics of Liquid Crystals*, Clarendon Press, Oxford (1993).

[2] I Musevic and Th. Rasing, *Surfaces and interfaced of Liquid Crystals*, Springer (2004)

[3] S. Chandrasekhar, *Liquid Crystals*, Cambridge University Press (1977).

[4] M. J. Stephen and J. P. Straley, *Physics of Liquid Crystals*, Rev. Mod. Phys. 46, 617 (1974).

[5] O. D. Lavrentovich, P. Pasini, C. Zannoni, S. Zumer eds., *Defects in Liquid Crystals: computer simulations, theory and experiments*, Nato Science Series, Springer (2001).

[6] A. Rastegar, M. Skarabot, B. Blij and Th. Rasing J. Appl. Phys. 89 (2001).

[7] M. Kleman, *Points, lines and walls*, John Wiley & Sons, New York (1983).

[8] V. Moshchalkov, M. Menghini, T. Nishio, Q. H. Chen, A. V. Silhanek, V. H. Dao, L. F. Chibotaru, N. D. Zhigadlo, and J. Karpinski, Phys. Rev. Lett. 102, 117001 (2009).

[9] I. Chuang, R. Durrer, N. Turok, and B. Yurke, Science 251, 1336 (1991).

[10] W.H. Zurek, Physics Reports 276, 177 (1996).

[11] M. J. Bowick, L. Chandar, E. A. Schiff and A. M. Srivastava, Science 263, 943 (1994).

[12] J. H. E. Cartwright and A. G. Checa, J. R. Soc. Interface 22, 491 (2007).

[13] P. Vukusic and J. R. Sambles, Nature 424, 852 (2003).

[14] M. Boamfa, M. W. Kim, J. C. Maan and T. Rasing, Nature 421, 149 (2003).

[15] M. Boamfa K. Viertler, A. Wewerka, F. Stelzer, P. C. M. Christianen and J. C. Maan, Phys. Rev. Lett. 90, 025501 (2003).

[16] I. O. Shklyarevskiy, M. I. Boamfa, P. C. M. Christianen, F. Touhari, H. van Kempen, G. Deroover, P. Callant and J. C. Maan, J. Chem. Phys. 116, 8407 (2002).

Chapter 2

Liquid crystals: fundamental aspects and magnetic field effects

2.1 Introduction

The combination of the two words −liquid and crystal− seems a *contradictio in terminis*, and immediately reveals the peculiar nature of the subject of this thesis. Liquid crystals have properties that are in between those of liquids and solid crystals. They exhibit long range orientatinal ordering over a distance that is much greater than the inter-molecular distance and yet they are able to flow like a liquid. This chapter summarizes the basic properties of liquid crystals and the effect of magnetic fields. The chapter is organized as follows. In section 2.2 we present the most important features of liquid crystals as they have been discovered in the past. In section 2.3 we consider the phase behaviour of liquid crystalline systems by varying the temperature. 8CB, the model system we investigate throughout this work, is presented in 2.4. The different phenomena that take place during the transition from the isotropic to the nematic phase are considered in the next sections: 2.5 deals with the energy associated to the coexistence region, 2.6 with phase ordering and cluster growth. Finally, the interaction with an applied magnetic field is the subject of section 2.7.

2.2 Liquids but still crystalline

The striking properties of liquid crystals arise from the shape of the constituent molecules. The highly anisotropic geometry of the molecules gives rise to a fascinating and technologically relevant behavior. In contrast to ordinary fluids, liquid crystals (LCs) are strongly anisotropic: their properties depend strongly on the direction. The anisotropy of their molecules produces the anisotropic optical behaviour of the system: birefringence. They share this characteristic with other systems in nature: polymers and materials of biological significance, such as DNA and membranes. All these building blocks of nature have complex 3D shapes.

Modern research on liquid crystals started in the 19^{th} century. An important invention in that time was the heating stage microscope by Otto Lehmann, a physicist from Karlsruhe, Germany. This microscope allowed detailed control of the temperature of the sample. In a later version, with polarizers added, it became the standard equipment in every research laboratory studying LC materials. In combination with digital imaging, polarized microscopy is the major investigation tool for the experiments presented in this thesis. We can combine polarized microscopy with very strong magnetic fields to create a rather extreme sample environment for liquid crystals.

Liquid crystals consist of moderate size organic molecules which tend to have an anisotropic shape. Because of their anistropic shape, under appropriate conditions, the molecules can exhibit

Figure 2.1: Liquid crystals are present in daily life. Examples are a Liquid Crystal Display (top left), a body cream (top right), a thermo-sensitive flexible film used in thermometers (bottom right) and an active separation wall that can switch from transparent to opaque (bottom left).

orientational order, such that all their axes line up in a particular direction. This bulk order has a profound influence on the optical and electrical properties of the material [1]. For example, if the direction of the orientation varies in space, the polarization of the light passing the material is affected by this variation. A well-known application of this phenomenon is the ubiquitous liquid crystal display (LCD), now comprising a $15b annual industry world-wide. Because of their optical and mechanical properties, large scale availability and low toxicity, LCs have entered many other industrial segments, including the world of cosmetics. Figure 2.1 shows examples of how LC technology has entered every-day life: a large size flat screen, a body cream, thermo-sensitive flexible films used in modern thermometers and an active separation wall that can switch from transparent to opaque.

2.3 Phase states in liquid crystals

Liquid crystals can flow like an ordinary liquid, but retain some features of a crystal regarding long range molecular correlations. In a solid crystal the centers of mass of the atoms and molecules are located on a more or less perfect three dimensional periodic lattice. A liquid crystalline mesophase – or intermediate phase– shows a similar long range orientational order, but with a positional order that is reduced or even completely absent [2].

The family of LCs is rather big, as schematically shown in figure 2.2. The nomenclature of LCs was invented by G. Friedel in 1920. We focus here on single component LC systems that show mesomorphic behavior in a defined temperature range. These are the thermotropic LCs. Lyotropic liquid crystalline phases, on the other hand, show mesomorphic behavior that strongly depends on both concentration and the solvent used. Above a certain temperature thermotropic LCs behave just like ordinary fluids: there is only very short range internal order of the molecular constituents as in a liquid and the system is macroscopically completely isotropic (isotropic phase). Upon lowering of

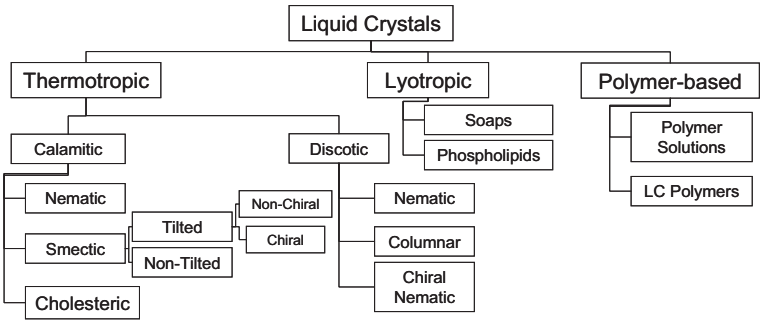

Figure 2.2: The liquid crystal family is rather large and consists of a large variety of different phases and materials. In this thesis we will focus on non-chiral thermotropic compounds in their nematic and smectic-A phases (non tilted).

the temperature, a liquid crystalline structure develops, of which the nematic phase is the most simple one. Here the centers of gravity of the molecules have no long-range translational order, while a long range orientational order is present: the molecules show a finite orientation distribution with respect to a common axis, labelled by a unit vector $\widehat{n}$, called the director, i.e. time averaged they point in the same direction, as shown in figure 2.3, left. However, opposite orientations of the director are indistinguishable, even if the molecules are asymmetric. Hence, the nematic order parameter is a second-rank tensor in 3D [1].

$$Q_{\alpha\beta} = S\frac{1}{3} < 3n_\alpha n_\beta - \delta_{\alpha\beta} >, \tag{2.1}$$

where $n_{\alpha\beta}$ are the components of a unit vector along the major symmetry axis of the molecules, $\alpha\beta = x, y, z$ in the laboratory frame, S is the degree of orientational order, $\delta_{\alpha\beta}$ is the Kronecker tensor with $\delta_{\alpha\beta} = 1$ when $\alpha = \beta$ and $\delta_{\alpha\beta} = 0$ when $\alpha \neq \beta$. The notation $< ... >$ indicates a statistical average. The order parameter Q as defined by Herman in 1944 is a measure of the alignment of the molecules along the director. We have $S = 0$ for a completely disordered system and $S = 1$ for a perfectly ordered situation where all molecules lie parallel to the director $\widehat{n}$. When the molecules are all perpendicular to the director $S = -0.5$ [3].

In a realistic situation, the nematic phase is constituted by molecules oriented at a small angle α_i with respect to $\widehat{n}$, as shown in figure 2.3 (right). Therefore we can write the local order parameter S for molecules sharing the same director $\widehat{n}$ as

$$S =< \frac{3\cos^2\alpha_i - 1}{2} > . \tag{2.2}$$

The word nematic (from the Greek "nema" $\nu\eta\mu\alpha$ = thread) refers to thread-like topological defects observed in nematics, as shown in the middle panel of figure 2.3. Many different textures are observed and explained in liquid crystals [4].

Another phase that is rather common is the smectic phase. Characteristic of all smectic phases is the existence of a certain positional order, which is often described as a one-dimensional density wave: the molecular centers are, on average, arranged in equidistant planes, leading to a layered structure, on average $20 - 30$ $\AA$ thick, as is schematically shown in figure 2.4. This positional correlation is not related to the orientational order of the long molecular axis, typical of the nematic phase; true long-range order is absent due to the logarithmic divergence of smectic layer displacement, due to the

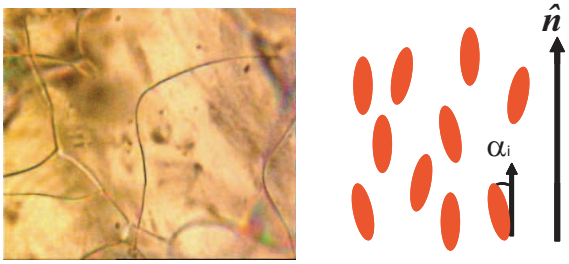

Figure 2.3: The word nematic (from the Greek "nema" $\nu\eta\mu\alpha$ = thread) refers to thread-like topological defects observed in nematics, see picture in left panel. The nematic phase is characterized by a long range orientational order of the molecules along a direction called the nematic director $\widehat{n}$. Each molecule is positioned at a small angle α with respect to $\widehat{n}$, see right panel, and the degree of order is given by the order parameter $S =< \frac{3\cos^2\alpha_i - 1}{2} >$.

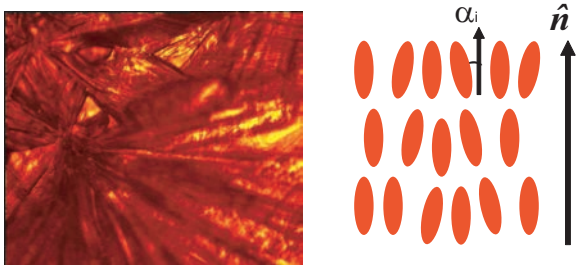

Figure 2.4: The smectic-A phase shows some properties of a crystal, as visible in the structure in the picture on the left, but it retains the ability to flow. This phase shows a long range orientational and positional order of the molecules along $\vec{n}$. The positional correlation is not rigid, but it can be described by q density wave, with the molecules arranged along layers, see right panel. The molecular centers are, on average, arranged in equidistant planes, leading to a layered structure, on average $20 - 30\ \mathring{A}$ thick.

thermal fluctuations known as Landau-Peierls instability. This is a result of the dimensionality of the system [1].

It is remarkable that deviations from the equilibrium position in the smectic planes can be quite large, making undulations in the layers responsible for the absence of a true long-range order in smectic materials [2]. Moreover the liquid crystal composition is not static and molecules can move during time from layer to layer. In the smectic A phase, the molecules point perpendicular to the layer planes, as shown in figure 2.4, whereas in the smectic C phase, the molecules are tilted with respect to the layer planes. In both cases the layers can slip over each other, with the only strict requirement to keep the inter-layer distance fixed.

LC molecules may form a stack of layers along one direction, but remain liquid $-$ in terms of the absence of translational order$-$ within the layers. As the system changes from one of these phases to another, a variety of physical parameters such as susceptibility and heat capacity, will exhibit "pre-transitional behavior", [9], [7], [11], [12], [9], [15]. Based solely on symmetry, this behavior may be described by the same mathematical framework as found in other physical systems, such as super-

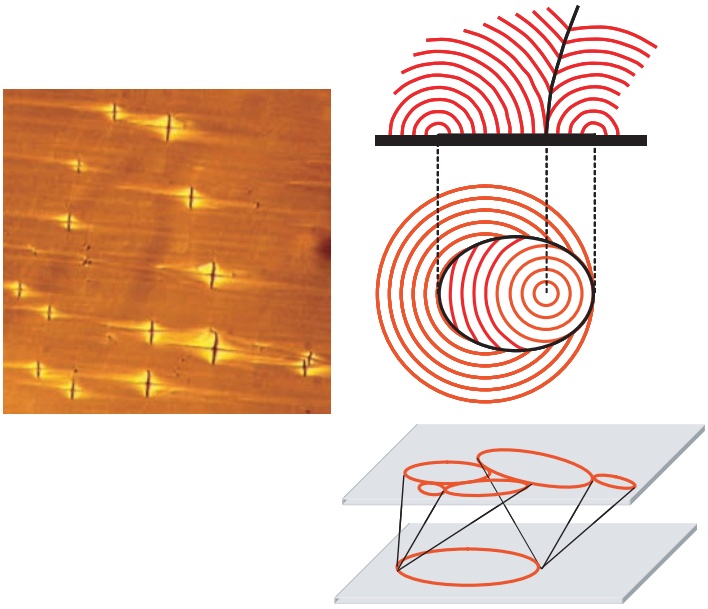

Figure 2.5: Left: optical pattern of focal conics observed under polarized microscopy in the smectic A phase. Right: schematic explanation of the nature of focal conics as result of distortions at the surface causing defects in the layered structure. When a smectic sample is sandwiched between two surfaces, the layers can rotate around a singularity, producing the observed focal conics.

conductivity, magnetism, or superfluidity; this is the so-called "universality" of these phase transitions.

Due to the layered structure, interesting optical phenomena can be observed, such as focal conics [16], known structures that form at the sample cell surface in smectic liquid crystals. G. Friedel deduced the layers structure of the smectic phase from the observed focal conic domains and not vice versa [17]. Their existence is linked to the wavy character of the smectic layers, as shown in figure 2.5. In general, focal conics develop around two singular lines [12]. Let us consider a limiting case of layers wrapped around a singular line forming concentric cylinders. By bending and closing these cylinders we get a torus with a singularity as a circle; adding further layers to close a hole of a circle we a singular line orthogonal to the plane of a singular circle and passing through its centre. This is the limiting case, since in general focal conic is a pair of singular ellipse and a hyperbola passing through its focus forming a cylinder.

2.4 Model system: 8CB

In this thesis the LC octylcyanobiphenyl $-$ 8CB$-$ is chosen as a model system for our studies. The properties of 8CB are well known since it is widely used from the very beginning of the research on liquid crystals. $-$ 8CB$-$ exhibits both a nematic and a smectic A phase. The molecule is characterized by an intrinsic anisotropy of its chemical structure, as shown in figure 2.6, which is the cause of a different refractive index along two perpendicular directions: the fast (ordinary) refractive index n_o and the slow (extra-ordinary) one n_e. Such a behavior is called birefringence and it can be measured by the difference $\Delta n = n_e - n_o$. For 8CB we have $\Delta n = 1.6250 - 1.5336$. The optical anisotropy and

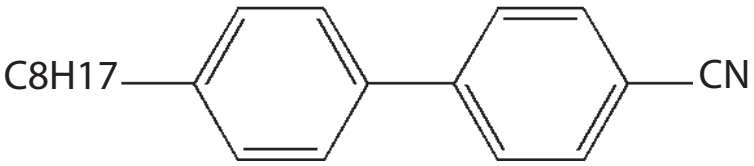

Figure 2.6: Structure of the molecule octylcyanobiphenyl (8CB).

the different LC phases give rise to the different textures under the polarization microscope, as shown in figure 2.7. The observed textures appear by lowering the temperature, when 8CB passes from the isotropic phase (I), dark image on the right, to a number of growing round domains (top images) which announce the nematic phase (N), where a multi-domain structure is visible. Subsequently the system starts to develop an even more solid-like structure with the smectic-A phase (SmA), image on the left. A further cooling brings the system in the full crystalline structure (K). The isotropic to nematic phase transition is a weak first order phase transition that is accompanied by a region in which the two phases coexist, between T_1 and T_3 in figure 2.7. Nematic domains (or clusters) nucleate, grow and merge within the isotropic phase, which appears as a black background. These different phases also give rise to changes in the overall birefringence signal of a 8CB sample as a whole, which is shown in figure 2.8 as a function of temperature.

Liquid crystals can show weak phase transitions, therefore it is appropriate to define a temperature range rather than a transition temperature. Nevertheless it is commonly accepted to indicate a transition temperature, with the convention of taking this temperature in the middle of the transition range. 8CB shows nematic and smectic-A phases in the liquid crystalline regime: I-40.85 °C-N-33.35 °C-SmA-25 °C-K. Above 40.85°C the liquid crystal is isotropic (I) [22]. No birefringence signal is detected, since no preferential molecular order is present in the liquid. Subsequently the system passes through the nematic phase (N) and the smectic phase (SmA), and loses its LC character becoming a crystalline solid (K) just below room temperature. Each phase transition produces an increase of the birefringence signal, corresponding to the development of internal order in the liquid.
From the isotropic phase the sample is cooled, producing a spontaneous increase of internal order, which characterizes each LC phase. Lowering the temperature produces a series of pre-transitional effects, with nematic clusters nucleation and growth, corresponding to the birefringence intensity jumping up and down. Upon further cooling the signal remains stable at a finite value when before the nematic phase (N) is fully formed.

Calorimetry is a more direct way of observing phase transitions; in particular differential scanning calorimetry (DSC) is a good tool for studying the kinematics of the transition, while modulation calorimetry (MC) is a practical tool for observing the phase dynamics [13].

2.5 The isotropic-nematic coexistence region

The transition from the isotropic liquid state to the nematic phase is often a weak first order phase transition, which involves latent heat. During such a transition, a system either absorbs or releases a fixed amount of energy. Because energy cannot be instantaneously transferred between the system and its environment, first-order transitions are associated with mixed-phase regimes in which some parts of the system have completed the transition and others have not. Such a system can be explained in relatively simple terms using the regular solution model [5]. Consider two phases A

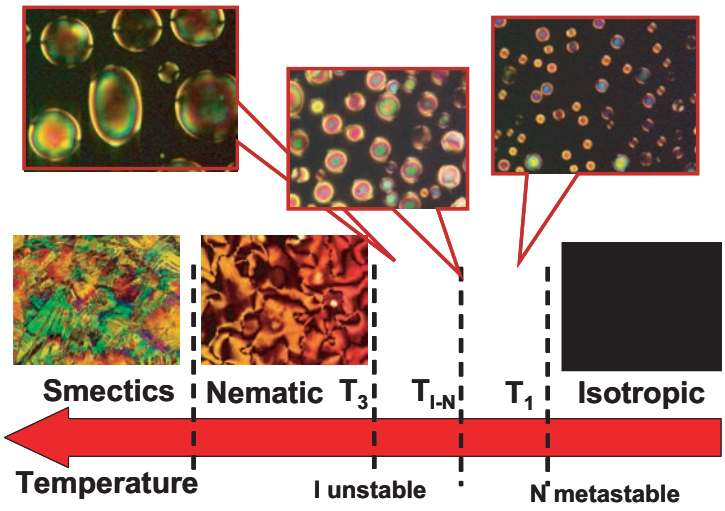

Figure 2.7: Textures observed for the different phase states of the LC system 8CB. By lowering the temperature 8CB passes from the isotropic phase (I) to the nematic phase (N) and then to the smectic-A phase (SmA). A further cooling brings the system in the crystalline structure (K). The isotropic to nematic phase transition is of weakly first order and it is accompanied by a region with a coexistence of the two phases. Nematic domains (or clusters) nucleate, grow and merge in a background formed by the isotropic phase, which appears as black in the images.

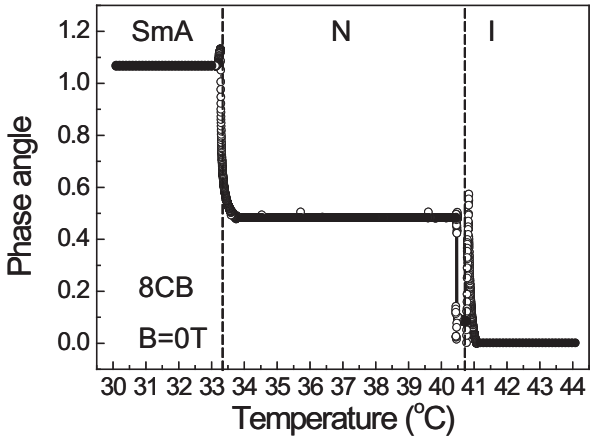

Figure 2.8: The birefringence signal of 8CB as a function of temperature. Our experiment starts in the isotropic phase (I), right side in the graph. The sample is cooled until the system undergoes a phase transition to the nematic phase (N) and then to the smectic phase (SmA). Each phase transition results in an increase of the birefringence signal from right to left, corresponding to the development of internal order in the material.

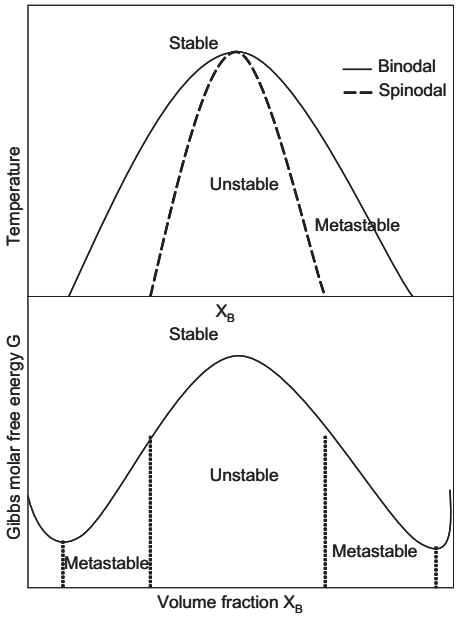

Figure 2.9: Top: Phase diagram of two phases of species A and B, with volume fractions X_A and X_B, as a function of temperature. The binodal (solid curve) and the spinodal (dashed curve) define the stability regions. Bottom: The Gibbs molar free energy plotted versus the molar fraction of the B species explains the stability regions: nucleation and growth take place when the curvature of ΔG_{mix} is positive. This phenomenon is also known as Kibble mechanism.

and B that can be phase separated (A, B) or mixed (A + B), depending on the volume fractions, denoted by X_A and X_B respectively with $X_A + X_B = 1$. The bottom panel of figure 2.9 schematically shows the difference in free energy of mixing ΔG_{mix} as a function of the volume fraction of phase $B(X_A = 1 - X_B)$. In the regime where the function of ΔG_{mix} is convex two phases can be present at the same time, each with a different composition. This regime is called the coexistence region and the locus of the coexisting compositions as a function of temperature is called the binodal (top panel of figure 2.9). Depending on the curvature of the ΔG_{mix} versus X_B function the way the phase transition proceeds can be described by two different mechanisms. When $\frac{\partial^2 \Delta G_{mix}}{\partial X^2} < 0$ the system is unstable against small fluctuations in composition. When one species gets more concentrated than the other this disbalance is amplified, leading to a decomposition of the system into the two phases, with a rapid spatial extension of the new phase. This mechanism is called spinodal decomposition and occurs until $\frac{\partial^2 \Delta G_{mix}}{\partial X^2} = 0$, defined by the inflection point in the ΔG_{mix} versus X_B curve. The locus of this inflection point as a function of temperature is the spinodal (top panel figure 2.9). Below the spinodal the mixture is unstable against phase separation. When $\frac{\partial^2 \Delta G_{mix}}{\partial X^2} > 0$ an arbitrarily small fluctuation in compostion will lead to an increase of the free energy. The system is locally stable against phase separation, although globally it is unstable. An energy barrier exists that should be overcome to accomplish the phase separation. Therefore, the region in between the bimodal and the spinodal the system is metastable. This can be described by the Kibble mechanism, which is a typical example of nucleation-growth. The Kibble mechanism has been studied in detail from the early 1970s [6], [7] and is the playground for many experiments described in this thesis.

2.6 From phase ordering to individual cluster growth

Phase ordering is of fundamental importance for the processing of different materials, including metal alloys, glasses and crystalline organic compounds for pharmaceutical applications. That crystallization from a melt, like other phase changes, does not necessarily occur at the equilibrium, had been established by G. Fahrenheit as early as in 1724.

We consider the homogeneous nucleation of the nematic phase from its liquid isotropic phase. By lowering the temperature from the high-temperature phase into a non-equilibrium state below the phase transition temperature T_c, the system enters a meta-stable region. At this point the new phase is thermodynamically favored and nucleation can occur, triggered by thermal fluctuations. Nematic phase formation requires a supercooling of the liquid phase in order to have a favourable chemical potential balance: $\mu_{nematic} < \mu_{liquid}$. The system is therefore brought into a meta-stable state, which evolves towards the stable equilibrium state via localized droplet fluctuations of a critical size. This is the case when the dominant contribution is given by surface tension. Alternatively, liquid crystals may show the formation of non spherical domains, when the anchoring force given by the surface becomes dominant [8]. In general the critical energy for the formation of the droplet is determined by the competition between a volume term, which favors the creation of the droplet, and a surface term, which favors its deformation and dissolution. For a cluster of radius R the free energy is given by a bulk and a surface term:

$$\Delta G = \Delta G_{bulk} + \Delta G_{surface} = \frac{4\pi}{3}\rho r^3 \Delta\mu_{s,l} + 4\pi r^2 \gamma_{s,l}, \tag{2.3}$$

where r is the position parameter, ρ is the density, $\Delta\mu_{s,l}$ is the difference in the chemical potential of the liquid and solid phases and $\gamma_{s,l}$ is the surface tension.

By imposing the condition of minimal free energy $\frac{\partial \Delta G}{\partial r} = 0$ we find $R_c = -\frac{2\gamma_{s,l}}{\rho \Delta\mu_{s,l}}$.

The critical size L_c to continue nematic growth is inversely proportional to $\Delta\mu_{s,l}$. For spherical nematic clusters L_c=R_c, thus droplets of size $r > R_c$ grow, while droplets with $r < R_c$ shrink. The probability that a molecule will leave a cluster diminishes with the size of the cluster, so that at the critical size a cluster has the same probability to grow and to shrink. A sketch of the difference in free energy for the two phases is depicted in figure 2.10. Experimental techniques have difficult access to the critical nucleus because of its small size. The early stage of nuclei formation is instead largely investigated by computer simulations [19], [23], [24].

Once nucleation has occurred, clusters of the new phase that could overcome the critical size grow surrounded by the mother phase. A quantitative description of the nucleation rate is given by the mathematical treatment introduced by Avrami in 1939 [18]. In the Avrami equation the volume fraction of crystalline material V is correlated to time:

$$-\ln(1 - V) = kt^m \tag{2.4}$$

and

$$V = 1 - e^{-kt^m}. \tag{2.5}$$

Here t is time, k is a rate constant and m is given by $m = \beta + \frac{\lambda}{2}$, where β is a parameter related to the nucleation mechanism: if the nucleation is instantaneous $\beta = 0$, while $\beta = 1$ when the nucleation rate is constant. The parameter λ gives the dimension in which growth takes place for needles $\lambda = 1$, for plates/disks $\lambda = 2$ and for spheres $\lambda = 3$.In the following we will focus on instantaneous nucleation events that take place in three dimensions. For short times we can approximate the Avrami relation to

$$V = kt^m. \tag{2.6}$$

For instantaneous nucleation the size R of a crystal is thus given by

$$R = kt^{\frac{1}{2}}. \tag{2.7}$$

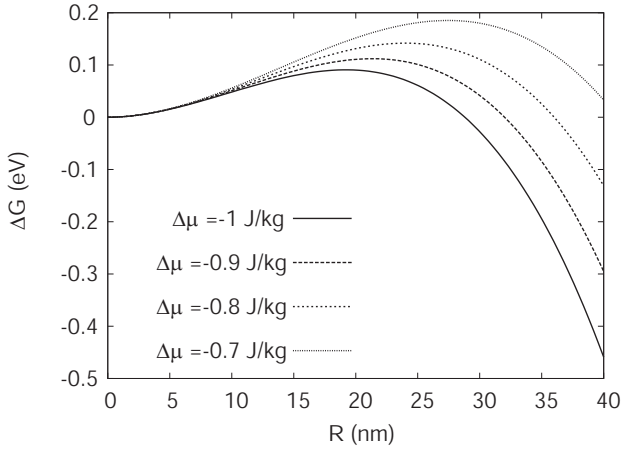

Figure 2.10: The difference in energy Δ_G for the formation of a cluster of the nematic phase inside the isotropic phase is sketched as a function of the radius R of the cluster. The critical radius corresponds to the maximum of the function.

A similar relation is valid for liquid crystals and follows from free energy considerations. Experimental observations performed by Ostner in 1973 revealed a time dependence of the radius of a nematic cluster R as

$$R(t) \sim t^{1/2} \tag{2.8}$$

[29]. This growth law is a special case of the Avrami model and has been predicted in 1961 by Lifshitz [30]. This model was further studied by Allen and Cahn [31] in the condition of vanishing free energy difference between the high and low temperature phases, i.e. close to the critical temperature T_c, as a result of a small quench.

The growth under consideration is somewhat similar to the growth of ferromagnetic domains in the kinetic Ising model, when the system is quenched below T_c, the paramagnetic-to-ferromagnetic phase transition temperature [34]. However, unlike the latter, which is of second order, the I-N phase transition is of first order. Therefore the latent heat generated at the I-N interface has to be conducted away. This heat transfer mechanism leads to the measured growth law, which is described by the solution of the diffusion equation [35]

$$\frac{\partial T}{\partial t} = D\nabla^2 T, \tag{2.9}$$

for the temperature field $T(r,t)$, function of the position r and time t, we apply the condition

$$LR = -D\left(\nabla T\right)_{r=R} \tag{2.10}$$

at the interface, where D is the diffusivity and L is the latent heat per unit volume. Imposing the boundary condition $T(r) = T_c$ at $r = R$ and $T(r) = T_\infty$ at $r = \infty$, for quasi stationary growth $\frac{\partial T}{\partial t} = 0$, we find the solution of the diffusion equation

$$T(r,t) = (T_c - T_\infty)\frac{R}{r} + T_\infty \text{ for } r > R. \tag{2.11}$$

Inserting the solution for $T(r,t)$ in equation (2.9) gives $\frac{dR}{dt} \sim \frac{1}{R,}$ and thus $R(t) \sim t^{1/2}$, as experimentally observed after small temperature quenches and as predicted by the Avrami law. However, if the

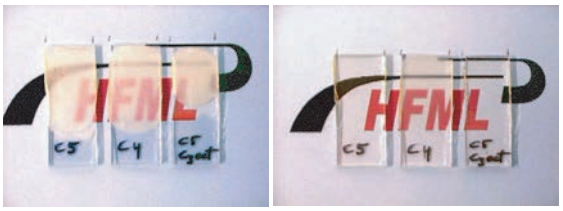

Figure 2.11: The macroscopic appearance of three polymeric LC compounds is affected by a magnetic field. The sample has been cooled from the isotropic phase to the liquid crystalline phase. With no applied magnetic field the material appears opaque, due to a strong light scattering from many micro-sizes domains with different orientation. In a magnetic field of 30 T the material appears transparent, because an orientated monodomain has formed and there is no light scattering.

size of the cluster is small, the released latent heat is also small and the rate at which this tiny amount of heat can be conducted away from the interface is very fast. The growth exponent gradually changes from $R \sim t^{1/2}$ to $R \sim t$ as a function of quench depth [32], [14].

For all times $t > t_0$ and for vanishing difference in the free energies of the two phases, the diffusive power law (2.8) is valid. A different power law is found for clusters growing far from the critical temperature T_c, i.e. after large quench depths, leading to a non negligible difference in the free energy of the high and low temperature phases [33], yielding a linear growth in time [37], [38]. Powerful tools to access the dynamics of microscopic system are molecular dynamics simulations (MDS). Results obtained from MDS bridge the different growth regimes; by this it is possible to explain the power law change for liquid crystals. Huisman and Fasolino [14] find that the growth of nematic clusters is driven by diffusion of latent heat. They solve the Landau-Ginzburg order parameter evolution equation by a multiscale approach in the same model system, 8CB [14]. For small quench depths the growth is slowed down by the latent heat released by the cluster that should diffuse away from it. This causes a transient regime, in which the exponent of growth increases with increasing quench depth towards the asymptotic value of 1. Upon varying the quench depth the growth law exponent follows a S-shaped curve. The relation 2.8 $R(t) \sim t^{1/2}$ is followed for growing clusters at quench temperature $T > T_C - R/C_p$, where C_p is the specific heat. For 8CB $C_p = 7.30 \cdot 10^2\ Jmol^{-1}K^{-1}$ [20].

2.7 Interactions with an applied magnetic field

2.7.1 Alignment

Diamagnetic materials create an induced magnetic field in a direction opposite to an externally applied magnetic field. Therefore a diamagnetic system tends to move away from the field maximum if a gradient is present. A spectacular application is the possibility of levitating diamagnetic objects, such as a frog, a strawberry or a water droplet [40], [41]. Apart from levitation, diamagnetic materials can also be aligned when the material is anisotropic. Diamagnetism is a tensorial additive property. Due to the collective behavior of LC molecules, the alignment induced by a magnetic field in a LC when cooled from the isotropic phase can result in enhanced macroscopic properties, such us high transparency see figure 2.11.

The extra energy per molecule in an external magnetic field is

$$E_{mag} = -\int_0^B \overrightarrow{m} \cdot d\overrightarrow{B} \tag{2.12}$$

and is linked directly to the molecular diamagnetic susceptibility, which is generally written as a second-rank symmetrical tensor $\dot{\chi}$. The diamagnetic susceptibility gives the magnetic moment $\overrightarrow{m}$ per molecule induced by the field:

$$\overrightarrow{m} = \frac{1}{\mu_0}\dot{\chi}_m \overrightarrow{B}. \tag{2.13}$$

It is convenient to consider the molar susceptibility tensor $\dot{\chi} = \dot{\chi}_m N_A$, with N_A Avogadro's number. Working out the components of $\dot{\chi}_m$can be cumbersome, but choosing the molecular coordinate system the susceptibility tensor can be diagonalised and written as

$$\dot{\chi}_m = \begin{pmatrix} \chi_{xx} & 0 & 0 \\ 0 & \chi_{yy} & 0 \\ 0 & 0 & \chi_{zz} \end{pmatrix}. \tag{2.14}$$

For the cylindrically symmetric case, which is a good approximation to describe a typical anisotropic LC molecule, we can write $\chi_{xx} = \chi_{yy} = \chi_\perp$ and $\chi_{zz} = \chi_{//}$, see figure 2.12.

Consequently the anisotropy of the diamagnetic susceptibility becomes $\Delta\chi = \chi_{//} - \chi_\perp$. For a general magnetic field orientation we write

$$\overrightarrow{B} = \begin{pmatrix} B\sin\theta\cos\phi \\ B\sin\theta\sin\phi \\ B\cos\theta \end{pmatrix} \tag{2.15}$$

and the magnetic moment $\overrightarrow{m}$ is

$$\overrightarrow{m} = \frac{1}{\mu_0 N_A}\begin{pmatrix} \chi_\perp & 0 & 0 \\ 0 & \chi_\perp & 0 \\ 0 & 0 & \chi_{//} \end{pmatrix} \cdot \begin{pmatrix} B\sin\theta\cos\phi \\ B\sin\theta\sin\phi \\ B\cos\theta \end{pmatrix} =$$

$$= \frac{1}{\mu_0 N_A}\left[\chi_\perp \begin{pmatrix} B\sin\theta\cos\phi \\ B\sin\theta\sin\phi \\ B\cos\theta \end{pmatrix} + \begin{pmatrix} 0 \\ 0 \\ (\chi_{//} - \chi_\perp)B\cos\theta \end{pmatrix}\right]. \tag{2.16}$$

We can now calculate the magnetic energy for a LC molecule:

$$E_{mag} = -\int_0^B \overrightarrow{m}\cdot d\overrightarrow{B} = -\frac{1}{2\mu_0 N_A}\left[\chi_\perp B^2 + (\chi_{//} - \chi_\perp)B^2\cos^2\theta\right]. \tag{2.17}$$

The first term can be omitted, since it is isotropic in B. Therefore the increase in magnetic energy of a molecule as a function of its orientation, expressed by θ, is

$$\Delta E_{mag} = -\frac{(\chi_{//} - \chi_\perp)B^2}{2\mu_0 N_A}\cos^2\theta = -\frac{\Delta\chi B^2}{2\mu_0 N_A}\cos^2\theta. \tag{2.18}$$

Now the link between an applied magnetic field and the molecular orientation is evident: this extra energy is minimized by an orientational force, tending to bring the molecule with its axis of smallest diamagnetic susceptibility parallel to the field direction. For the liquid crystal system studied here – 8CB– this means that the long axis of the molecule is aligned along the field direction. Unfortunately, when considering a single molecule, the diamagnetic susceptibility is never large enough to make the magnetic energy overcoming the randomizing thermal energy $k_B T$, even for the strongest available magnetic fields. For example, in an external field of 100 T at room temperature, for a typical anisotropic organic molecule like benzene, the ratio

$$\frac{\Delta E_{mag}}{k_B T} \approx 10^{-4}. \tag{2.19}$$

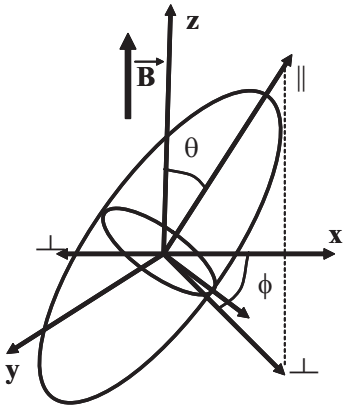

Figure 2.12: The molecular frame: the molecular director forms an angle *theta* with the *z* axis, which coincides with the direction of the external field B. The direction perpendicular to the molecular director forms an angle ϕ with the x axis.

However an array of N molecules stacked in a uniform way gives a total magnetic energy $N\Delta\chi B^2$ that can be larger than the thermal energy. This is what happens in liquid crystals, where molecules show a collective behavior. In this thesis we report the direct observation of micrometer-sized LC clusters, for which $N \sim 10^6$, aligning in magnetic field $\geqq 0.1$ T. To be able to measure this phenomenon we make use of birefringence microscopy, as described in chapter 3.

2.7.2 Nucleation and growth dynamics

The effect of an external magnetic field on nucleation is basically unknown. Experiments are scarce, conflicting results are reported and a detailed, comprehensive understanding is clearly missing. Two main experimental problems are the extremely small size of the critical nucleus and the stochastic nature of the nucleation process, which make it very difficult to probe the actual nucleation process itself. Therefore, most of our knowledge has been obtained as a side product of crystallization experiments under applied external fields. The main motivation of those works has been to improve the quality of the crystals with an external magnetic field, rather than understanding nucleation. Possible effects of a magnetic field on crystal growth include magnetic alignment of the crystals [28], suppression of convection in field gradients [47], [48], [49] and damping convection in conducting metal melts [54]. There is indeed a large body of work describing nucleation in different fields. However, the differences between those fields are mainly in the strength of the interaction parameter, not in the final effect.

Theoretically, crystal nucleation from a solution in an external electric field has been described by Kashchiev [50]. Depending on the ratio of the dielectric constants of the crystal and the solution nucleation can be enhanced or inhibited by an electric field. A similar argument is proposed for a magnetic field with the ratio of the dielectric constants replaced by the ratio of magnetic permeabilities [50].

Experimentally the application of a magnetic field reduced the number of nuclei during the growth of hen egg-white lysozyme and horse-spleen ferritin [27] and inhibited the nucleation of calcium carbonate in water [43]. Some evidence is reported that the application of a magnetic field leads to a widening of the metastable region during nucleation of cholesterol [45]. Finally, several studies report that the nucleation during metal solidification is inhibited by an external field [51], [52], [53], [54], [55],

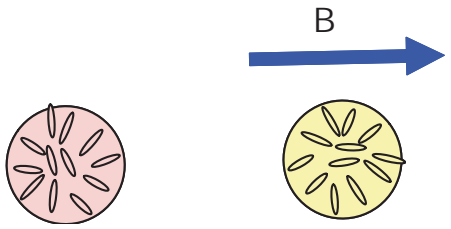

Figure 2.13: The magnetic field tends to align the molecules in a direction parallel or perpendicular to its direction. This causes a different appearance of the nematic domain under cross polarized light.

although some papers report the opposite [56] or no effect at all of an applied field [52]. Recently, an explanation for these effects has been proposed, namely that heterogeneous nucleation is hindered through an increase in contact angle between the liquid and the crucible as a result of an additional surface tension, which is induced by the interfacial magnetic pressure [57].

In the isotropic nematic transition the formation of the nematic phase implies the formation of nematic clusters. The shape of the clusters depends on the competition between surface tension, which is rather small at T-N-I, and the surface anchoring. We observe spherical nematic clusters, which appear faceted, almost square, when illuminated with monochromatic light. A magnetic field tends to align the molecules along or perpendicular to its direction, competing against the cluster structure, where the molecules are perpendicular to the surface to minimize surface tension, see figure 2.13. Therefore the curvature energy might be increased by the presence of a magnetic field.

The results of this magnetic effect on the isotropic-nematic transition in unclear. Few studies report the observation of a wider metastable region during nucleation of crystals [45] and focus on industrial applications [26].

The unique experimental set-up allowed us to study the effect of a magnetic field systematically and to analyze the role of interfaces, which is not only of fundamental interest, but also important to technological application. The magnetic field induces the same orientation in each cluster. This facilitates the formation of few large clusters rather than many small ones. This effect has been observed in crystal growth experiments where it results in bigger and high quality crystals [48], [49]. For liquid crystal this would result in a easier merging of clusters during the I-N transition, called coarsening regime, where clusters oriented in the same direction merge together to form the nematic phase.

References

[1] P. G. de Gennes and J. Prost, *The Physics of Liquid Crystals*, Clarendon Press, Oxford (1993).

[2] G. Vertogen, W. H. de Jeu, *Thermotropic liquid crystals, Fundamentals*, Springer-Verlag (1988).

[3] S.Meng, *Molecular Theory of Liquid Crystal Thin film*, Purdue University (2008)

[4] I. Dierking, *Textures of Liquid Crystals*, Wiley-VCH (2003).

[5] R.A.L. Jones, *Soft Condensed Matter*, OUP Oxford (2002).

[6] J.S. Huang, S. Vernon, and N. C. Wong, Phys Rev. Lett. 33,140 (1974).

[7] H. Kneppe, F. Schneider and N. K. Sharma, J. Chem. Phys 77, 3203 (1982).

[8] V. Popa-Nita and P. Oswald, J. Chem. Phys. 127, 104702 (2007).

[9] J. Thoen, H. Marynissen and W. Van Dael, Phys. Rev. A 26, 2886 (1982).

[10] P.K. Mukherjee, J. Phys.: Condens. Matter 10, 9191 (1988).

[11] P.J. Keyes, Phys. Lett. A 67, 132 (1978).

[12] M.A. Anisimov, *Critical Phenomena in Liquids and Liquid Crystals*, Gordon and Breach Science Publisher, Philadelphia (1991).

[13] D. Sharma, J.C. Mac Donald, G.S. Iannacchione, J. Phys. Chem. B, 110 (33), 16679 (2006).

[14] F. Mercuri, R. Pizzoferrato, U. Zammit and M. Marinelli, Applied Physics letters 81, 4148 (2002).

[15] I. Dierking, J. Phys. Chem. B 104, 10642 (2000).

[16] M. Kleman, *Points, Lines, Walls*, Wiley (1982).

[17] M. Kleman, O.D. Lavrentovich, *Soft Matter Physics. An Introduction*, Springer (2004).

[18] M. Avrami, J. Chem. Phys. 7, 1103 (1939).

[19] S. Auer and D. Frenkel, Nature 409, 1020 (2001).

[20] G. Iannacchione and D. Finotello, Liquid Crystals, 14, 4, 1135 (1993)

[21] A.J. Bray, Physica A 194, 41 (1993).

[22] N.A. Clark, T. Bellini, R.M. Malzbender, B.N. Thomas, A.G. Rappaport, C.D. Muzny, D.W. Schaefer and L. Hrubesh, Phys. Rev. Lett. 71,3505 (1993).

[23] A.J. Bray and K. Humayun, Phys Rev. E 48, 1609 (1993).

[24] A.J. Bray, Advances in Physics 51, 481 (2002).

[25] P.R. ten Wolde and D. Frenkel, Science 277, 1975 (1997).

[26] H. Sheibani, S. Dosta, S. Sakaia and B. Lent, Journal of Crystal Growth 258, 283 (2003).

[27] G. Sazaki, E. Yoshida, H. Komatsu, T. Nakada, S. Miyashita and K. Watanabe, Journal of Crystal Growth 173, 231 (1997).

[28] N. I. Wakayama, M. Ataka and H. Abe, Journal of Crystal Growth 178, 653 (1997).

[29] W. Ostner, S.-K. Chan and M. Kahlweit, Berichte der Bunsengesellschaft 77, 1122 (1973).

[30] I.M. Lifshitz, Sov. Phys. JETP 15, 939 (1962).

[31] S.M. Allen and J.W Cahn, Acta Met. 27, 1085 (1979).

[32] H.K. Chan and I. Dierking, Phys Rev. E 70, 021703 (2004).

[33] K. Diekmann, M. Schumacher and H. Stegemeyer, Liq. Cryst. 25, 349 (1998).

[34] K. Binder, Rep. Prog. Phys 50, 783 (1987).

[35] D. Frenkel, Mol. Phys. 60, 1 (1987).

[36] S. Bronnikov and I. Dierking, Phys. Chem. Chem. Phys. 6, 1745 (2004).

[37] I. Dierking, Appl. Phys. A 72, 307 (2001).

[38] H. K. Chan and I. Dierking, Phys Rev. E 70, 021703 (2004).

[39] B. A. H. Huisman and A. Fasolino, Phys Rev. E 76, 021706 (2007).

[40] A. K. Geim, Physics Today 51, 36 (1998).

[41] M. V. Berry and A. K. Geim, European Journal of Physics 18, 307 (1997).

[42] I. Dierking, J. Phys. Chem. B 104, 10642 (2000).s

[43] S. Kobe, G. Dražić, A.C. Cefalas, E. Sarantopoulou and J. Stražišar, Cryst. Eng. 5, 243 (2002).

[44] G.J. Evans, J . Chem. Soc. Faraday Trans. 1, 81, 673 (1985)

[45] N. M. Sandarac, M. Ashok and S. N. Kalkura, Acta Crystallogr D Biol Crystallogr 58, 1711 (2002)

[46] H. Sheibani, S. Dosta, S. Sakaia and B. Lent, Journal of Crystal Growth 258, 283 (2003)

[47] D.C. Yin, N.I. Wakayama, K. Harata, M. Fujiwara, T. Kiyoshi, H. Wada, N. Niimura, S. Arai, W.D. Huang, Y. Tanimoto J. Cryst. Gr. 270, 184 (2004)

[48] P.W.G. Poodt, M.C.R. Heijna, K. Tsukamoto, W.J. de Grip, P. C. M. Christianen, J.C. Maan, W. J. P. van Enckevort and E. Vlieg: Appl. Phys. Lett. 87, 214105 (2005)

[49] M.C.R. Heijna, P.W.G. Poodt, K. Tsukamoto, W.J. de Grip, P.C.M. Christianen, J.C. Maan, J.L.A. Hendrix, W.J.P. van Enckevort and E. Vlieg: Appl. Phys. Lett. 90, 264105 (2007)

[50] D. Kashchiev, Nucleation Basic Theory with applications, J. Cryst. Gr. 13/14, 128 (1972)

[51] M. Hasegawa and S. Asai, J. Mat. Science 27, 6123 (1992)

[52] Y.K. Zhang, Y.L. Zhou, J.R. GAO, J.C. He Materials Science Forum 649, 281 (2010)

[53] C.J. Li, H. Yang, Z.M. Ren, W.L. Ren and Y. Q. Wu, Progress In Electromagnetics Research Letters, Vol. 15, 45 (2010)

[54] T. Liu, Q. Wang, F. Liu, G. Li, J. He, J. of Crys. Gr. 321, 167 (2011)

[55] C.J. Li, Z.M. Ren, W.L. Ren and Y.Q. Wu, Trans. Nonferrous Met. Soc. China 22, s1?s6 (2012)

[56] Y. Aoki, S. Hayashi and H. Komatsu, Journal of Crystal Growth 108, 121 (1991)

[57] Z.H.I. Sun, X. Guo, M. Guo, C. Li, J. Vleugels, Z. Ren, O. Van der Biest, and B. Blanpain, J. Phys. Chem. C 116, 17676 (2012)

Chapter 3

Experimental Techniques

3.1 Introduction

Several experimental techniques are combined to study the structure of liquid crystals in a magnetic field. In section 3.2 we describe the optical properties of liquid crystals through cross-polarized filters and in section 3.3 we describe the low field (2 T) set-up for experiments. In section 3.4 the image analysis technique is explained which allows a qualitative analysis of the magnetic manipulation experiments. We focus on the thermal aspects to study the isotropic nematic coexistence region in section 3.5, while in section 3.6 the relationship between the nematic director orientation and the measured intensity is formally described. In this way we extract information on the orientation and phase state of the liquid crystals. In section 3.7 we present the experimental details for magnetic manipulation in the Smectic A phase. Finally in section 3.8 the high field (up to 20 T) set-up is described and used to observe smectic reorientation and pattern formation.

3.2 Light transmitted through a birefringent object

Any object with an intrinsic anisotropy of its molecular structure may exhibit different refractive indices for light polarized along two perpendicular directions. This phenomenon is called birefringence. Light polarized along the so-called fast axis experiences the(ordinary) refractive index n_o, whereas light polarized along the slow axis feels the (extra-ordinary) refractive index n_e. The two light components travel with different speeds through the material causing the built-up of a phase difference between them. Due to this phase difference the polarization state of the light after crossing the sample has changed with the amount: $\Delta\varphi = 2\pi\frac{d}{\lambda}(n_e - n_o)$, where d is the thickness of the material and λ is the wavelength of the light [1]. Thus the birefringence of a material is characterized by the difference $\Delta n = n_e - n_o$. The condition $n_e > n_o$ defines a positive uniaxial material, as for instance a nematic liquid crystal [3], [5]. For typical nematic liquid crystals n_o is approximately 1.5 and the corresponding phase difference Δn may range between 0.05 and 0.5.

It is important to consider the thickness d of the sample, which determines the phase shift: any polarization state can be produced with different values of n_e, n_o and d. A phase difference of $(2m + 1)\frac{\pi}{2}$, i.e. when $d = \frac{\lambda}{4(n_e - n_o)}(2m+1)$, will result in a linearly polarized wave; when $2\pi\frac{d}{\lambda}(n_e - n_o) = \frac{\pi}{4}$ a circularly polarized wave will be the result [4], [6].

An effective way to visualize the birefringence of materials is to position it in between two perpendicularly oriented polarizers. Light passing through non-birefringent parts of the sample will be blocked. Birefringent parts of the sample causes the polarization of the light to rotate, resulting in transmitted light, unless the polarizers are aligned along the fast or slow axis of the material [7], [8]. In our experiments the magnetic field induces a parallel orientation on the LC sample director. In order

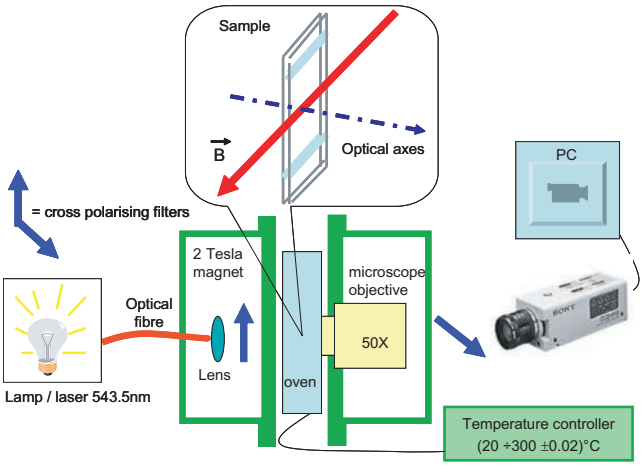

Figure 3.1: Set-up for experiments in 2 Tesla. The oven between the pole-shoes of the magnet can accomodate an optical cell, where the temperature of the system can be controlled with a precision of $2/1000$ of degree. The sample is positioned between two cross-polarized filters and is illuminated by a light source (lamp or laser).The birefringent signal from the probed area is magnified by a lens system and it is collected by a CCD camera. Note that light travels perpendicular to B in this configuration.

to maximize the contrast we orient the cross-polarized filters and the magnetic field direction at 45 degrees with respect to each other. In this way an oriented material appears the brightest. On the other hand when the LC material is heated up to its isotropic phase the molecular order is destroyed and the sample, loosing its birefringence, appears black through cross-polarized filters. A black state is also detected whenever the LC is oriented at 45 degrees with respect to the magnetic field, because of our orientation choice on the directions of the magnetic field and the cross-polarized filters.

We perform experiments both in static and in transient magnetic fields. In transient magnetic fields we measure the dynamics of the magnetic alignment and the relaxation to the non perturbed state by birefringence microscopy. Unfortunately the relaxation and alignment times are of the same order of the sweep rate (1 to 5 s) of the magnetic field. Therefore the results obtained in transient fields are excluded from this thesis. Having oriented the two cross-polarized filters at 45° with respect to the magnetic field direction, we observe an increasing intensity of nematic clusters while the magnetic field intensity increases.

3.3 Low magnetic field Set-up in 2 T

The set-up for experiments up to 2 T is schematically shown in 3.1. Between the pole-shoes of a water-cooled electromagnet, manufactured by Varian, we place an oven with a glass window facing a microscope objective, mounted directly on the oven. The distance between the pole-shoes is 41 mm wide and can host a massive aluminum oven, 40 mm x 40 mm x 400 mm, where the temperature stability of the sample is controlled up to $2/1000$ of degree by symmetric heating and cooling. Picture 3.2 shows the oven as it as been designed and manufactured at the HFML for our experiments. A resistive heater is controlled by a *lake shore 340* device, which receives feedback from the temperature sensor and drives the heating, adjusting the proportional, integral and differential settings. A copper plate (zone 1 in the picture) fits the optical cell containing the sample. This occupies the central part

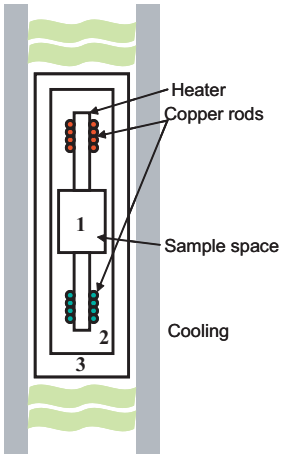

Figure 3.2: The oven consists of a copper plate (1) that can accomodate an optical cell containing the sample. This occupies the central part of the oven and it is in thermal contact with a water-based refrigerated copper chamber (2). The rest of the oven contains air (3), allowing heat distribution by convection.

of the oven and it is in thermal contact with a water-based refrigerated copper chamber (zone 2 in the picture). The rest of the oven contains air (zone 3 in the picture), allowing heat distribution by convection. During all experiments the temperature is measured by a $Pt100$ sensor, in contact with the cell in the zone 1. In the oven we can accomodate an optical glass cell containing the pure liquid crystal. Both commercial Hellma Benelux B.V. path length 1 mm, or smaller cells with optical path 0.1$\div$0.5 mm can be used. The latter cells are fabricated in our laboratorium. The system can be observed at different magnifications just by changing the microscope objective. This oven allows a fast and symmetric heating and cooling of the sample. The accuracy in controlling the temperature of the sample is verified by introducing a second sensor in the oven, right into the optical cell containing 8CB. This allows also a temperature calibration. In figure 3.3 the temperature readings at the $Pt100$ sensor (bottom line) and another resistive sensor immersed into the cell (top line) are showed for different values of ΔT. We find a close relationship of the temperature inside the cell with the measuring sensor positioned outside of the cell. This is an evidence of the reliability of our quench experiments.

3.4 Image acquisition and analysis

Video imaging and image analysis enable us to study liquid crystals during their phase transition and to detect the changes induced by an external magnetic field. We use either polarized light from a He-Ne laser (1 mW output, Melles-Griot) with wavelength λ=543.5 nm as a monochromatic light source. Such a monochromatic light source eliminates noise from diffraction fluctuations but may give rise to interference effects between the laser wavelength and the optical path length. Alternatively unpolarized light guided to the sample through an optical fiber is used in order to avoid interference fluctuations. Two Glan-Thompson cross polarized filters (Melles-Griot, extinction ratio 10^{-5}) are positioned outside the magnet, before and after the sample. The optical signal is collected by a 3CCD video camera with a PC interface. The image acquisition rate can be chosen between 1 and 25 frames per second. We record videos in AVI format on a PC and extract image frames in BMP format. We convert these

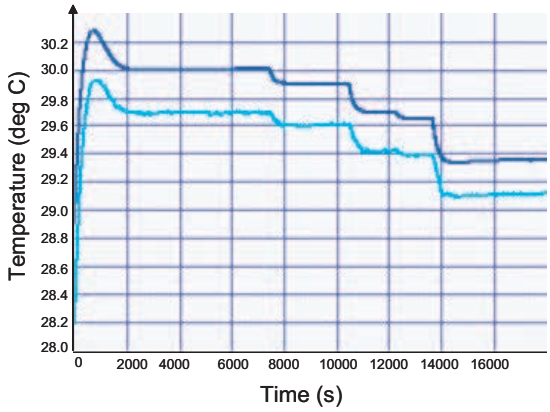

Figure 3.3: During the quench experiments the temperature inside (top line) and outside (bottom line) the cell rapidly follow the induced variations, showing that our quench experiments are reliable for temperature variations smaller than 0.5 °C.

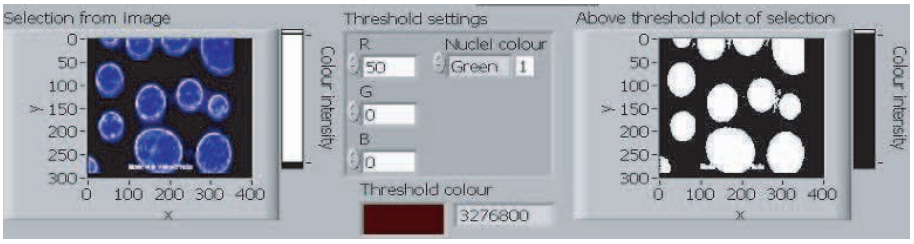

Figure 3.4: The image frames from the acquired videos are processed by a Labview routine. All the intensity values above a defined threshold give the area occupied by the nematic phase. The background corresponds to the isotropic phase, with intensity values below the threshold.

images in a $4x4$ bit pixmap and consider the corresponding RGB values. When studying the isotropic to nematic transition we detect the coexistence region by the presence of both isotropic and nematic phases. By image analysis we are able to distinguish the two phases defining threshold RGB values below which only the isotropic phase is present. All the values above the threshold are detected in Labview and correspond to the area occupied by the nematic phase, as shown in figure 3.4. The Labview routine allows to scan thousands of consecutive frames in few minutes. By running this program on a restricted area around a single nematic area, we can measure the size of an individual nematic cluster. When we evaluate the percentage of nematic coverage during the transition we consider the total probed area in the field of view. Furthermore, in order to extract information about the degree of alignment within each nematic domain, we convert the RGB values into luminance values. In a similar way the intensity variation within a nematic region is obtained and the director angle θ is measured from the equation

$$I_{tot} = A\left(\cos^2\theta - \frac{1}{2}\right)^2, \tag{3.1}$$

as described in section 3.8.

3.5 Experimental details for magnetic manipulation in the Smectic A phase

When cooling liquid crystals close to the smectic phase the degree of order increases and a significant energy difference is required to modify their molecular orientation. Experiments on the Smectic phase are therefore performed in high magnetic fields, up to 20 T. By suddenly rotating the smectic sample, while keeping the magnetic field direction constant, we observe how the system recovers its equilibrium. In fact, as a result of the rotation, the smectic domains are oriented along an unfavorable direction with respect to the magnetic field, so the system rearranges towards a more favorable energy balance.

The optical cell for our experiments consists of two borosilicate glass disks 0.4 mm thick (Schott Desag AG **)** and a teflon ring 1.6 mm thick used as spacer. The choice of a round confinement reduces singularities at the borders, while the special glass ensures the best imaging quality, having a high transmission rate in the desired wavelength range. As for all the experiments above, the cell is filled in the isotropic phase, taking good care of avoiding air bubbles, which would dramatically affect the dynamics of our experiment.

3.6 Set-up in 20 T

Data on the dynamics after a sudden rotation of the smectic sample are detected by our optical system, as shown in figure 3.5. A cylindrical lens and two cross polarized filters are placed between the pole-shoes of a 20 T Bitter magnet. The probing light is guided by an optical fiber (3M, multimode, 600 μm core diameter) and it homogeneously illuminates the sample. Two mirrors mounted aside the sample allows to bring the light at normal incidence to the cell and collect the optical signal while keeping the cell walls parallel to the applied magnetic field. The signal is then transmitted to a zoom lens mounted on a 3CCDs camera. The total magnification of this system is about 30X. A quick rotation of the sample is essential to observe reorientation phenomena. Our stepper motor Phytron IXE is able to complete a 360° rotation in 2400 steps, at a maximal frequency of 25 Hz, with accuracy $\Delta\phi = \pm 3°$. The temperature of the sample is varied using a water based circular AKE system, which stabilizes the temperature of the whole magnet bore with an accuracy of 0.1°C.

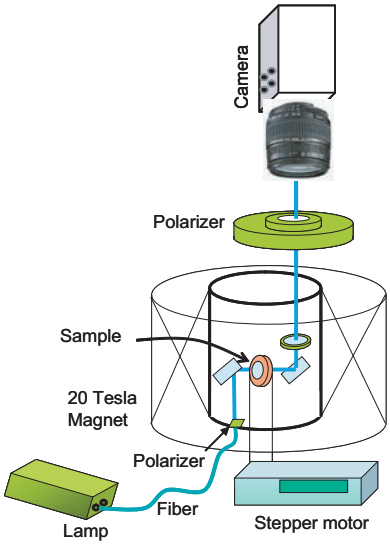

Figure 3.5: The set-up for experiments in 20 T combines birefringence microscopy with a rotation device controlled by a stepper motor.

3.7 Thermal details for magnetic manipulation at the I-N phase transition

As discussed above, phase transitions in thermotropic liquid crystals are observed by inducing sudden temperature changes in the system. When studying liquid crystals during the isotropic to nematic phase transition we need both to control with great accuracy the temperature of the system and at the same time to be able to modify the energy balance of the system. This is possible by applying an external magnetic field up to 2 T, which can be changed from 0 to 2 T in 5 s, sufficient to change the energetic equilibrium of our system when it is in a metastable state, which is very sensitive to small energy differences.

Different optical cells are prepared to observe the isotropic nematic transition. The cell consists of two flat glass surfaces separated by teflon spacers. The liquid crystal is thus confined in an optical cell of minimal thickness 0.1 mm in order to observe volume phenomena and not only surface effects. A sample thickness of 1 mm is also used to reproduce the results obtained in 0.1 mm. The sample is then heated above the Isotropic transition to a temperature two degrees above T_c, the I-N phase transition, and kept at constant temperature for at least 10 minutes. Two different cooling techniques, quench and slow cooling, are used, as described below.

Our quench experiments are performed in different background fields, from 0 T to 2 T. A constant magnetic field is applied when the system is stable in its isotropic phase, before cooling to the boundary of the I-N coexistence. The dynamics of the process is studied in thermally stable conditions to exclude any external driving force to the growth and a quench is realized by a sudden temperature reduction with a step ΔT between 0.1 and 0.45 °C. In a thick cell of 1 mm variations of the temperature throughout the cell volume are more important, therefore the quench amplitude is reduced to 0.25 °C to guarantee the realization of experiments at thermal equilibrium. We call a quench successful when growing domains can be observed within 400 s after the end of the quench. When domains

appear before the temperature becomes constant the experiment is considered fault and not taken into account. It also happens that no nematic cluster can be observed after the quench. In this case, after 400 s, a second quench is applied. Again, if no growing domain is observed the temperature is lowered by another, identical step ΔT until a successful quench occurs.

We verify that the presence of a magnetic field does not affect the reading of our temperature sensor, the accuracy of which remains $\delta T = 0.002°$C. Upon varying the magnetic field $\delta T = 0.005°$C is measured. This latter systematic error does not affect our experiments, since no magnetic field variation is required. As shown in figure 3.6 the temperature reading is thus not affected by a magnetic field sweep.

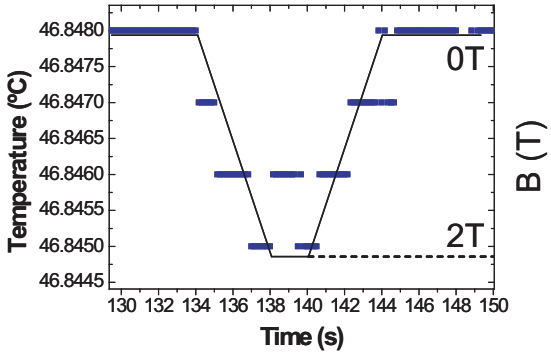

Figure 3.6: The temperature of the cell upon varying the magnetic field from 0 to 2 T and back to 0 T is minimally affected. This shows that electromagnetic interference is negligible for the temperature control of our experiments.

Another cooling technique is used to observe the Isotropic to Nematic phase transition for a long time. The liquid crystal is heated up to its isotropic phase and then the temperature is stabilized. Subsequently the system is cooled slowly down to the I-N transition temperature, within the coexistence region. We program the cooling with a progressively slower rate, from 0.1° C/min to 0.01° C/min. In this way the phase transition is slowed down and observed on a time scale from few minutes to many hours. In this way the meta-stable coexistence region can be locally considered as a stable state. This allow us to study the effect of a transient external field on the coexistence of the two phases, neglecting the fact that the phase transition is slowly progressing. Experimental results on the effect of a transient magnetic field on nematic domains are presented in chapter 4.

3.8 Relation between the nematic director orientation and the measured intensity

Here we work out the relation between the orientation of the nematic director of a LC cluster and the light intensity at the detector. Let us first consider the two dimensional case, where the director lies in the plane of the field of view. In the liquid crystalline phase the nematic material behaves as phase changer operator, thus, when its director is parallel to the x axis, we can write it as:

$$S_{al} = \begin{pmatrix} e^{i\varphi_x} & 0 \\ 0 & e^{i\varphi_y} \end{pmatrix}$$

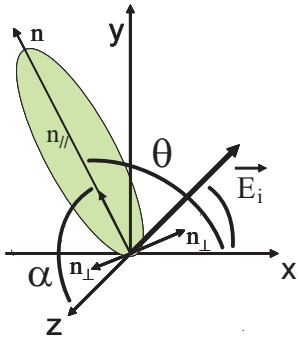

Figure 3.7: In the molecular frame the director of a three dimensional molecule can be rotated by an angle θ in the plane and can be tilted by an angle α out of this plane.

.

The phase differences φ_x and φ_y are directly related to the path length, i.e. to the thickness of the birefringence material d:

$$\varphi_x = n_x \frac{d}{\lambda},$$
$$\varphi_y = n_y \frac{d}{\lambda},$$

where n_x and n_y are the diffraction index along the corresponding axis.

The expression above corresponds to a fully oriented sample when the magnetic field is parallel to the x axis. On the other hand, when the director is not oriented along the field, but forms an angle θ with respect to the x axis in the plane perpendicular to the optical axis, the matrix associated with the sample becomes: $S = R \cdot S_{al} \cdot R^{-1}$, with

$$R = \begin{pmatrix} \cos\theta & -\sin\theta \\ \sin\theta & \cos\theta \end{pmatrix}$$

The intensity I at the detector is: $I = E_f^* \cdot E_f = |E_f|^2$, with

$$E_f = P_{-45} \cdot E_i,$$

where $E_i = \begin{pmatrix} 1 \\ 0 \end{pmatrix}$ is the incoming polarized light and the elements associated with each polarized filters P, at 45° with respect to the x axis, are:

$P_{\pm 45} = \begin{pmatrix} 1 & \pm 1 \\ \pm 1 & 1 \end{pmatrix}$.

We obtain

$$I = \frac{1}{2}\cos^2(2\theta)\,(1 - \cos(\Delta\varphi)) \tag{3.2}$$

where $\Delta\varphi = \varphi_x - \varphi_y$ is the total phase difference induced by the birefringent material.

In a more general and realistic case we have to consider that the nematic director may be tilted by an angle α out of the plane of the field of view, as sketched in figure 3.7.

An expression for the intensity in three dimensions can be calculated extending all the matrix elements in three dimension in the Jones formalism [10].

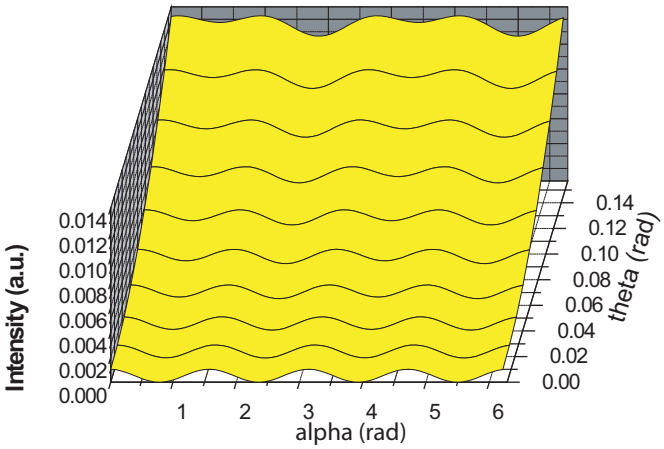

Figure 3.8: Qualitative behavior of the intensity for small values of θ.

We have now $S_{al} = \begin{pmatrix} e^{i\varphi_x} & 0 & 0 \\ 0 & e^{i\varphi_y} & 0 \\ 0 & 0 & 1 \end{pmatrix}$; $E_i = \begin{pmatrix} 1 \\ 0 \\ 0 \end{pmatrix}$;
$P_{\pm 45} = \frac{1}{2}\begin{pmatrix} 1 & \pm 1 & 0 \\ \pm 1 & 1 & 0 \\ 0 & 0 & 1 \end{pmatrix}$; $n = \begin{pmatrix} n_{//} & 0 & 0 \\ 0 & n_\perp & 0 \\ 0 & 0 & n_\perp \end{pmatrix}$
in the axis frame the outgoing electric wave E_f becomes:

$$E_f = P_{45} \cdot R_\alpha \cdot R_\theta \cdot S \cdot R_\theta^{-1} \cdot R_\alpha^{-1} \cdot P_{-45} \cdot E_i$$

with $R_\alpha = \begin{pmatrix} 1 & 0 & 0 \\ 0 & \cos\alpha & -\sin\alpha \\ 0 & \sin\alpha & \cos\alpha \end{pmatrix}$, $R_\theta = \begin{pmatrix} \cos\theta & -\sin\theta & 0 \\ \sin\theta & \cos\theta & 0 \\ 0 & 0 & 1 \end{pmatrix}$.

In the frame of the molecule, considering that the molecule sees E_i and $P_{\pm 45}$ rotated by $-\theta$ and that n remains the same, being the rotation of the birefringence included in the rotation of S_{al}, we have:

$$E_f = R_\theta^{-1} \cdot R_\alpha^{-1} \cdot P_{45} \cdot R_\theta^{-1} \cdot R_\alpha^{-1} \cdot S \cdot R_\theta^{-1} \cdot R_\alpha^{-1} \cdot P_{-45} \cdot R_\theta \cdot R_\alpha \cdot R_\theta^{-1} \cdot R_\alpha^{-1} \cdot E_i. \tag{3.3}$$

Therefore the detected intensity for both calculations is:

$$I = |E_f|^2 = E_i^t \cdot P_{-45} \cdot R_\theta \cdot R_\alpha \cdot S^* \cdot R_\theta^{-1} \cdot R_\alpha^{-1} \cdot P_{45} \cdot R_\theta \cdot R_\alpha \cdot S \cdot R_\theta^{-1} \cdot R_\alpha^{-1} \cdot P_{-45} \cdot E_i. \tag{3.4}$$

Including all the Jones elements results in a rather complex expression for the intensity:
$I = \frac{1}{4}(1 - \cos\varphi_y) + \frac{1}{4}\cos^2\theta\left(1 + \cos^4\alpha\right) +$
$(1 - \cos\varphi_x + \cos\varphi_y - \cos(\varphi_x - \varphi_y)) +$
$+\frac{1}{4}\cos^4\theta(\cos(\varphi_x - \varphi_y) - 1)\left(1 - 6\cos^2\alpha + \cos^4\alpha\right) +$
$+\frac{1}{2}\cos^2\theta\cos^2\alpha\left(\cos\varphi_x - \cos\varphi_y + 3\cos(\varphi_x - \varphi_y - 3\right) +$
$+\sin\theta\cos^3\theta\cos\alpha(\cos(\varphi_x - \varphi_y) - 1)\left(1 - \cos^2\alpha\right) +$

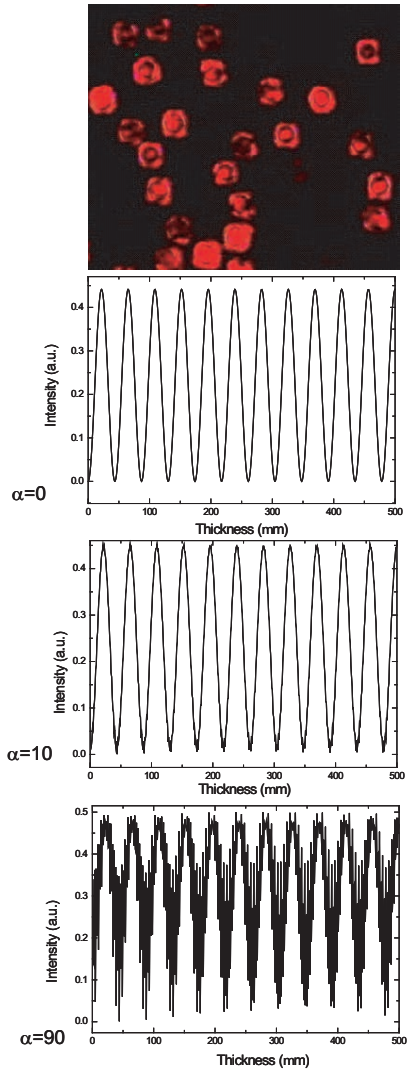

Figure 3.9: Top: image of the coexistence region near the phase transition under monochromatic light (red laser), showing nematic clusters with same order parameter S and different nematic director orientation with respect to the detection system. Note the alternation of bright and dark rings in the domains. Bottom: In the three panels the intensity profile through the samples is calculated for different values (in $^\circ$) of the angles α as a function of the sample thickness. The series of maxima and minima is due to alternating constructive and destructive interference; this clarifies the nature of the observed bright and dark rings in the nematic clusters under laser light.

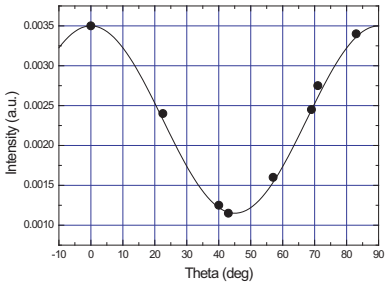

Figure 3.10: An experimental curve of the birefringent intensity of a 8CB nematic sample as detected as a function of the angle θ. The calculated intensity (solid line) interpolates the experimental intensity values for an aligned sample(dots).

$+\frac{1}{4}\sin 2\theta\cos\alpha(1-\cos\varphi_x+\cos\varphi_y-\cos(\varphi_x-\varphi_y))\left(1-\cos^2\alpha\right)+$
$+\frac{1}{4}\cos^2\alpha\left(1-\cos\varphi_x+\cos\varphi_y\right)-\cos(\varphi_x-\varphi_y)+\frac{1}{4}\cos^4\alpha\left(\cos\varphi_x-1\right).$

The qualitative behavior of the intensity for small values of θ is shown in figure 3.8. We calculate the intensity profile as a function of the sample thickness for any value of the angles α and θ. When illuminated with monochromatic light, the intensity shows a series of maxima and minima, as shown in figure 3.9. The same minima and maxima are experimentally observed by illuminating the sample with a monochromatic source (red laser) and are visible as a serie of bright and dark rings. When $\alpha=0$ the long expression above is simplified into the two dimensional case and the total intensity at the detector can be obtained by integrating I on the plane xy :

$$I_{tot}=\int Idxdy=\int_{\alpha=0}\left(\left(1-\cos\left(\Delta\varphi\right)\right)\left(\cos^2\theta-\frac{1}{2}\right)^2\right)dxdy \tag{3.5}$$

We observe nematic clusters both under white light and by monochromatic laser light. In the case of a monochromatic source the nematic domains appears squared, but under white light a round shape is observed. Based on our observations, we assume that nematic clusters have a spherical shape. It is thus convenient to pass to radial coordinates. We have

$$x^2+y^2+z^2=R^2-\left(\frac{d}{2}\right)^2=r^2 \tag{3.6}$$

with $r=0, d=2R$ in the center of the domain and $r=R, d=0$ outside of it.
In these coordinates the total intensity can be written:

$$I_{tot}=\frac{1}{2R^2}\int_0^{2R}I\left(d\right)\partial d \tag{3.7}$$

This expression can be written explicitly:
$I_{tot}=\left(\cos^2\theta-\frac{1}{2}\right)^2\left(1-\frac{\lambda}{\Delta nR}\sin\left(\frac{2\Delta nR}{\lambda}\right)+\frac{1}{2}\left(\frac{\lambda}{\Delta nR}\right)^2\cos\left(\frac{2\Delta nR}{\lambda}\right)-\frac{1}{2}\left(\frac{\lambda}{\Delta nR}\right)^2\right)$
In the following we will indicate with A the quantity:
$A=\left(1-\frac{\lambda}{\Delta nR}\sin\left(\frac{2\Delta nR}{\lambda}\right)+\frac{1}{2}\left(\frac{\lambda}{\Delta nR}\right)^2\cos\left(\frac{2\Delta nR}{\lambda}\right)-\frac{1}{2}\left(\frac{\lambda}{\Delta nR}\right)^2\right)$
and use the proportionality relation between nematic director orientation and detected intensity:

$$I_{tot}=A\left(\cos^2\theta-\frac{1}{2}\right)^2 \tag{3.8}$$

The validity of this expression can be verified by a simple experiment. By letting rotate a fully aligned nematic sample from $\theta = 0^\circ$ to 90°, we obtain the intensity calibration curve, as shown in figure 3.10. The calculated intensity (solid line) interpolates the experimental intensity values (dots). Thus in the vicinity of nematic (S=1) to isotropic (S=0) phase transition the intensity depends only on the orientation with respect to our detection system and not on the degree of internal alignment S, which is the same for all clusters.

References

[1] P. G. de Gennes and J. Prost, *The Physics of Liquid Crystals*, Clarendon Press, Oxford (1993).

[2] I. Dierking, J. Phys. Chem. B 104, 10642 (2000).

[3] E. Hecht *Optics* Pearson (2001).

[4] E. Hecht and A. Zajac *Optics*Addison-Wesley pub. Co. (1974).

[5] T. Scharf, *Polarized Light in Liquid Crystals*John Wiley and sons (2000).

[6] S. Chandrasekhar, *Liquid Crystals*, Cambridge University Press (1977).

[7] I Musevic and Th. Rasing, *Surfaces and interfaced of Liquid Crystals*, Springer (2004)

[8] G. Maret, A. Blumstein, Molecular crystals andliquid crystals, 88, 1-4, Taylor and Francis (1982).

[9] I. Dierking, *Textures of liquid crystals*, Wiley (2003).

[10] R. A. L. Jones, *Soft Condensed Matter*, OUP Oxford (2002).

Chapter 4

Magnetic manipulation of 8CB at the I-N phase transition

4.1 Abstract

We present an investigation of the phase dynamics of the liquid crystal 8CB around the isotropic-nematic (I-N) transition in static magnetic field. Using polarization microscopy we image the nucleation-growth of nematic domains within the isotropic background and the subsequent development of the full nematic phase. We find that nucleation is suppressed by the magnetic field and that in a field a deeper undercooling is required before the I-N transition occurs. After nucleation the phase transition is found to proceed faster in a magnetic field, which is attributed to the fact that it is easier for individual domains to merge when all of them are aligned in the same direction by the magnetic field. Finally, no effect of the magnetic field is observed on the growth of individual domains. The radius R of a growing domain always scales with time as $R(t) \sim t^{1/2}$, in agreement with a volume diffusion growth process.

4.2 Introduction

Nucleation phenomena occur in a variety of materials in many different circumstances, but always under non-equilibrium conditions. It is thus in this region that an external force can produce considerable effects. Homogeneous nucleation takes place in the coexistence region of two species when concentration and temperature conditions allow the formation of one phase within the other [1], [2], [3]. For liquid crystals in the isotropic phase (I) the nematic phase (N) begins with the coupling of a few molecules to form a cluster. The I-N transition in 8CB is known to be a weak first-order transition, as it can be deduced by its small associated latent heat of 612 ± 5 J/mol [4]. Therefore the nucleation theory, as it has been introduced in Sec. 2.6 for the liquid crystalline case, can be applied. The major complication in the study of the phase transition, both from the theoretical and the experimental point of view, is the small latent heat. Theoretical models [5], [6] describe often the case of a second order transition and although they are adjusted to be used with the I-N transition [7], there are aspects still far from being understood.

From the experimental point of view the coexistence region makes that phase transitions occur not just at a single temperature but in a wider temperature range, where the two phases coexist. The kinetics of the transition, and therefore the evolution in temperature of one phase into the other, is dependent on the experimental conditions [8], [10]. This triggered new experiments, which combined calorimetry investigation with in-situ optical studies [9], [11]. However in all the previous studies the effect of a static magnetic field has not been considered. The goal of our study is to show with experimental data whether and how the I-N phase transition is affected by the magnetic field. The

contact free magnetic force is the ideal tool to act on the liquid crystal system without interfering with its molecular structure. Moreover magnetic field effects can be discovered by in situ microscopy during a thermal cycle.

The global dynamics of the I-N transition in three dimensions is studied here by monitoring the percentage of nematic phase converted from the isotropic phase. We also consider individual nematic clusters, their number and their size, and study a sample area large enough to allow statistically relevant conclusions. We follow the nematic clusters from their early stage, through their growth and the merging phase, up to the full nematic conversion (see the overview in figure 4.1). By those two approaches, global dynamics and single cluster evolution, we obtain complementary information on the phase transformation: the number of clusters is a measure of the effect of a field on the nucleation and merging dynamics, while the global conversion rate is connected to the speed of the phase transition. The results are presented for each aspect of the phase transition. The experimental details are presented in section 4.2. The number of nematic clusters during time and the total nematic coverage are studied in section 4.3. In section 4.4 we consider the individual growth rate of a nematic cluster and the effect of the magnetic field on its dynamics. Finally all the results are discussed in section 4.5 and linked to theoretical expectations to provide a deep understanding of all observed phenomena.

4.3 Experimental details

Thermal quenches are applied in order to bring the system from the Isotropic phase into the I-N metastable region where we can observe growing nematic domains at constant temperature. A quench is realized by a sudden temperature reduction below T_c with a step δT between 0.1 and $0.45\ ^\circ C$, depending on the cell thickness.

After a quench δT, or more quenches of total depth ΔT the system rapidly passes from the homogeneous high temperature phase into a non equilibrium state below the critical temperature T_c, where an isothermal condition is established at $T = T_c - \Delta T$, with ΔT the quench depth. Now the low-temperature phase is thermodynamically favored, but after a successful quench the system is still in its mother (isotropic) phase. In a metastable state nucleation is likely to happen, but does not always begin immediately after a quench. Often a waiting time of minutes is recorded before the first event is observed. Once the system is quenched below T_c, thermal fluctuations induce the nucleation of the low temperature (nematic) phase, giving rise to the formation of nematic clusters, which grow spontaneously once a critical size is exceeded. Impurities in the system can also act as nucleation centers. Here we briefly summarize the entire experimental procedure: the liquid crystal 8CB is confined in an optical cell with a thickness of 0.1 mm in order to observe volume phenomena and to minimize surface effects. A cell thickness of 1 mm is used to reproduce and verify the results obtained in the 0.1 mm thick cell. In all cases we observe volume phenomena and we study the isothermal growth. Thermal quenches bring the system into the I-N metastable region. For 8CB we find the I-N coexistence region in the temperature range I-40.5°C-37.5°C- N. Here nucleation takes place and growing nematic domains are observed at constant temperature. We define the time t=0 indicated as t_0, as the time at which the successful temperature quench is concluded and the temperature is constant. We denote as $t^* = 0$ the time at which the first nematic domain is observed, so t^* measures the time from the appearance of the first domain.

The experimental conditions and definitions are summarized in figure 4.1. The growth dynamics of individual nematic droplets after a quench from the Isotropic phase into the I-N coexistence region is studied by video imaging, as described in section 4.5. After nucleation has occurred we observe isolated nematic domains, i.e. clusters for which the distance to other droplets is larger than their own diameter. About 100 isolated spherical domains are considered in different cells and experimental conditions. Making suitable temperature quenches to observe cluster growth at constant temperature

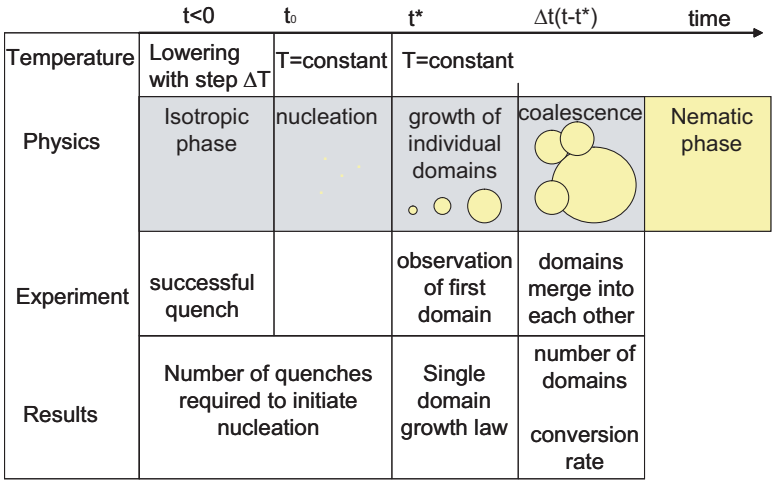

Figure 4.1: In this table the experimental conditions and definitions are summarized and compared to the physics of the isotropic-nematic transition.

requires an accurate control of the system temperature. Our oven allows controlled temperature steps ΔT as small as 0.02°C, while the maximal depth of a quench depends on the possibility to observe clusters at constant temperature after the quench. Under the experimental conditions we are using it is not possible to vary the temperature faster than $1°C/min$. Therefore, by imposing a large ΔT, the nucleation may occur while the temperature is still varying, altering the results for its dynamics. On the other hand a very small ΔT creates the risk of not observing any nucleation for a long time after the quench, since the system can remain stable in its mother phase. This restricts our experiment to temperature steps between 0.05°C and 0.45°C, depending on the cell thickness, which determines the thermal gradient and therefore the importance of local temperature fluctuations on the isothermal growth. Given this, we could not study the effect of the quench depth on the dynamics in three dimensions as extensively as reported in two dimensional experiments [10]. In a 1 mm thick optical cell temperature fluctuations are more important, therefore the quench amplitude is reduced to guarantee the realization of experiments at thermal equilibrium. In a successful quench growing domains can be observed after the conclusion of the quench [12]. When the domain growth starts before the temperature becomes constant the experiment is considered invalid. It also happens that no nematic cluster can be observed after a quench [13]. In this case, after $400s$, a second quench is applied. Again, if no growing domain is observed the temperature is lowered by another, identical step until a successful quench is found.

4.4 Experimental results

Figure 4.2 shows the global evolution of the transition from the isotropic (black region) to the nematic (light colored) phase, as observed through birefringence microscopy. These images are captured after a thermal quench of Δ T= 0.15 °C in 0 T at intervals of 20 s. Without magnetic field nematic domains appear as colored spherical objects, showing different optical patterns, due to their different director's orientation. Upon growing and merging, a variety of birefringence textures is observed. Clusters exhibit a quite different behavior when a magnetic field is applied (see figure 4.3). In $B \neq 0$

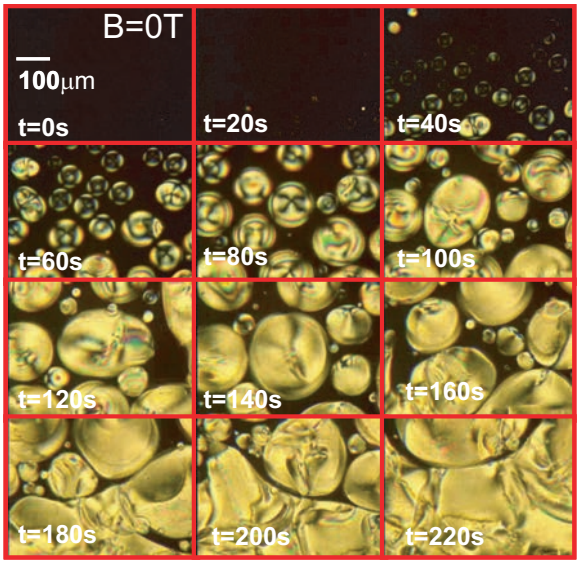

Figure 4.2: The global evolution of the transition from the isotropic (black region) to the nematic (colored regions) phase observed through birefringence microscopy without the presence of a magnetic field. Note the variety in the internal patterns for the nematic clusters, corresponding to a random orientation of their director.

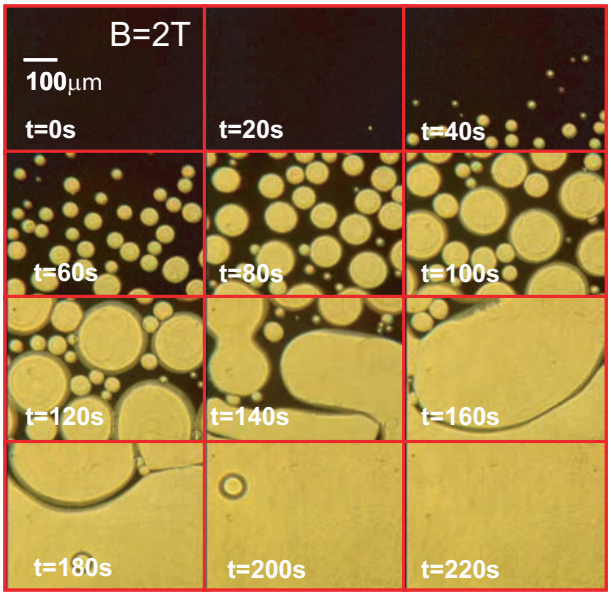

Figure 4.3: Nematic clusters observed by birefringent microscopy after a thermal quench in 2 Tesla. In magnetic field the nematic domains show high and regular brightness and no internal pattern.

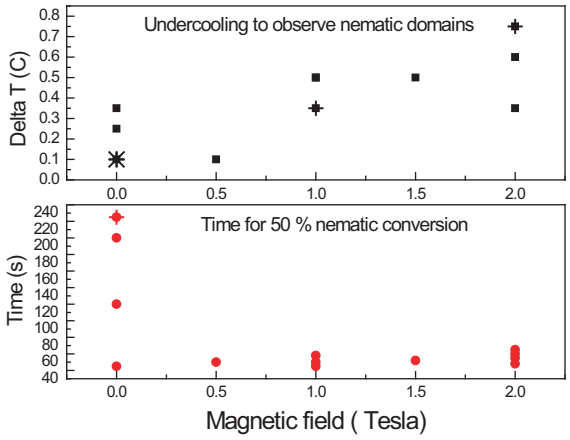

Figure 4.4: Top: the size of the under-cooling (ΔT) that is required to induce nucleation as a function of magnetic field. ΔT is given by the total temperature difference after one of more thermal quenches δT. Bottom: Time in seconds to reach 50% of nematic conversion during the I-N phase transition at thermal equilibrium after one or more thermal quenches. In both graphs each point corresponds to one experimental result (full symbol) or two (cross and full symbol) or three (double cross and full symbol) identical values.

the nematic clusters do not show any internal pattern but a constant and intense birefringence signal, because they are aligned by the magnetic field. These images are captured after a successful thermal quench in 2 T at intervals of 20 s, as for the series of images described above. At the end of the phase transition a uniform nematic monodomain is present. In the following we will describe the consecutive regimes.

4.4.1 Nucleation

Figure 4.4 summarizes our results on the total depth of the under-cooling to initiate nucleation as a function of the applied magnetic field (top part) in a 0.1mm thick cell. The under-cooling ΔT is given by the total number of temperature steps δT needed in order to observe nematic domains. The bottom part of the figure represents the time to reach 50% of nematic conversion. Each point corresponds to one experimental result (full symbol) or two (cross and full symbol) or three (double cross and full symbol) identical values.

When no magnetic field is applied, the minimal thermal quench depth is ΔT=0.1°C. Such a small undercooling is often enough to nucleate nematic, although in same cases larger quenches were required. At 1 T the same ΔT does not produce any growing cluster and the liquid crystal still appears completely isotropic. Therefore more quenches are applied, until growing nematic domains are observed. In general with increasing fields a larger number of quenches is needed before the first nematic droplet can be detected, increasing up to 4 to 7 quenches at 2 T and a δT as large as 0.75°C. In the bottom part of figure 4.4 the conversion rate is measured by the time to reach 50 percent of nematic conversion. The observed phenomenon of faster conversion rate of the nematic phase in magnetic field is reproduced at different quench depths, implying that the total undercooling in a magnetic field is usually larger than ΔT=0.25°C. When no magnetic field is applied a δT=0.1°C

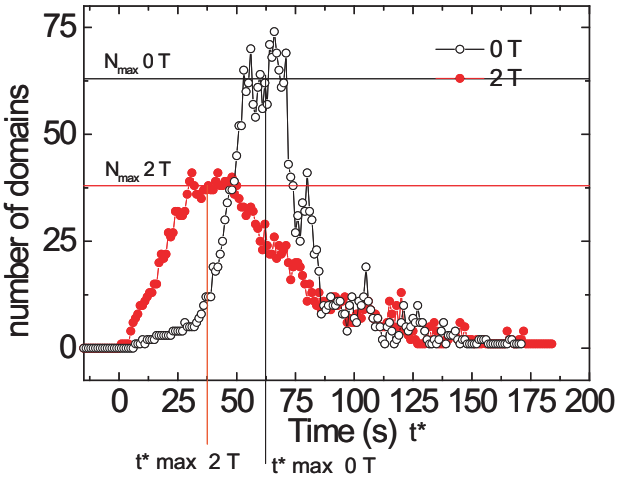

Figure 4.5: The number of nematic domains observed in the isotropic background after a successful quench at B=0T and B=2T, as a function of the time t^* after the observation of the first nematic domain. In both situation the number of observed clusters first increases and then decreases, due to merging of domains. Note the effect of magnetic field: it reduces the maximum number of domains N_{max} and it decreases the corresponding time t^*_{max} to detect the maximum number of clusters. In 2 T N_{max} is lower with respect to the zero field case, while t^*_{max} is shorter.

is sufficient to observe growing nematic clusters. We thus find that the application of a magnetic field reduces the nucleation of nematic domains.

4.4.2 Number of nematic domains

Next we consider the number of nematic clusters observed during the phase transition. Figure 4.5 shows the result of a representative experiment. Similar trends have been observed multiple times in separate experiment runs. The number of nematic clusters is plotted as a function of time t^* after the appearance of the first domain. Without magnetic field (open symbols) the number of nematic clusters rises up to a maximum of about 63 and then decreases again, until at the end a single domain remains. Indeed when the number of nematic domains is high, they also get closer and start to merge into each other. We observe the coarsening regime until the number of domains reaches the limit value 1, corresponding to the end of the I-N coexistence and the formation a homogeneous nematic phase. In a magnetic field of 2 T (solid symbols) we find a more rapid increase of the number of domains, while the maximum number clusters is reduced to 38. Note that the number of domains does not give any information on their size, since the phase transition proceeds by growing and merging domains.

From all these results we can determine two magnetic effects on N_{max} and t^*_{max}. The maximum number of nematic clusters N_{max} is reduced, while the time to reach the maximum t^*_{max} is shorter. In fact,in finite fields the maximum number of clusters is lower and reached at earlier times with respect to the zero field case (figure4.6). Interestingly, the behaviour of the number of domains at later times (after 100 s in figure 4.5) seems not to be affected by the field strength, which implies that the time to reach complete (100$\%$) nematic conversion does not depend on field (see also discussion of figure 4.7).

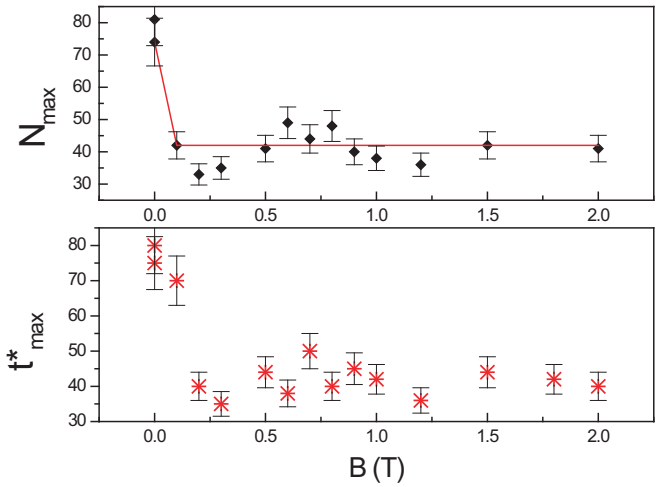

Figure 4.6: The maximum number of nematic domains N_{max} and the corresponding time t^*_{max} as a function of magnetic field B. This summarizes the two observed magnetic effects: t^*_{max} is shortened by B (bottom) and N_{max} is lowered by B (top).

4.4.3 Nematic coverage

The dynamics of the I-N transition can also be considered in terms of nematic coverage, by looking at the percentage of nematic regions with respect to the whole sample region probed by our microscopy tool. In our experiments the nematic coverage during the phase transition is detected as the area occupied by nematic clusters.

Comparing our experiments with and without magnetic field we find that upon increasing the field strength the observed I-N phase transition speeds up considerably, as evident by comparing figure 4.2 to figure 4.3.

The field effect is quantified by calculating the nematic coverage. In figure 4.7 we compare the conversion rate during the whole transition. This represents a typical experimental situation: the nematic coverage as a function of time t^* is plotted with and without magnetic field. The faster dynamics in magnetic field is associated with an enhanced merging regime between aligned nematic clusters.

4.5 Growth rate of individual nematic domains

In figure 4.8 the radius R of a spherical nematic domain growing at B=0 (triangles) and B=2 T (squares) is plotted as a function of time t^* for a single experiment. The observation is performed in a cell of 1 mm thickness after a temperature quench $\Delta T = 0.05\ ^\circ C$. Both sets of data are fitted with the function $R(t^*) = (t^*)^\alpha$, where α is a fit parameter plotted in figure 4.9 as a function of B. The fit results are rather scattered, since each individual domain may experience different local fluctuations. Thus the growth rate is fitted after taking the average of at least 3 data points for each magnetic field intensity. As shown in figure 4.9 the constant linear fit gives the experimental value $\alpha = 0.45 \pm 0.10$. Therefore the growth rate of isolated nematic clusters does not appear to be affected by the magnetic field and the it is governed by a diffusion law $R(t^*) \sim t^{*1/2}$ as expected from the model presented in

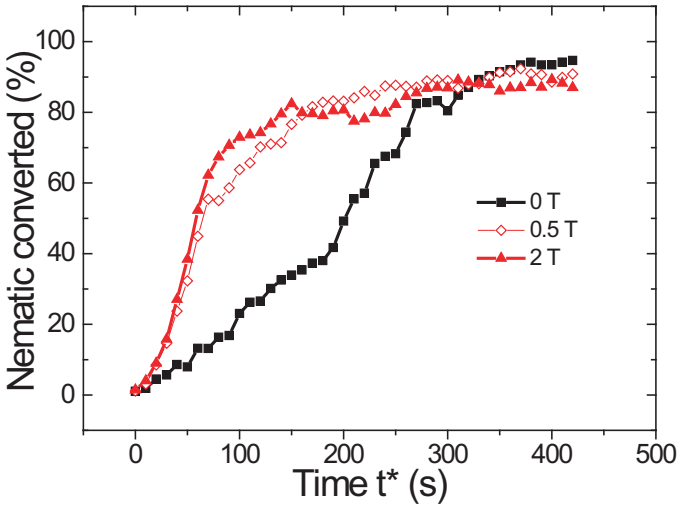

Figure 4.7: The effect of an applied magnetic field on the conversion rate during the I-N phase transition. Note the initial faster conversion in a magnetic field.

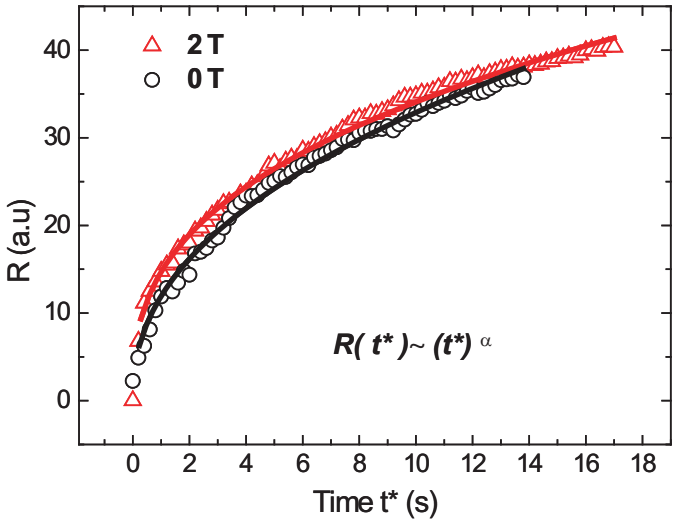

Figure 4.8: The radius R of an isolated, spherical, nematic domain growing in zero field (triangles) and in B=2 T (circles) after a temperature quench of ΔT=0.05°C, as a function of time t^*. The data are fitted with the general power-law $R(t^*) \sim t^{*\alpha}$ in order to extract the growth exponent α.

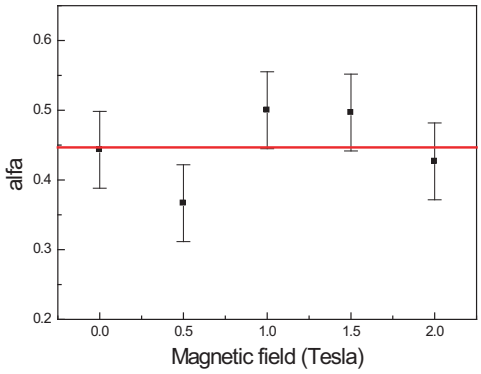

Figure 4.9: The growth rate exponent α of growing single domains for several magnetic field strengths. Within the experimental error α shows no field dependence: $\alpha = 0.45 \pm 0.10$.

section 2.6.

4.6 Discussion

A schematic overview of our results on the 3D nucleation of nematic clusters, individual cluster growth and phase conversion rate is depicted in figure 4.10.

Growing nematic clusters are observed by quenching the system below its critical temperature. They appear as spherical and their growth rate follows the power law $R(t) \sim t^{1/2}$. Successively the clusters begin to interact with each other and merge into large domains. Here the domain density is too high and single domain growth is no longer studied. In this coalescence regime the total number of domains starts to diminishes until the whole space is filled by a single nematic phase, i.e. 100% nematic conversion.

In the presence of a constant magnetic field the phase dynamics described above is reproduced, but with some important differences. The schematic pictures in figure 4.11 explain our experimental results by showing the magnetic effects on the LC molecules and can be understood as follows.

1. The nematic clusters appear uniformly because of the fixed orientation of their director along the field induced direction, leading to a homogeneous high birefringence.

2. In magnetic field often nematic domains could not be observed after a single quench. The system appears to be trapped in its mother phase. A series of thermal quenches is thus applied in order to observe the phase transition and nucleation of nematic clusters is found to be inhibited by the magnetic field. We can explain this by taking into account the orientation of the LC molecules within a nematic cluster (see also paragraph 3.8 and figure 3.9, 4.2 and 4.3). At zero field the droplets exhibit a complex birefringence pattern due to competition between the nematic alignment of the molecule in the core of the droplet and the preferential radial alignment of the molecule at the surface. With increasing field this radial surface alignment is increasingly unfavourable, which possibly explains why nucleation is found to be inhibited. When nucleation finally occurs the nuclei grow into fully aligned droplets without internal texture visible by our experiments (figure 4.3).

3. The growth of individual nematic domains is unaffected by the magnetic field. Their growth is regulated by volume diffusion. The range in which this individual growth can be observed is small compared to the time scale of the whole isotropic-nematic phase transition. After about 20 s from the

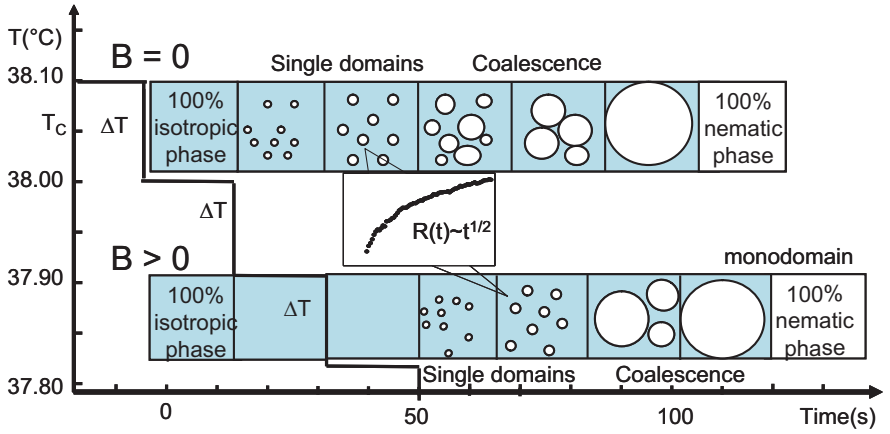

Figure 4.10: Schematics of the Isotropic-Nematic transition as observed in our experiments. Without magnetic field (top panel) nematic clusters grow after a thermal quench until the coalescence regime starts, having domains merging into each other to obtain full nematic coverage. In magnetic field a single quench of ΔT is often not sufficient to observe the phase transition. Growing nematic domains are only observed after several quenches. They rapidly start merging into each other, so that the total number of observed domains is lower than in zero field. The full nematic coverage is reached after a shorter time. In all cases the growth fits with a diffusive power law.

first appearance of the clusters, their density is too high to consider them as isolated.

4. When the distance of two consecutive domains becomes of the same order as their size, the growth dynamics is strongly influenced by the neighboring conditions. Only by considering the whole probed space we are able to study the development of the late I-N phase transition and find relevant magnetic effects.

5. Once the I-N transition has started the phase conversion evolves much faster toward the nematic phase in an applied magnetic field, as compared to the zero field case. This is observed in two ways: the nematic coverage rate as well as the number of nematic clusters evolve faster by increasing the field and the maximum number of nematic domains is lower, since bigger clusters are observed. These findings evidence an easier merging between aligned domains, which share the same field-induced orientation. Considering the global evolution of the phase transition we find a shorter time to observe single cluster growing without being affected by neighboring domains. The time to reach full nematic conversion is not affected by the magnetic field. Upon increasing the magnetic field intensity, we find a longer isotropic regime and a faster initial advancing of the transition, reducing the total time of the Isotropic-Nematic coexistence. The contribution of each single cluster to the nematic conversion is important. The orienting effect of an applied magnetic field on each nematic cluster influences the merging properties. In fact nematic clusters growing in magnetic field align their director in the field-induced direction. Therefore, in an external field, nematic domains are all oriented in the same way. Consistently, we find that the initial dynamics is not further enhanced at field strengths above 0.7 T, when the domains are already perfectly oriented. As a consequence of the easier merging of nematic clusters, the maximum number of domains detected in time is lower in magnetic field. We can explain the observed initial faster advancing of nematic conversion in terms of difference in Gibbs free energy of the liquid crystal molecules between Isotropic and Nematic phase.

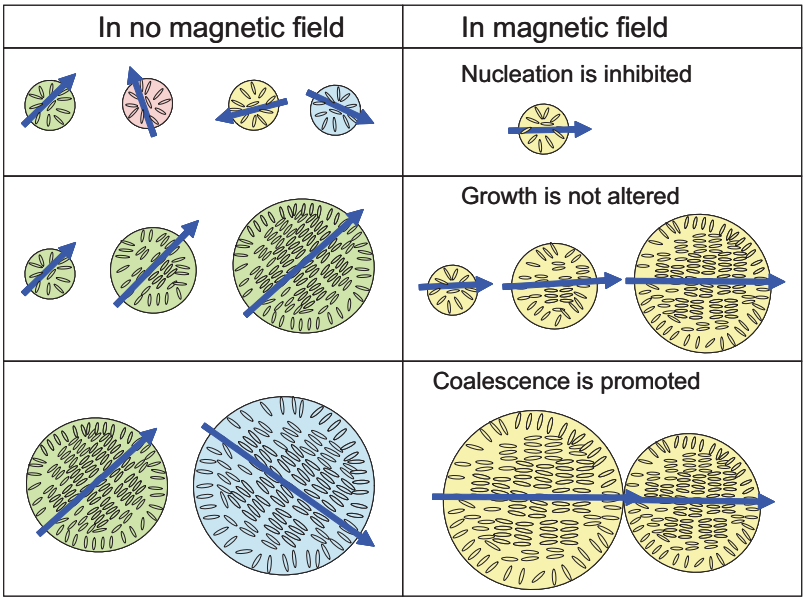

Figure 4.11: Without magnetic field nematic cluster show different nematic director orientation. In a magnetic field nematic clusters have their director oriented along the same field induced direction. In this case clusters nucleation is hindered, since the magnetic force compete with the cluster surface tension, but clusters merging is promoted, resulting in a faster conversion rate of the isotropic into the nematic phase.

4.7 Conclusion

Multiple effects of magnetic field are observed during the Isotropic Nematic phase transition. The nematic clusters in a field appear uniform because of their identical directors orientation, along the field induced direction. In a magnetic field the system appears to be trapped in the isotropic phase and the formation of nematic clusters is hindered. No magnetic effect is found for isolated growing clusters finding that the cluster's radius *R* scales in time as $R(t) \sim t^{1/2}$, as predicted when the growth is dominated by volume diffusion [14]. Fluctuations due to the presence of neighboring domains make the growth exponent difficult to measure with accuracy. Once the transition has started it proceeds faster in magnetic field. We observed the number of domains raising faster, while the maximum number of domains is lower with respect to the zero field case. In the later stage of the isotropic to nematic phase transition, the coarsening regime is found to be promoted in high fields on the cost of the isolated growth regime, which becomes shorter, as the magnetic field induces the same director orientation in all the nematic clusters and facilitates their merging. Finally in magnetic field the whole phase transition, even if more difficult to observe, proceeds faster, through the formation of oriented clusters which grow and merge to form a fully aligned nematic phase. Indeed the applied field reduces the total time of the Isotropic-Nematic coexistence, while the time to reach 100 percent conversion is not altered.

References

[1] R. A. L. Jones, *Soft Condensed Matter*, OUP Oxford (2002).

[2] I Musevic and Th. Rasing, *Surfaces and interfaced of Liquid Crystals*, Springer (2004)

[3] A. Rastegar , M. Skarabot, Blij B. and Th. Rasing J. Appl. Phys. 89 (2001)

[4] J. Thoen, H. Marynissen and W. Van Dael, Phys. Rev. A 26, 2886 (1982).

[5] P. G. de Gennes and J. Prost, *The Physics of Liquid Crystals*, Clarendon Press, Oxford (1993).

[6] G. Vertogen, W. H. de Jeu, *Thermotropic liquid crystals, Fundamentals*, Springer-Verlag (1988).

[7] P. K. Mukherjee, J. Phys.: Condensed Matter 10, 9191 (1988).

[8] S. Auer and D. Frenkel, Nature 409, 1020 (2001).

[9] F. Mercuri, R. Pizzoferrato, U. Zammit and M. Marinelli, Applied Physics letters 81, 4148 (2002)

[10] S. Bronnikov and I. Dierking, Phys. Chem. Chem. Phys. 6, 1745 (2004).

[11] I. Dierking, J. Phys. Chem. B 104, 10642 (2000).

[12] I. Dierking, Appl. Phys. A 72, 307 (2001).

[13] H. K. Chan and I. Dierking, Phys Rev. E 70, 021703 (2004).

[14] B. A. H. Huisman and A. Fasolino, Phys Rev. E 76, 021706 (2007).

Chapter 5

Realignment of the smectic-A phase in high magnetic fields

5.1 Abstract

The reorientation dynamics of a smectic-A (SmA) phase within 8CB is studied by time-resolved birefringence microscopy. The reorientation occurs when a magnetically aligned SmA monodomain is suddenly rotated over an angle. These experiments were performed within a constant magnetic field (up to 20 T), for several temperatures below the Nematic Smectic-A phase transition temperature (T_{N-A}) and for several rotation angles. We observe that the reorientation starts after an induction time, during which the SmA phase remains fixed in its initial orientation. This induction time increases with lowering the temperature further below T_{N-A}. After this induction time the system relaxes back to the new equilibrium state. It is found to reorient via complex, transient local structures, forming elongated patterns that are oriented perpendicularly to the smectic layers, propagating through the system. Overall, we find that the equilibrium state is achieved faster with increasing rotation angles and increasing magnetic field strengths. From these observations we conclude that the SmA phase does not reorient as a simple monodomain.

5.2 Introduction

In this chapter we investigate the reorientation dynamics of a Smectic-A liquid crystal. Reorientation phenomena found great application in modern display technology, which makes use of the fast switching of LC molecules under the effect of an external field. Most displays employ nematic LCs, which show a fast orientational dynamics. Currently also smectic phases are considered to improve the orientation performances. Tilted chiral smectic phases have a rapid electro-optical response resulting from the reorientation of molecules within an existing layered structure, rather than the reorientation of the layers [1]. More recently the use of encapsulated smectic-A liquid crystals has opened the way to flexible flat displays [2],[3].

In all cases an external field, either magnetic B or electric E, is used to manipulate the optical properties of LCs. Investigation of the effect of an external field, acting on the molecules, allows to gain insight into the internal molecular structure and on the inter molecular interactions. For instance in LC displays a weak electric field is applied to a thin film of liquid crystal contained between transparent electrodes. Magnetic fields however are an important alternative for the study of the optical properties of many materials, since they allow to probe the dynamics in different geometries and over larger thicknesses compared to E. Furthermore the contact-free, non destructive magnetic force leads to highly oriented bulk samples as well as thin films applying B-fields of a few Tesla.

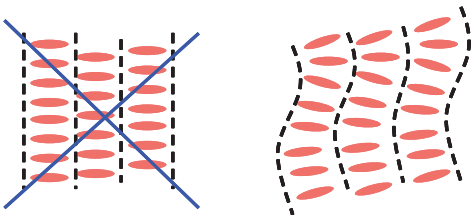

Figure 5.1: The smectic A phase consists of molecules oriented along a director and organized in layers. This structure cannot be thought as rigid, since the intermolecular order is just of short range. This makes the layered structure very flexible and the system able to flow like a liquid.

The understanding of the alignment dynamics of LCs in different smectic phases is less advanced than for nematics. Smectic systems show a higher complexity in their structure, leading to an entirely different behaviour whose understanding is of fundamental and technological relevance.

We consider here the Smectic-A phase consisting of LC molecules oriented along a director and organized in layers. The centers of mass of the molecules show a short range correlation and the layered structure is very flexible, so that layers are able to slip over each other, see figure 5.1. Only the inter-layer distance stays constant, while the molecules may diffuse within and among the layers, as already stated by De Gennes [4]. It is thus the presence of this extra degree of order brought by the layers that makes the re-orientational behavior of the smectic phase entirely different from the case of the nematic phase.

The investigation of the alignment dynamics is generally performed by reorientation experiments. An oriented sample is prepared in an external field, after which a perturbation is applied in order to be able to observe the way in which the equilibrium is re-established. In our experiments a LC system is cooled in an external magnetic field from the isotropic phase, resulting in a perfectly oriented (mono-domain) smectic-A structure. What happens if we suddenly change the direction of the magnetic field? Naturally the smectic-A structure, subject to an abrupt change of the forces determining its energetic equilibrium, will tend to recover its equilibrium to decrease its total energy. Here we investigate how this really happens. Figure 5.2 shows six out of many different scenario's. In the first one the system rotates as a whole rigid structure to the equilibrium position (1). Another possibility is the breaking of the structure in smaller smectic domains, each of them rotating as islands to the equilibrium (2). Alternatively the smectic structure could change phase, becoming smectic-C (3), nematic (4), or even isotropic (5), as an intermediate step to reach a new ordered smectic-A state. Finally the smectic structure could be so flexible to allow great distortions (6), which would correspond to the rotation and diffusion at the molecular scale. Note that only in the first and last cases we can formally describe the reorientation process by a rotation of the LC director along the field induced direction.

This chapter is organized as follows: in the following section the results from previous experiments by different techniques are presented and the reasons for our in-situ birefringence microscopy investigation are explained. The experimental details are discussed in section 5.4, while in the subsequent sections our results are presented as a function of the rotation angle (5.5), the temperature (5.6) and the applied magnetic field (5.7). The role of the fluctuations in the layered structure is presented in section 5.8 and a general discussion follows in section 5.9.

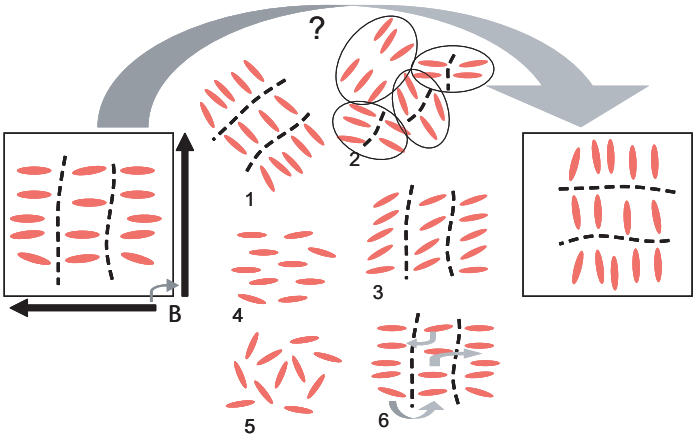

Figure 5.2: Illustration of some possible results of a reorientation experiment. A smectic structure, previously aligned in an external magnetic field, is suddenly rotated, in this example over 90°. The system will try to recover its equilibrium position, i.e. to minimize its internal energy by orienting itself according to the new field direction. This can actually take place via different transient structures. 1) Rotation of a rigid structure. 2) Breaking of the monodomain structure in smaller smectic domains . 3) Phase change to smectic-C, although energetically unfavoured. 4) Phase change to nematic. 5) Phase change to isotropic. 6) Distortions of the smectic structure, with molecular rotation and interlayer diffusion.

5.3 Smectic reorientation: state of the art

The reorientation of smectic A layers in a field depends on the cell thickness, thus on the amplitude of the interaction between the LC layers and the surface. Two different reorientation mechanisms are known: in thin samples reorientation is achieved through complete disordering and reordering of the smectic layers, while in thick samples the layers can also appear to rotate continuously as a monodomain [6]. We focus on the intermediate situation where both bulk and surface influence the properties of smectic liquid crystals. The reorientation dynamics in nematic and smectic liquid crystals has been extensively studied by time-resolved nuclear magnetic resonance (NMR) spectroscopy [7], [8]. In those experiments the sample is aligned in a magnetic field and then exposed to an extra torque produced by a rapid spinning. When a macroscopically ordered liquid crystal is subjected to a new torque of sufficient magnitude, the direction of the macroscopic order changes in response to the new torque. Therefore the LC director aligns along the spinning axis. By suddenly stopping to spin the sample the LC molecules reorient along the magnetic field direction. With this technique the spontaneous system reorientation can be observed at the molecular level, providing that no extra flow is produced by stopping the spin.

These experiments have revealed that the dynamics of the smectic reorientation is qualitatively different from the nematic case. Unfortunately NMR spectroscopy does not provide any information on the motion of the smectic layers during the reorientation and also it provides average results on the whole sample, while as we will see, local structures are very important. Only by using synchrotron radiation in time-resolved X-ray diffraction experiments it has been possible to probe the behavior of the smectic layers on the liquid crystal 8CB at the DUBBLE SAXS/WAXS beamline BM26B at the ESRF in Grenoble [10][11] [6]. X-ray diffraction experiments can capture diffraction patterns on a time

scale faster than the re-alignment of the smectic layer in 7 T, opening the way to the detailed study of the smectic reorientation dynamics [12], [13], [14].

The angular dependence of the reorientation experiments by X-ray diffraction in 7 Tesla can be summarized by distinguishing two regimes. Rotations below 45° produce a smooth intensity profile, typical of a monodomain structure. The monodomain shows a smooth alignment, slower than a nematic domain, but still rather rapid realignment of smectic layers to the field-induced direction. For rotation angles above 45° the regular reorientation profile is perturbed by the appearance of smectic regions oriented at different angles and reorienting by different pathways. Those deviations from the regular monodomain reorientation can be associated to a twisting of the smectic structure or more likely to the existence of different domains. Moreover the measured intensity distributions at large rotation angles suggest that the smectic monodomain can break into domains with different reorientation processes, even though it is not possible, by X-ray diffraction, to quantify the relative amounts of sample following a specific reorientation pathway. Another puzzling result from these experiments at large rotation angles is the apparent loss of intensity during the reorientation. This suggests that the smectic layers are being strongly deformed or even that parts of the sample are changing phase.

A special case is represented by a rotation angle of $\phi = 90^\circ$. Here a longer induction period is measured. The system appears to be trapped in a metastable position because it can rotate either clockwise or anticlockwise. Director fluctuations, producing a small torque are required to break the symmetry before the reorientation starts. After this longer induction period the system finds itself in a highly unfavorable energetic configuration and therefore shows the fastest reorientation of the smectic layer normals to the magnetic field-induced direction.

The high complexity of the process, and in particular the finding that dramatic fluctuations occur during the reorientation by increasing the rotation angle above 45°, makes the dynamics of the process difficult to be understood only by a time resolved investigation. Moreover the intense collimated X-ray beam can alter the liquid crystalline sample, making such experiments sensitive to the duration of the experiments because of possible damage to the sample. The need for spatial resolution in a large probed area (larger than 300x300 μm probed by X-rays) and at the same time using a non-destructive probe stimulated our birefringence microscopy experiments in magnetic fields. These experiments do not have the previously mentioned disadvantages and provide extra spatially resolved information leading to a better understanding of the reorientation dynamics.

5.4 Experimental details

Birefringence microscopy is a complementary technique to the X-ray diffraction allowing to extend the probed area, while assuring not to modify or destroy the samples. Even though no direct information on the layers is obtained, the combination of time- and space-resolution offers an extra insight in the study of the molecular directors distribution during the reorientation.

In figure 5.3 a schematic representation of the experimental set-up is depicted. White light from a halogen lamp (continuum spectrum in the visible range) passes through a linear polarizer so that polarized light reaches the sample. The transmitted intensity is guided through an analyzer, which is oriented at 90° with respect to the polarizer, in order to exclude all light that does not pass through birefringent areas of the sample. The birefringent signal is detected by a CCD camera with a standard acquisition rate of 25 frames per second. The optical system allows a time resolution of 0.04 s and a spatial resolution of 1.8 μm in a field of view of 0.7 x 0.65 mm^2.

The sample cell is sketched in the top left part of the figure. The liquid crystal 8CB is injected in its isotropic phase into a round cell, 1.6 mm thick and 4.5 mm diameter, with glass windows. The cell is filled completely, carefully excluding the presence of air, and then placed into a rotation device positioned in a Bitter magnet with maximum field strength of 20 T. The rotation device is connected to a stepper motor Phytron IXE, which allows to rotate the cell within 20 ms per step, within an accuracy

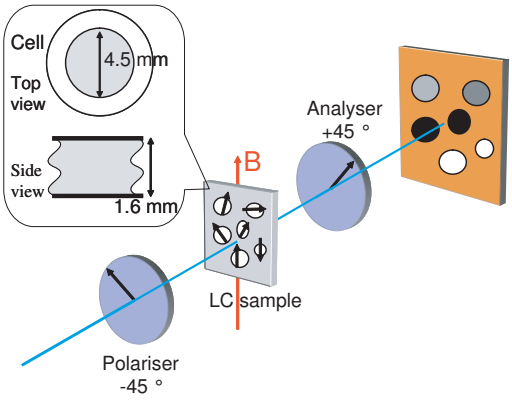

Figure 5.3: Schematic overview of the experimental set-up for birefringence microscopy in high magnetic field. See figure 3.5 for the complete set-up. The optical system consists of two polarizing filters, one before and one after the sample, oriented at 90° to each other. It allows to detect only the birefringent light signal from the liquid crystalline sample, which is contained in a round glass cell 1.6 mm thick with teflon walls positioned in a 20 T magnet. A CCD camera records the signal with a time resolution of 0.04 s and a spatial resolution of 1.8 μm in a field of view of 0.7 by 0.65 mm^2.

of $\delta\phi = 3°$. A smectic monodomain structure is prepared by cooling from the isotropic through the nematic, down to the smectic phase in a constant background field. Then the system is brought out of its equilibrium by an abrupt rotation of the whole sample about an angle ϕ with respect to the magnetic field direction, while the magnetic field orientation is kept fixed. This is conceptually identical to keeping the sample fixed and changing the magnetic field direction, but much easier to do. The reorientation process is filmed in-situ. The magnetic field is applied parallel to the cell windows. Nominally the orientation of the polarizer is $\pm$ 45° relative to the field direction. Then the transmitted light is maximal (bright image) when the bulk of the sample is aligned along the field. The transmitted light is minimal (dark image) when the sample is in the isotropic phase, or when it is aligned in the viewing direction, or along one of the polarizer directions. In some cases the angle of the polarizer is changed. In chapter 2 we have described all the other optical aspects of birefringence microscopy.

The temperature of the cell is controlled within an accuracy of 0.1°C and the birefringent response of the sample is tested *in-situ* in no external field, as shown in figure 2.8 in chapter 2. The liquid crystal 8CB is contained in a round glass cell with different surface treatments that can either induce a homeotropic or planar alignment of the LC molecules. In most cases clean untreated glass is used, whereas we also use spin-coated layers of polyvinyl alcohol (PVA) to obtain a hydrophilic substrate, which induces a planar molecular alignment. When the surface is not treated the substrate is hydrophobic and it induces a homeotropic alignment. The opposite action of homeotropic surface and magnetic field results in a striated pattern close to the surface boundaries, as discussed in the next chapter. Here we focus on bulk properties and therefore neglect what happens at the surface.

The standard protocol for all measurements was the following: the sample was heated to the isotropic phase, and after a stabilization period of at least 10 min, a constant magnetic field between 0 and 20 T was applied. Reorientation experiments are performed for different values of the rotation angle ϕ and at temperature differences ΔT=0.25-2.75 °C below T_{N-A}. Within the same experimental conditions two different cells are used, with surface inducing homeotropic or planar molecular alignment, giving two independent set of data.

5.5 Smectic reorientation as a function of the rotation angle

Having prepared the system as an oriented smectic-A structure at a chosen temperature below the N-SmA phase transition, the cell containing the sample is suddenly rotated and the re-orientation dynamics is studied. We have verified that the liquid crystal sample rotates together with the cell, at any angular velocity.

In figure 5.4 typical snapshots from reorientation experiments in a magnetic field of 7 T at the same temperature T=32 °C, i.e. ΔT_{N-A}=1.75°C, are presented for different values of the rotation angle ϕ. In each column, from left to right, representative frames illustrate the reorientation at $\phi = 33°$,$45°$, $66°$, $90°$, respectively. The sample is always rotated at a time defined as $t = 0s$. To understand the results it is important to realize that the intensity depends on the structure of the LC, but also on the direction of this LC structure with respect to the polarization of the set-up. Before any rotation a homogeneous aligned smectic structure $-$monodomain $-$ is prepared ($t = 0^{-}s$), by cooling the sample from its isotropic phase in a constant magnetic field. Note the presence of surface line patterns, which are explained in the following chapter. Immediately after the rotation the system retains its monodomain structure ($t = 0^{+}s$). In this configuration, as a result of the rotation, the molecular directors - thus the smectic layer normals- are oriented at an angle $\phi \neq 0°$ with respect to the energetically favored field-induced orientation. Before the rotation the aligned structure shows a high and uniform brightness, corresponding to a smectic monodomain having the director oriented at $45°$ with respect to the polarizing filters. The same aligned monodomain system appears less bright if the angle between its director and the polarizers is changed from its maximum of $45°$ to a lower value, and it appears totally dark when this angle is zero, i.e. when the liquid crystalline director and the polarized filters are parallel. Therefore, depending on the extent of the rotation angle, the same aligned smectic system shows different transmitted intensities. A rotation of $33°$ brings the liquid crystalline director at an angle of $12°$ with respect to the filters. This angle becomes $21°$ rotating the sample by $66°$ and it stays at $45°$ after a rotation of $90°$. A rotation of $45°$ makes the liquid crystalline director parallel to the polarized filters, resulting in no birefringence signal. Concluding, the transmitted brightness of a smectic monodomain indicates the orientation of the liquid crystalline director with respect to the polarizing filters. After the rotation the system appears to be trapped for some time in the new high energy configuration. This can last as long as one or more minutes, depending on the rotation angle. The equilibrium configuration resembles the initial monodomain structure, even though some defects are present.

In general the reorientation process is not smooth: dramatic changes are observed in the reorienting structure. Indeed, at any rotation angle, we measure a large variation in the birefringence signal from the bulk of the smectic system. This difference in birefringent intensity is associated to local fluctuations propagating through the sample. Subsequently the local variation of the intensity becomes more pronounced, especially for rotation over large angles. Only after passing through complex transient configurations the system reaches its equilibrium position at a timescale of 75-400 s, depending on the rotation angle.

Let us now consider in detail each single reorientation experiment in order to clarify the role of the rotation angle in the reorientation dynamics. For $\phi = 33°$ (first column) the reorientation proceeds rather smoothly. In the first 50 s the pre-rotational smectic configuration remains. Only after about 1 minute($t = 55$ s) the brightness gradually increases, until approximately 400 s, after which no further change in the structure in observed.

For $\phi = 45°$ (second column) the rotated monodomain structure leads to a dark image because the smectic domain is aligned along the axis of the polarizers. The image remains dark for about 50 s, after which the reorientation proceeds smoothly, as evidenced by a homogenous increasing of the intensity. The equilibrium is reached after about 350 s from the rotation, when the molecular directors are again parallel with the magnetic field.

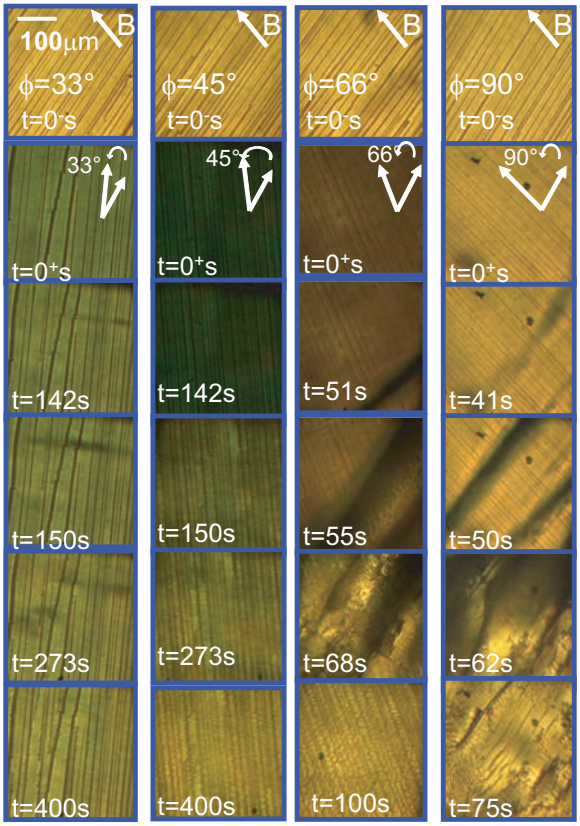

Figure 5.4: Snapshots of representative events during the reorientation of the smectic A phase in 8CB in magnetic field. In each column the image frames represent a different reorientation experiment in 7 T. All data are taken at the same temperature T=32 °C, i.e. ΔT_{N-A}=1.75°C below the N-SmA transition. The four sequences in the four columns refer to experiments in the bulk, with cell thickness of 1.6 mm, and they differ only by the rotation angles, which increases from left to right: $\phi = 33°$,$45°$, $66°$, $90°$. The arrows indicates the angle ϕ at which the sample has been rotated. Note the presence of surface line patterns, which are the object of the following chapter. Before any rotation, a homogeneous smectic structure aligned in magnetic field $-$monodomain $-$ is prepared. This corresponds to the time $t = 0^{-}s$ in our representation. Immediately after a rotation, at the time $t = 0^{+}$ s, the system is observed to retain its monodomain structure for a certain period, appearing fixed in the pre-rotational orientation. Subsequently the system reorients via a series of transient phenomena, which alter the original monodomain structure. The resulting equilibrium structure is never as perfect as the initial one.

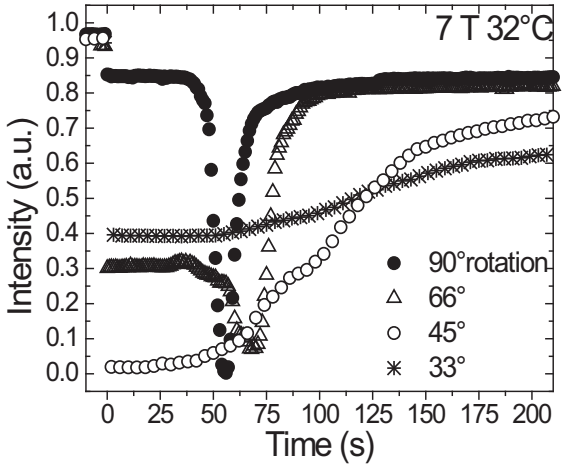

Figure 5.5: The transmitted birefringence intensity integrated over the detected area through the smectic sample during a serie of reorientation experiments. Experiments are performed at ΔT_{N-A}=1.75°C in 7 T for different rotation angles ϕ. After the rotation the system remains fixed in its initial orientation, while the measured intensity drops to a value consistent with the corresponding rotation angle. The reorientation is faster for large rotation angles. Moreover the qualitative behaviour of the curve changes for $\phi > 45°$, where a dip appears.

A less gradual reorientation is measured for rotation angle larger than $\phi = 45°$. Indeed, at $\phi = 66°$ and $\phi = 90°$, significant dark regions arise in the image, respectively after 50 s and 40 s. Elongated dark patterns rapidly grow and propagate through the sample. Moreover the orientation of these elongated patterns is not random but it is linked to the domain structure, since it coincides with the orientation of the smectic layers. This has been graphically verified in all the frames showing dark stripes. Subsequently a rather in-homogeneous structure is observed, which rapidly evolves to an equilibrium state, which is reached after 100 s for the $66°$ rotation and after 75 s for the $90°$ rotation. Thus the largest rotation angle produced the fastest reorientation dynamics!

Up to now we considered the behavior of the local brightness within the investigated sample area. The average dynamical response of the system can be studied by determining the total integrated intensity, i.e. by adding all the signals from each pixel in the probed area. In figure 5.5 the total intensity from the whole detection area is shown for reorientation experiments at ΔT_{N-A}=1.75°C in 7 T for different rotation angles ϕ. The transmitted intensity is maximal before the rotation, corresponding to a perfectly oriented smectic structure, having the smectic layer normals parallel to the magnetic field. This intensity level is normalized to value 1, which means that all intensities are between 1 and 0.

In contrast to the rather complex behavior observed analyzing the local intensity, the average intensity shows a rather smooth profile, corresponding to the overall alignment of the LC material, averaging out the stripe surface pattern and the local variations and fluctuations. All the rotations, performed at t=0 s, result in a reduction of the total birefringent signal, dependent of the rotation angle. After the rotation the system initially keeps its original alignment at a different angle respect to the polarizer axis and field-induced alignment. The reorientation profiles show a different temporal behaviour for rotation angles $\phi < 45°$ and $\phi > 45°$. The intensity immediately after the rotation roughly follows a $\cos^2 \phi$ dependency, decreasing for small ϕ, minimal at $\phi = 45°$ and then increasing

again, see calibration in chapter 3.

In all cases we measure a certain time, up to 40 s, in which the smectic structure remains fixed in its pre-rotational orientation. Subsequently a rapid reorientation begins with a duration that decreases with increasing rotation angle. Thus the reorientation at $\phi = 90^\circ$ is the fastest, showing a rapid decrease of the intensity around 40 s and a full recovery at 75 s. Only at $\phi = 90^\circ$ the equilibrium structure is fully recovered within the experimental time, since the integrated intensity approaches its final value, roughly equal to the initial value. In all other cases the intensity does not recover completely, remaining at a lower final level, which decreases with increasing rotation angle. This is a consequence of the many defect structures remaining present in the smectic structure (see figure 5.4).

5.6 Smectic reorientation experiments as a function of the temperature

Let us now consider the temperature dependence of the smectic reorientation. In figure 5.6 representative frames during reorientation experiments in 7 T for different temperatures ΔT_{N-A} below the nematic to smectic-A transition are presented. In all cases the sample is rotated by $\phi = 66^\circ$ and the reorientation towards the equilibrium position is studied. In this set of experiments the focus of the imaging system is at the bulk structure. Therefore the defect line surface pattern is not visible and only some impurities on the glass surfaces are visible.

It is clear from figure 5.6 that the qualitative behavior is similar for all temperatures, but that the whole reorientation process becomes slower as ΔT_{N-A} increases. Always, after a rotation, the system is trapped in its pre-rotational orientation for a certain time. Subsequently the smectic structure reorients under the effect of the magnetic force. Note that, at low temperatures, when the reorientation is slow, we detect dark patterns (middle panels in figure 5.6).

Figure 5.7 shows the average intensity profiles obtained by integrating the intensity values over the entire detection area, leading to smooth curves. Close to the N-SmA transition temperature, i.e. for small ΔT_{N-A} (0.25 $^\circ C$), the reorientation is concluded in about $50s$, while at $\Delta T_{N-A} = 2.75\ ^\circ C$ it takes more than 3 minutes to reach an equilibrium stage, saturating to a value that is less than 70% of the initial intensity. Figure 5.7 also shows two different curves obtained at temperature $32^\circ C$, and the same rotation angle, where the results are reproduced. The same experimental conditions result in rather different intensity profiles, since local fluctuations have a large influence on the re-orientational dynamics at large rotation angles. In one case the reorientation is monotonic (squares), while in the other there is first a local maximum and then a minimum (stars), corresponding to a dark sample. In both cases large structural fluctuations are observed in the bulk, but a substantial difference is found in the transient structure formed during the reorientation. In the first case a heterogeneous structure is observed, showing local intensity variations, but on average the reorientation profile is a smooth monotonic curve. In the other case the structural fluctuations are so pronounced that they cover the whole probed area, producing for some time a total dark state, which rapidly evolves to the field-induced equilibrium.

5.7 Smectic reorientation experiments as a function of the magnetic field strength

Up till now we have presented results in a constant magnetic field of 7 T, chosen to have a rapid and complete system reorientation, but also a sufficiently slow response, to be able to study the system during the reorientation. Furthermore, a field of 7 T has been used previously in X-ray reorientation experiments [12], which permits to compare the results obtained. Here we consider the effect of the magnetic field strength on the reorientation dynamics of the smectic-A phase.

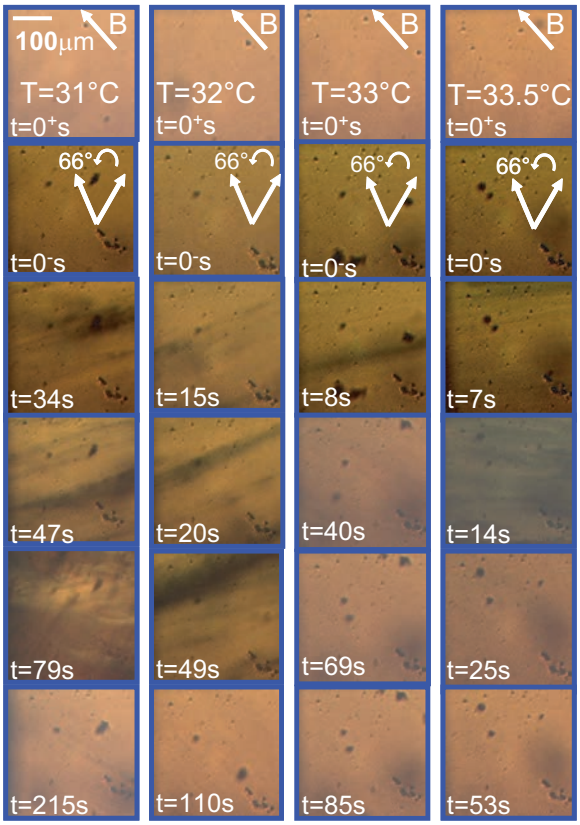

Figure 5.6: Snapshots of the reorientation dynamics of the smectic A phase in a 8CB sample. The image frames in each column represent reorientation experiments in a constant magnetic field of 7 T and for a rotation angle $\phi = 66°$ at different temperatures ΔT_{N-A} below the nematic to smectic-A transition. Note the faster recovery of the equilibrium state for temperatures closer to the SmA-N phase transition and the presence of dark elongated perturbations at intermediate times during the reorientation.

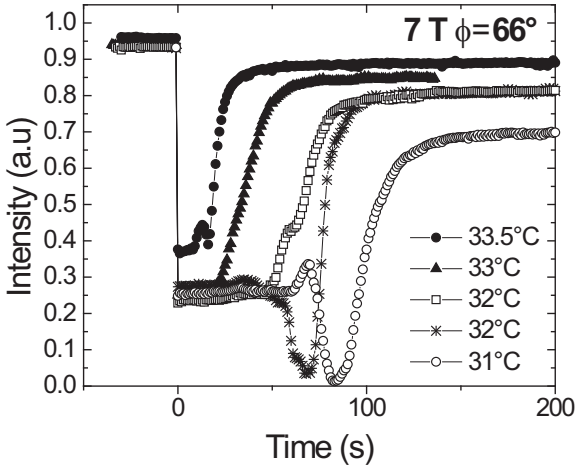

Figure 5.7: The area averaged birefringence intensity during single reorientation experiments in 7 T, rotation angle $\phi = 66°$, and for different temperatures ΔT_{N-A} below the nematic-smectic-A transition. The evolution of the total intensity towards the equilibrium is slower at larger ΔT_{N-A}. At large rotation angles, such as $\phi = 66°$, fluctuations have a great effect on the reorientation dynamics, exemplified by the two different curves obtained at T=32°C.

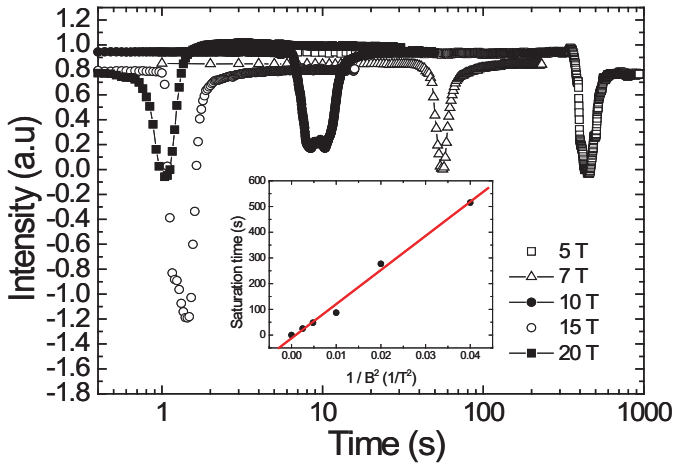

Figure 5.8: Birefringence intensity from reorientation experiments at different magnetic field strengths over time (logarithmic scale). A constant magnetic field between 5 and 20 T is applied for a rotation of $\phi = 90°$ at a constant temperature of 32°C, i.e. ΔT_{N-A}=1.75°C. By increasing the magnetic field strength the reorientation process becomes faster and the equilibrium intensity is reached in a time - the alignment time- inversely proportional to B^2, as shown in the inset.

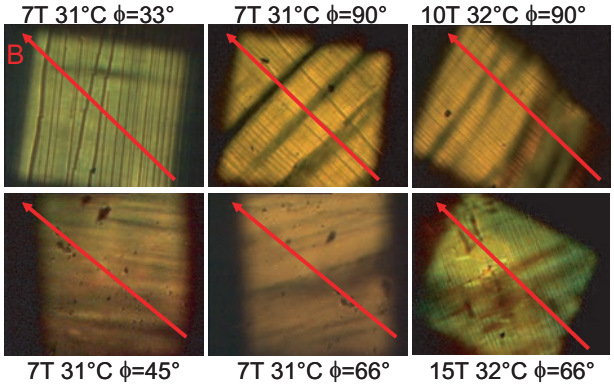

Figure 5.9: Elongated order fluctuations (dark patterns) are observed at different temperature and for rotation angles larger than $\phi = 45°$. They propagate through the sample, in a direction parallel to the smectic layers, inducing dramatic changes in the structure and a rapid recovering of the equilibrium.

As for the previous experiments the smectic structure is prepared and then abruptly rotated over an angle of $\phi = 90°$in a constant magnetic field at ΔT_{N-A}=1.75°C. The resulting total intensity is shown in figure 5.8. With increasing the field strength the re-orientation process becomes considerably faster (almost a factor 1000), though its qualitative behavior is the same. The time at which the transmitted birefringent intensity reaches the equilibrium value (the alignment time) is plotted in the inset of figure 5.8. We find a linear dependence of the time with the inverse of the square of the magnetic field. The orientational force is proportional to B^2 as also observed for a monodomain aligning by rotating as a single structure under the effect of the magnetic force. Thus although many fluctuations perturb the complex smectic structure, on average its reorientation can still be described as a rigid structure rotating towards the field-induced direction. The reorientation time is for a smectic structure much longer than for a nematic system. It is thus not possible to study nematic domains reorientation with our experimental set-up.

5.8 Role of fluctuations in the smectic reorientation

Figure 5.9 shows structural fluctuations occurring during the system reorientation at different temperatures and only for rotation angles ϕ larger than $45°$. Such fluctuations always appear as dark regions through our imaging system. The bulk reorientation of a smectic-A liquid crystal is perturbed by fluctuations, especially in the early stage of the actual reorientation. In our experiments we observe the smectic system rearranging via a transient heterogenous structure.

Even though those structural order fluctuations can appear as a random dark pattern perturbing the smectic system, we find that elongated fluctuations show a well defined orientation. This orientation is not determined by the field direction but by the smectic structure. Indeed the orientation of stripe-like fluctuations is always found to coincide with the orientation of the smectic layers, while their propagation direction is along the layer normals. In time the dark structural fluctuations become larger and, for large rotation angles, they happen to cover the whole probed area, inducing a transient dark state. We find that large order fluctuations in the system do speed up the reorientation of the smectic sample to the equilibrium structure. We observe that the most dramatic transient structures and the fastest and total recovering of the equilibrium are both measured at large rotation angles, where the

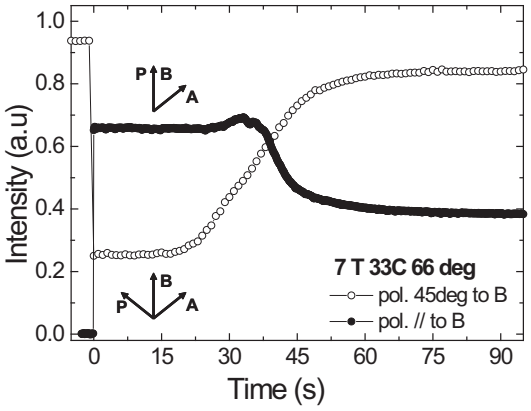

Figure 5.10: Integrated intensity profile from a reorientation experiment in 7 T, at ΔT_{N-A}=0.75°C and $\phi = 66°$ in two different acquisition settings. In our usual experimental configuration the polarizing and analyzing filters -always at $\phi = 90°$ to each other- form a $45°$ angle with respect to the magnetic field direction, the open circles curve is obtained, while the full circles profile corresponds to one polarizer parallel to B. The results from these two configurations indicate that the observed dark perturbation in the smectic structure do not correspond to regions oriented at the dark angle of the optical set-up, revealing that in those patterns the LC order is not present.

structural fluctuations are also more important. The same transient phenomena were observed in the X-ray diffraction experiment, during the early stage of the reorientation process [17], [18], [14]. Here the distribution of the smectic normals shows large fluctuations, while the diffraction patterns exhibit intensity distributions from different sectors at the same time.

In order to clarify the nature of the structural fluctuations observed during the reorientation, we have modified our measuring set-up. In our original situation the polarizing filters are oriented at 45° with respect to the magnetic field orientation. This is the standard experimental configuration in all the results presented above. A modified set-up is obtained by rotating the polarizers together until one polarization direction coincides with the magnetic field direction. Therefore two experiments in the same physical conditions gives opposite reorientation profiles, due to the different measuring conditions. Both configurations are sketched in figure 5.10 and the total birefringence intensity is plotted for a reorientation experiment in 7 T, at $T = 32\,°$ and $\phi = 66°$. For $t < 0$ s the aligned smectic structure shows a maximum of intensity when the crossed polarizers are at $45°$ with respect to the magnetic field - usual set-up- (open circles), while the same initial state is completely dark when the magnetic field is parallel to one of the polarizers - modified set-up (full circles).

After the rotation the integrated intensity from the birefringent signal increases or drops, respectively, to reach the equilibrium state. In the usual experimental conditions dark regions are observed during the reorientation. If those regions would correspond to smectic areas oriented along the dark angle of our detector, they would therefore appear bright when the measuring set-up is modified in the way explained above. Instead, by measuring with the modified set-up, the reorientation does not show any bright pattern, remaining dark. This allows us to exclude the possibility of having - during the reorientation- smectic regions oriented at the dark angle of the optical set-up and it suggests a loss of long range order in the system.

5.9 Discussion

The overall reorientation dynamics of the smectic-A phase in 8CB strongly depends on the three experimental parameters that have been varied: rotation angle, temperature and magnetic field strength. By rotating the sample in a magnetic field at constant temperature we observe that immediately after the rotation the smectic monodomain structure is conserved at an unfavourable orientation angle with respect to the magnetic field direction, resulting in an orientational force on the diamagnetic LC molecules. In all cases it takes some time before the smectic structure responds to the magnetic force, during which the birefringence signal is constant. This induction time becomes longer with decreasing temperature below T_{N-A} (figure 5.7). At a given temperature and rotation angle $\phi = 90$, the induction time becomes faster with increasing magnetic field strength (Figure 5.8) with an alignment time that is inversely proportional to B^2 (inset). This effect can be readily understood as the result of the increasing magnetic torque that scales quadratic with the field strength (section 2.7). After this initial period the actual reorientation begins towards the new equilibrium situation. Roughly we find that the equilibrium state is achieved faster after large rotation angles and higher B and ΔT, but the detailed behaviour strongly depends on the conditions.

The system dynamics, both the induction time and the reorientation dynamics, is slower at larger ΔT_{N-A} (see figure 5.7). We attribute this temperature sensitivity to the changing viscosity of the compound, which is found to increase significantly with cooling just below the nematic-smectic-A phase transition [14]. In any case the reorientation of the smectic phase is much longer than that of the nematic phase: the equilibrium is reached in minutes or even hours in the smectic phase, while it is established in a few seconds in the nematic case [6].

In general, at a given temperature the birefringence signals are monotonic for rotation angles $\phi \leq 45$, while they show a dip for rotation angles $\phi > 45$ (figure 5.5). For small angles the system reorients in a continuous, smooth way, whereas at larger angles the behaviour is more complex, in accordance with the results of previous X-ray experiments [10]. For larger angles a series of fluctuations perturb the system during the reorientation (figures 5.4 and 5.6). We find that the order fluctuations are not randomly distributed, but form elongated patterns oriented perpendicular to the smectic layers. Those patterns propagate through the system in a direction parallel to the smectic layers and precede the rapid transformation of the initial monodomain into a transient heterogeneous structure, which recovers the initial state. This complex local behaviour corresponds to the dip in the spatially averaged birefringence signal (figures 5.5, 5.7 and 5.8). Moreover, the occurrence of transient patterns is consistent with the irregular reorientation of smectic domains studied by X-ray diffraction [10], where the average distribution of the molecular directors revealed several anomalies, especially at rotation angles $\phi > 45$. In particular, large deviations from a smooth reorientation behaviour were observed at $\phi = 90$. At this critical angle the system can rotate either clockwise or anticlockwise, and, indeed, the reorientation profile appeared to be divided in two parts. One part first stayed fixed, hanging in the pre-rotational orientation before reacting to the magnetic force and reorienting quickly; another part appeared later oriented at $\phi = 45$ and first moved towards the unfavourable direction of the pre-rotational orientation, then stays fixed, before merging with the other domain. Thanks to the spatial resolution of our experiment we can follow the onset and the propagation of these local inhomogeneities. Most interestingly, a clear relation exists between the orientation of the smectic structure and the orientation and the propagation of the dark patterns. Even though fluctuations may arise in all directions, only the ones oriented along the layer normals will grow and propagate. As a consequence, the ordered smectic phase becomes locally unstable. In the X-ray study this is accompanied by a decreasing scattering intensity of the smectic layers indicative of a temporal loss in layer integrity [10]. This is consistent with our observation of dark, unordered domains that travel in a smectic background. We are not able to investigate the local order within the dark domains at molecular level. The absence of birefringence in these areas seems to suggest that the LC order has disappeared altogether or to a

great extent.

5.10 Conclusion

The reorientation dynamics of a smectic-A (SmA) phase within 8CB is found to be strongly dependent on temperature, rotation angle and magnetic field strength. We observe that the reorientation starts after an induction time, during which the SmA phase remains fixed in its initial orientation. This induction time increases with lowering the temperature further below T_{N-A}. After this induction time the system relaxes back to the new equilibrium state, which is found to be reached achieved faster with increasing rotation angles, increasing magnetic field strengths and temperatures closer to T_{N-A}. It is found that the reorientation process proceeds via complex, transient local structures, forming elongated patterns that are oriented perpendicularly to the smectic layers, and that propagate through the system. Our results demonstrate that the SmA phase does not reorient as a simple monodomain.

References

[1] A. Findon, H. Gleeson and J. Lydon, Phys. Rev. E 62, 5137 (2000).

[2] G.P. Crawford, *Flexible Flat Panel Displays*, A. C. Lowe ed., 313 (2005).

[3] E. A. Büyüktanir, M. Mitrokhin, B. Holter, A. Glushchenko and J. L. West, Japanese Journal of Applied Physics 45, 4146 (2006).

[4] P. G. de Gennes and J. Prost, *The Physics of Liquid Crystals*, Clarendon Press, Oxford (1993).

[5] I. Dierking, *Textures of liquid crystals*, Wiley (2003).

[6] S. D. Siemianowksi, P.D. Brimicombe, S. Jaradat, P. Thompson, W. Bras and H.F. Gleeson, Liquid Crystals 39, 1261 (2012).

[7] A. Sugimura and A.V. Zakharov, Phys. Rev. E, 84, 021703 (2011)

[8] G. R. Luckhust, T. Miyamoto, B. A. Timimi, A.Sugimura, J. Chem. Phys. 117, 12, 5899 (2002)

[9] G. R. Luckhust, B. A. Timimi, M. Nakatsuji, K. Okumoto, A. Sugimura and H. Zimmermann, Mol. cryst. Liq. Cryst. 398, 235 (2003).

[10] W. Bras, J. Macromol. Sci. Phys. 37, 557 (1998).

[11] W. Bras, I. P. Dolbnya, D. Detollenaere, R. van Tol, M. Malfois, G. N. Greaves, A. J. Ryan and E. Heeley, J. Appl. Crystallogr. 36, 791 (2003).

[12] W. Bras, J. W. Emsley, Y. K. Levine, G. R. Luckhurst, J. M. Seddon and B. A. Timimi, J. Chem. Phys. 121, 4397 (2004).

[13] P. D. Brimicombe, S. D. Siemianowski, S. Jaradat, Y. K. Levine, P. Thompson, W. Bras and H. F. Gleeson, Phys. Rev. E 79, 031706 (2009).

[14] S. D.Siemianowksi, P. D Brimicombe, S. Jaradat, P. Thomson, W. Bras and H. F. Gleeson, Liquid Crystals 127 (2012)

[15] H. Ogaki, K. Okumoto, A. Sugimura and H.Zimmermann, Thin Solid Films 499, 249 (2006).

[16] F. Schneider, Phys. Rev. E 74, 021709 (2006).

[17] C. Ortiz, C.K. Ober and E.J. Kramer, Polymer, 39, 16, 3713 (1998).

[18] W. Quevedo, C. Peth, G. Busse, M. Scholz, K. Mann and S. Techert, Int. J. Mol. Sci., 10, 11, 4754 (2009).

[19] Y. Levine and A. Polimeno, private communication.

Chapter 6

Defect-pattern at the interface in 8CB Smectic-A liquid crystals

6.1 Abstract

We report the observation of a double periodic surface defect-pattern within the liquid crystal 8CB, formed during the nematic - smectic A (N-SmA) phase transition in an applied magnetic field. The pattern results from conflicting alignment requirements of the 8CB molecules, i.e. homeotropic at the surface and planar in the bulk of the sample cell. The formation of a defect pattern is observed by in-situ polarization microscopy as a function of temperature and magnetic field strength. The defect pattern, which appears as stripes, forms at the cell walls, which are oriented perpendicularly to the magnetic field direction. A second structure, in between the stripes, is formed with lines parallel to the magnetic field direction. We find that the defect pattern formation speed decreases with increasing magnetic field. When the field direction is changed, the stripes break and rotate to a direction that corresponds to the new field direction. Using the continuum Landau-deGennes theory, the double periodicity of the pattern is explained. The long period ($\approx$10 μm) is determined by the balance of the surface anchoring and the elastic bending within the defect curvature walls. The short term period ($\approx$1 μm) is attributed to the effect of the saddle-splay term in the elastic energy of a SmA liquid crystal, causing the curvature walls to break up.

6.2 Introduction

The understanding of the microscopic structure of liquid crystalline phases is closely related to the study of topological defects, both from bulk and interfacial instabilities. Especially in thin films, defects play an important role in defining the macroscopic characteristics of the materials. They do not simply disturb the LC phase locally, but instead act to stabilize the director field configuration. This is of great importance for technological applications, such as small size displays, where local defects may influence the performance drastically.

As defined in chapter 3 smectic-A layers are flexible and easily distorted, but tend to preserve the interlayer spacing. As the structure adjusts itself to surface conditions, the layers can slide over another. These distortions at the surface are the cause of many defects, which under a polarizing microscope give rise to beautiful optical patterns.

Interfacial instabilities have been investigated extensively theoretically as well as experimentally in the last decades [1]. On the theoretical side mostly numerical approaches have been used, since the analytical treatment of the problem is rather difficult, apart from the stability analysis of a few planar, circular and dendritic solutions [2]. The two basic numerical methods are the sharp interface models

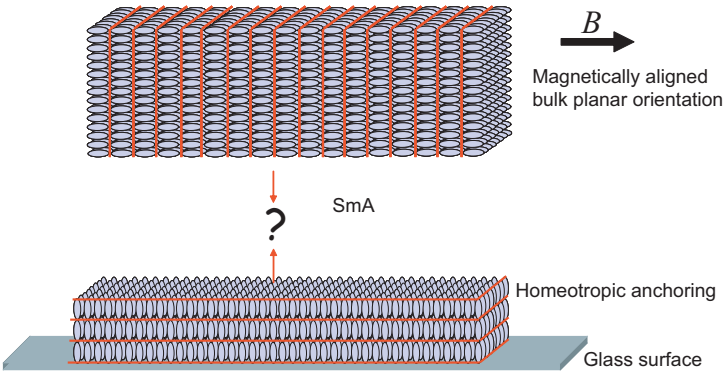

Figure 6.1: Two opposing forces act on the molecules within a SmA LC phase: the magnetic field-induced planar alignment in the bulk and the homeotropic anchoring at the surfaces. At the interface of the two regions, indicated with a question mark, these forces balance, giving rise to a frustrated structure.

[3], [4], and the phase fields models, which are dynamic extensions of the Cahn-Hilliard theory of first-order phase transformations [5]. On the experimental side the literature reports a great variety of optical studies on liquid crystals thanks to their optical and thermodynamical properties. In liquid crystals many complex patterns have been observed, such us undulations of the smectic layers in applied magnetic field (Helfrich-Hurault instability)[6],[7], or other periodic structures, like stripes[8], squares [9] or hexagons [10]. Usually those structures are explained by the formation of focal conic domains or curvature walls [11], [12]. Solidification [13], viscous fingering [14], electrochemical deposition [15], as well as growth of bacterial colonies have been studied. An impressive variety of regular patterns have been observed and understood, at least macroscopically [16], [17]. A regular undulated pattern has been observed in the homologous series of the cyano-biphenyl LC systems [18]. The inner structure of the singularities in a smectic system at the interface has been observed by a X-ray diffraction investigation [8]. A fundamental study on defects in smectic liquid crystals dates back to 1975 [19], when Cladis and Torza published a long article on a corrugated nematic layers in smectic phase, with planes oriented in two different directions. By polarization microscopy they observed stripes in CBOOA oriented parallel to the applied magnetic field. The stripes observed by Cladis and Torza showed a stable double periodicity, as a transition to a honeycomb texture. They explained the stripes to be a trapped nematic texture formed close to the critical transition temperature [26]. The stripes develop at 0.2°C above the nematic /smectic-A transition temperature T_c by slowly cooling the smectic towards T_c. The stripes are sensitive to the magnetic field strength: in a lower field intensity the stripes are not stable and disappear by cooling to the nematic phase, while the period of the stripes decreases as the field increases. Upon increasing the cooling rate close to the nematic transition temperature, the stripe's periodicity also decreases.

In this chapter we report the observation of a stripe defect pattern formed during the nematic-smectic A phase transition in an applied magnetic field. The pattern shows a double periodicity, a long one (≈10 μm) along the field direction and a short one (≈ 1 μm) perpendicular to the field. We explain the formation of these structures with the competition of two opposite forces acting on the LC molecules: the magnetic field-induced planar alignment in the bulk and the homeotropic anchoring at the surfaces, as illustrated in figure 6.1. At the interface of the two regions these forces balance, giving rise to a frustrated structure, where the smectic layers are deformed, but the inter-layer distance

is kept constant.

This chapter is organized as follows. In section 6.2 the technical aspects of our experiments are explained. In section 6.3 we describe the dynamics of the defect formation at the interface, during the N-SmA transition in 8CB, in a background magnetic field. The competition between the surface anchoring force and the field-induced aligned structure in the bulk, results in the bending of the smectic layers, which gives rise to the observed defects. In section 6.4 the defects pattern are characterized by polarization microscopy. The substrate and field dependence of the surface defects formation are described, respectively, in sections 6.5 and 6.6. The speed of the defect formation, as well as the periodicity of the pattern, are described for field strengths between 5 and 20 T. The growth speed is found to decrease in higher magnetic fields, where less defects are observed. In section 6.7 the reorientation of the defects lines is studied by varying the alignment of the bulk. Finally in section 6.8 the microscopic defects structure is discussed and compared with other recent results.

6.3 Experimental details

For the experiments we have used time-resolved birefringence microscopy in high magnetic fields. The experimental set-up is the same as in chapter 5 and it is schematically shown in figure 6.2. Light from a halogen lamp is transmitted through the liquid crystalline sample 8CB and is imaged on a video CCD camera, with a field of view of 1.1 x 0.9 mm^2 and with 2 μm resolution. The cell containing the sample is positioned in between two polarizers, oriented at 90° to each other, in order to exclude all isotropic contributions. The orientation of the polarizers is chosen at $\pm 45^\circ$ with respect to the magnetic field, which means that the intensity of the transmitted light is high when the molecules are aligned along the field. No light is transmitted (dark image on CCD) for non oriented (isotropic) materials, or when the molecules are either aligned parallel to one of the polarizers or along the viewing axis.

The liquid crystal 8CB (4'-Octyl-4-biphenylcarbonitrile) is contained within two 0.4 mm thick borosilicate glass plates, spaced by a teflon ring of 4.5 mm inner diameter and of 1.6 mm thickness, as shown in the inset of figure 6.2. The liquid crystalline structure in the vicinity of the glass surface shows different patterns, the actual surface texture being strongly dependent on the surface treatment of the glass. The surface treatment can induce a homeotropic or planar alignment of the LC molecules. In most cases clean untreated glass is used, whereas we also use spin-coated layers of polyvinyl alcohol (PVA), polydimethyilsilizane (PDMS) and hexamethyldisilzane (HMDS). By coating the cell with PVA we obtain a hydrophilic substrate, which induces a planar molecular alignment. When the surface is not treated, or when it is coated with PDMS or HMDS a hydrophobic substrate is obtained, inducing a homeotropic alignment. The anchoring strength gradually increases for HMDS, untreated glass to PDMS. The standard protocol for all measurements was the following: the sample was heated to the isotropic phase. After a stabilization period of at least 10 min, a constant magnetic field between 0 and 20 T was applied. Subsequently the system was cooled at a rate of 0.4 °C/min to a temperature within the smectic phase, just below the N-SmA phase transition ($\Delta T_{N-A} = T_{N-A} - T$). During this process the birefringence microscopy images were recorded. After the experiments one of the three following actions were done: 1) the cell was taken out of the magnet to be investigated at higher magnification in a polarization microscope. 2) the sample was heated again to 38 °C, in to the nematic phase, in order to prepare the sample for the next measurement. 3) the cell was rotated about an angle ϕ in order to study the stability of the observed patterns.

6.4 Formation of surface defect pattern in high magnetic field

We first consider the formation of a regular pattern of line-defects in the plane of the cell, during cooling the cell through the N-SmA phase transition in the presence of a magnetic field stronger that 3 T. A

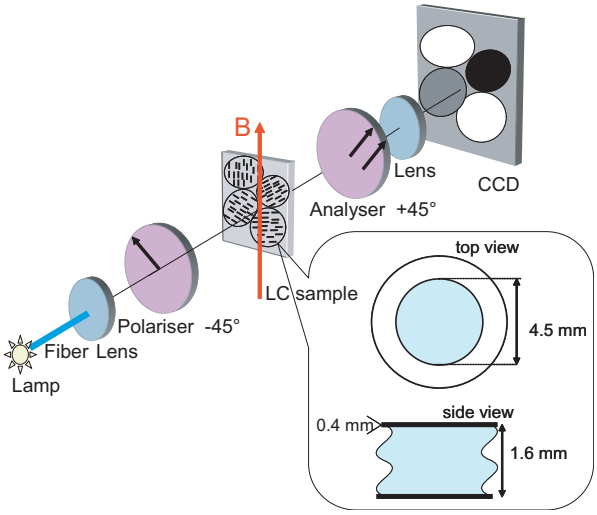

Figure 6.2: Schematic of the optical path for birefringence microscopy in high magnetic field. See also figure 3.5 for a complete set-up. The LC sample is placed in the center of a 20 T Bitter magnet. The temperature of the whole magnet bore can be controlled with an accuracy of 0.1°C. The sample is positioned between two crossed polarizers at $\pm 45^\circ$ with respect to the field direction. LC domains appear bright on a video CCD camera when oriented parallel to the field direction. The LC cell is made of two 0.4 mm thick borosilicate glass plates, spaced by a teflon ring of 4.5 mm inner diameter and of 1.6 mm thickness.

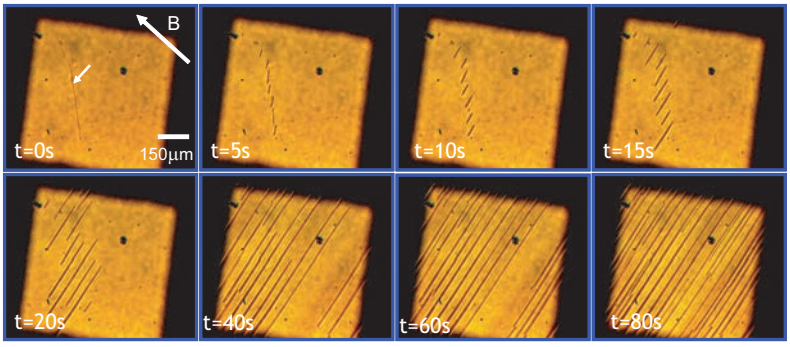

Figure 6.3: Birefringence images of the formation of line defects during the N-SmA phase transition in a background magnetic field of 7 T. At $t = 0$ s the temperature is $T = 33.75$ °C and the system is cooled at a rate of 0.4 °C/min. Line-defects appear and develop in the plane of the cell. In this particular case a line defect is presented at $t = 0$ s, as indicated by the arrow. Upon cooling, the defect breaks up ($t = 5$ s), rotates ($t = 10$ s), and grows in a direction perpendicular to the magnetic field. Finally ($t \geq 80$ s) the full sample surface is covered by a defect pattern.

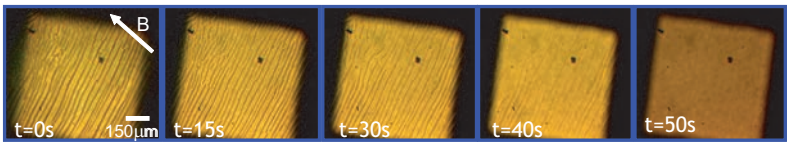

Figure 6.4: Birefringence images of the annealing of line defects by heating through the SmA-N transition, to T=37.35°C, at rate of 0.45°C/min in a 7 T background field. The line-defects have completely disappeared in the nematic phase ($t = 50$ s).

typical example using untreated glass is shown in figure 6.3. The formation of a striated defect pattern is observed in a background field of 7 T and it is reproducible. At $t = 0$ s the temperature is $T = 33.75$ °C and the cooling sequence is started. The average transmitted light intensity is high because in the bulk of the sample the LC phase is aligned parallel to $\vec{B}$. In this particular case an elongated defect is present, as indicated by the arrow in the $t = 0$ s image. Upon cooling, the defect breaks up in shorter lines ($t = 5$ s), which rotate towards an orientation perpendicularly to the magnetic field direction ($t = 10$ s). Subsequently the defects rapidly grow ($t = 20$ s), covering the entire surface with straight lines, all oriented at an angle of $90°$ with respect to the magnetic field direction. Finally, a homogeneous and stable pattern is obtained, with a periodicity of approximately 10 μm ($t = 80$ s and later). Heating the system through the SmA-N transition induces the reverse phenomenon: the line-defects shrink and finally disappear in the nematic phase, as shown in figure 6.4.

6.5 Microscopic characterization of the surface line pattern

The field-induced line texture is not perturbed by further cooling the system to room temperature and the subsequent switching-off the magnetic field. The resulting material appears stable, which allows the investigation by a polarizion microscope. Representative images are shown in figure 6.5, obtained by adjusting the focus at different depths of the sample. Clearly, the line-defects are formed on both top and bottom surfaces of the cell, while there are no stripes in the bulk.

In figure 6.6 representative pictures of the same part of the cell are shown for different magnifications. The line pattern is already visible at 100X magnification, but it becomes more clear at 200X magnification. Here we observe dark lines similar to those of the in-situ images taken at a comparable magnification. In fact, as shown in figure 6.7, the brightness of the lines depends on the focus, because well focussed stripes appears bright (right panel), in contrast to the black lines observed out of focus (left panel). Here the same region of the line pattern is shown at 500X magnification. At this higher magnification the line pattern reveals a finer structure: between adjacent lines smaller elongated defects are visible with 1 μm periodicity and perpendicular to the main pattern. This secondary structure develops where the primary defect structure is more dense and regular, i.e. in between straight defect lines. In contrast, no secondary structure is formed in the vicinity of an interrupted line pattern.

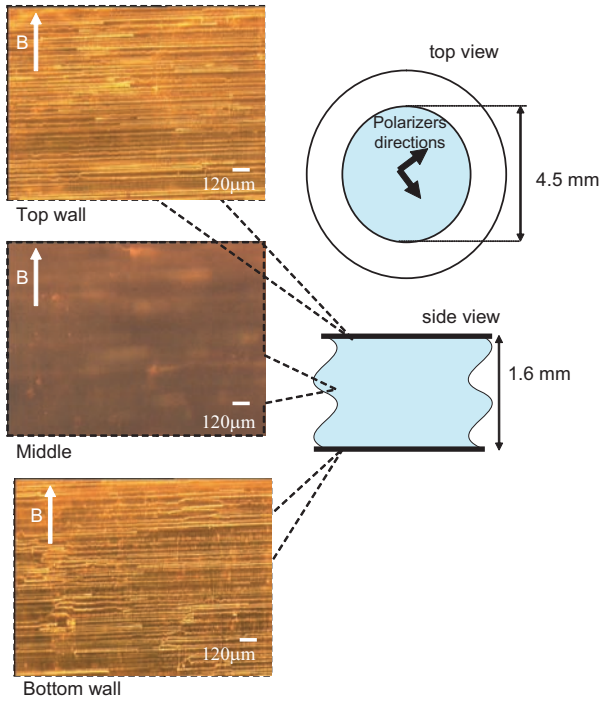

Figure 6.5: Ex-situ investigation of the aligned structure prepared in high magnetic field, after cooling through the N-SmA transition in 7 T. Line-defects are formed at the cell walls, while there are no stripes in the bulk. In the sketched cell the orientation of the polarizing filters is depicted.

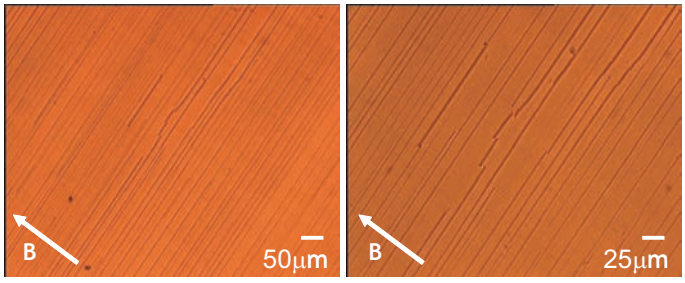

Figure 6.6: Line patterns observed at different magnifications in a polarization microscope. Left: 100X magnification; right: 200X magnification

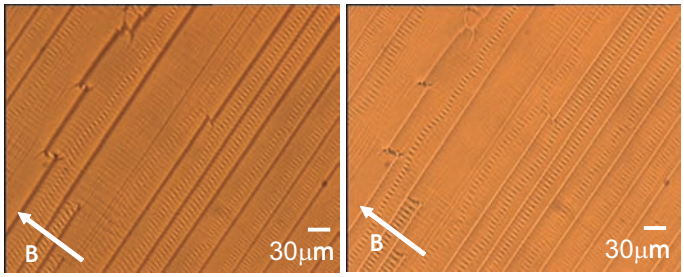

Figure 6.7: Line patterns observed at 500X magnification in a polarization microscope. The brightness of the lines depends on the focus. Well focussed stripes appear bright (right panel), in contrast to the black lines observed out of focus (left panel). At this magnification a finer structure is observed: between consecutive lines there are other smaller elongated defects, about 1 μm thick, perpendicular to the main stripes.

6.6 Influence of the surface anchoring

The precise defect structure strongly depends on the surface treatment of the cell walls, as shown in figure 6.8. Very similar defects pattern are obtained for cells made by untreated glass and using glass coated by polydimethyilsilizane (PDMS). In both cases a hydrophobic substrate is formed, which leads to an homeotropic alignment of the LC molecules at the surface. In fact for the PDMS coated glass the wall controlled homeotropic alignment produces a beautiful line pattern, which is much more regular than the pattern on untreated glass, as shown in bottom left and right images. Here a regular undulation is observed in the inner structure of the line pattern, giving rise to a zig-zag pattern. In contrast the formation of stripes does not occur on cell walls coated by hexamethyldisilizane (HMS) (top right of figure 7.8), which induces a low surface anchoring, and by polyvinyl alcohol (PVA), which is a hydrophilic surface and induces a planar molecular alignment. Instead, a well oriented monodomain is found in this case, with some focal conic defects, as shown in the top left of figure 6.8.

For our study it is interesting to remember that focal conics are observed at the interface between the substrate and a region where planar forces act on smectic layers. In contrast the stripe defects as described in the previous sections form at the interface due to the effect of two antagonistic non planar forces that induces an orientation of the molecules perpendicular to each other, see figure 6.1.

6.7 Effect of the magnetic field strength

The previous experiments were performed in a background field of 7 T, which is strong enough to observe the formation of the stripe pattern during the N-SmA transition, in a reasonable measurement time. Upon varying the magnetic field strength we change the balance between the substrate anchoring force and the magnetic aligning force. Thus we change the conditions for the formation of the stripe pattern. Indeed, as shown in figure 6.9, at a magnetic field of 20 T the planar alignment becomes dominant also at the surface and therefore few stripes are observed. We have monitored the defect formation at field strengths between 5 T and 20 T, finding that with increasing the field strength, the the line-defect coverage gradually decreases. Moreover a strong magnetic field remarkably influences the growth speed of the lines, as shown in figure 6.10, which displays the length of a line as a function of time.

The length of a line is graphically measured in each frame recorded during the pattern formation,

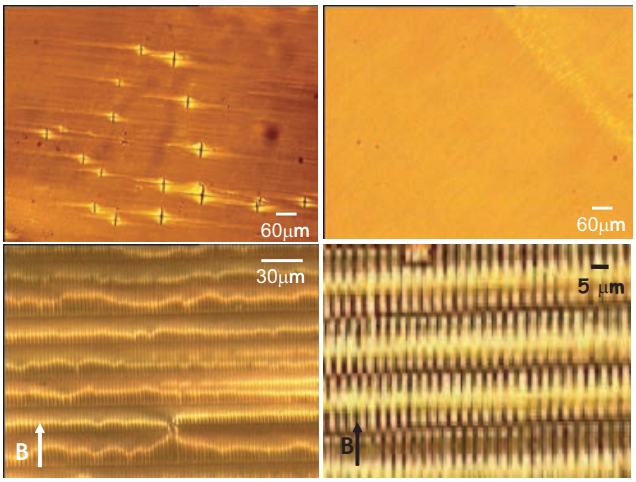

Figure 6.8: Using cells with different surface coatings leads to different surface anchoring forces and therefore to different surface structures. Top left: polyvinyl alcohol (PVA) induces planar surface anchoring and focal conics are observed when exposed to a planar magnetic force, top right: hexamethyldisilizane (HMS) induces a weak anchoring and no surface defects are observed. In this case a beautiful monodomain is present. Bottom: polydimethyilsilizane (PDMS) induces homeotropic surface anchoring and regular stripes defects are observed (left), with a zig-zag inner structure (right).

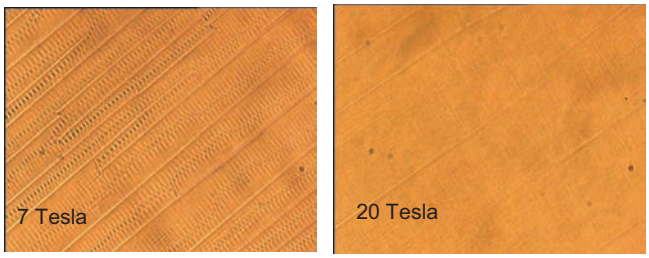

Figure 6.9: Surface patterns obtained at 7 T (left) and 20 T (right). At higher field strengths less stripe defects cover the surface.

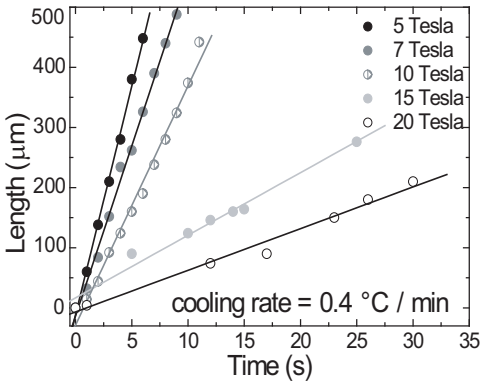

Figure 6.10: Length of the line defects as a function of time at different field strengths between 5 and 20 T, during cooling the LC system with a rate of 0.4 °C/min. The slope of the curves corresponds to the growth speed of the defects, which slows down with increasing the field strength. A stronger magnetic field changes the balance between the planar field-induced orienting force and the homeotropic anchoring force at the surface.

as shown in figure 6.3. In good approximation, in all cases the growth is found to be linear in time, with a slope that corresponds to the growth speed of the stripe pattern. Our results show that the growth speed of the stripes strongly decreases with B. This is consistent with the role of the counteracting forces acting on the sample: when the planar alignment becomes dominant there are less chances for the homeotropic surface to equilibrate the two forces near the surface, giving rise to the stripes. Since the system is being cooled, and therefore the viscosity of the system is rapidly rising, these results explain also why less stripes are obtained in higher field. In fact, a slower growth rate implies that less lines are formed within the available time in which the system stays in the temperature range of the N-SmA transition. At lower temperature the system is fixed in the smectic phase and the surface anchoring always dominates. On the other hand, as long as we remain in the N-SmA transition region a balance between the two aligning forces is possible. This balance is investigated in the following section, by varying the direction of one of the forces.

6.8 Reorientation of surface pattern in high magnetic field

Given a fixed anchoring force at the substrate, the result of the competition between the magnetic force and the surface alignment depends on the orientation of the magnetic field. In our previous experiments we always consider the case of highest frustration, since the two forces are perpendicular to each other. Now we study what happens when the direction of the magnetic field is suddenly changed, but kept in the plane of the cell walls. For this experiment we use a substrate inducing homeotropic anchoring at the surface, thus the magnetic orientation is in the plane perpendicular to the surface molecular orientation. After a rotation the balance of the forces producing the frustrated structure is the same, but the new direction of the magnetic field produces a change of alignment of the bulk molecules. This influences the interfacial region and thus the stripes pattern. For simplicity, instead of changing the magnetic field direction we perform a sudden rotation of the cell containing the liquid crystal sample. A rotation by an angle ϕ in a constant background field and at a temperature

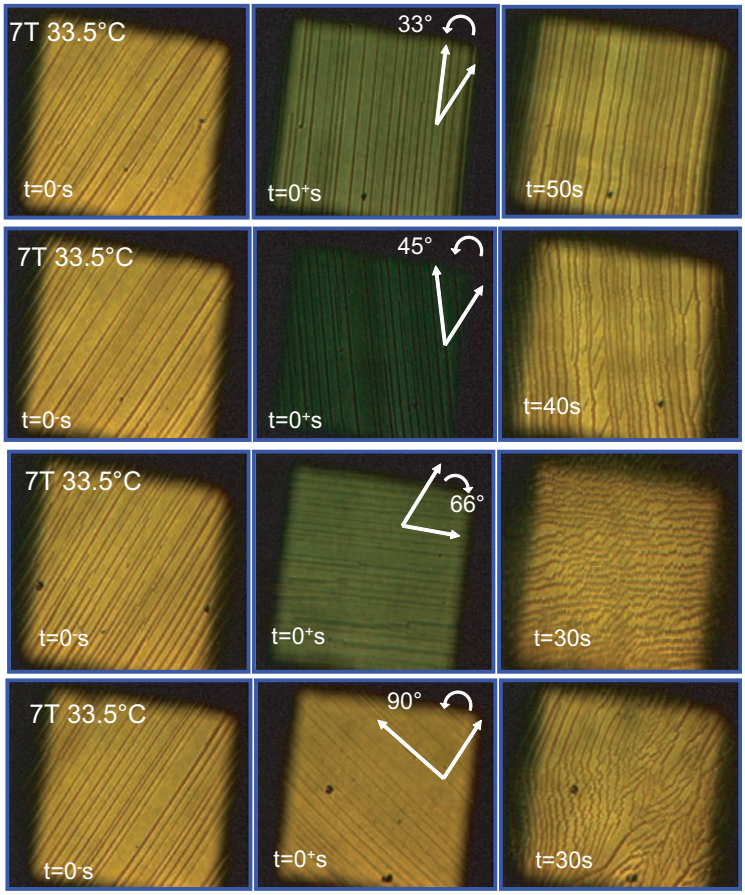

Figure 6.11: Surface pattern reorientation experiments in 7 T at ΔT_{N-A}=0.25°C, for rotation angles ϕ=33°, ϕ=45°, ϕ=66° and ϕ=90°. By increasing the amplitude of the rotation angle the stripes tend to reorient in the field-induced orientation, by breaking and rotating or by forming new stripes in between the old defects.

T, ΔT_{N-A} below the N-SmA transition produces different results depending on the values of ΔT_{N-A} and ϕ. The most interesting results are obtained at 33.5 °C, i.e at $\Delta T_{N-A} = 0.25$ °C, as shown in figure 6.11. In the upper row results are presented for a rotation of ϕ=33°. The pattern is observed immediately before the rotation ($t = 0^-$ s), immediately after the rotation ($t = 0^+$ s) and when the system is again in equilibrium and the bulk structure has re-aligned, as described in chapter 5 at the time $t = 50$ s. For small rotation angles the stripe pattern remains fixed in its pre-rotational orientation. By increasing the amplitude of the rotation angle the line-defects become unstable and tend to recover the initial orientation. At ϕ=45° (second row) we observe the formation of new line-defects in the field-induced orientation, i.e. oriented at $45°$ with respect to the old defects. The formation of new lines occurs where no other defect is present, thus in between the old defects. The presence of a differently oriented planar force becomes more pronounced at ϕ=66° (third row), where lines break and rotate towards the field direction, and at ϕ=90° (lower row), where a zebra pattern is obtained.

6.9 Discussion

The formation of the stripe defects observed close to the surface during the nematic-smectic-A phase transition is the result of two competing forces acting on the liquid crystalline system: magnetic field and surface anchoring. The applied magnetic field tends to orient the liquid crystalline director parallel to its direction, which is, in our geometry, planar to the glass surfaces. This force is dominant in the bulk. On the other hand a not treated surface, as well as a surface coated with polydimethyilsilizane, induces a homeotropic alignment, with the rod-like liquid crystalline molecules aligning perpendicularly to the substrate. At the interface between the bulk and the surface the two forces are in balance, giving rise to a frustrated region, where the smectic layers readjust by bending, forming the observed defects. The pattern observed in our experiments is compatible with the half tube-shaped defect structure observed in a X-ray study on ultrathin 8CB films [8]. In this study the interfacial structure of a very thin liquid crystalline films is as well frustrated by two opposing anchoring forces acting on the smectic phase. In this particular case the surface was coated with MoS_2 (molybdenum disulfide), which imposes a strong planar unidirectional anchoring, antagonistic to the homeotropic anchoring at the 8CB-air interface. The relaxation of the constraints imposed by the competing anchoring forces occurs through the formation of a periodic network of flattened hemi-cylinders, parallel to the substrate [20]. This defect formation causes a rotation of the smectic layers, which is measured in that experiment for the first time. The defect cores revealed by X-ray diffraction consist in half tube-shaped rotating grain boundaries (RGB), with the diameter of the tubes laying on the surface. In our experiment the two antagonistic forces are oriented in opposite direction with respect to the above case, thus the geometry of our defects corresponds to half tube-shaped structures with the diameter opposing the surface. In both experiments the spacing between the observed defect-lines can be calculated balancing the magnetic energy, the surface anchoring, the bending energy and the defect energy. The result of the calculation gives a typical dimension: d = 5 - 10 μm [22], [23]. In our experiment the typical distance d between lines is found to be 20-30 μm.

We recall here the theoretical description in the nematic phase (above the transition temperature $T > T_c$ ($T_c \equiv T_{\mathrm{N-SmA}}$)), which is described by a unit vector $\mathbf{n}$ called the director, pointing along the averaged orientation of the LC molecules. In the bulk the director is aligned parallel to the magnetic field, while close to the glass surface the molecules are orientated along the normal to the surface (homeotropic anchoring). The director $\mathbf{n}$ reorients by bending within a boundary layer [24] in order to minimize the sum of elastic and magnetic free energy:

$$\mathcal{F}_{\mathrm{nem}} = \frac{1}{2}\int_V dV\,\{K|\nabla\mathbf{n}|^{\mathbf{2}} - \chi_{\mathbf{a}}\mathbf{B}^{\mathbf{2}}(\mathbf{n}\cdot\mathbf{e_x})^{\mathbf{2}}\}. \tag{6.1}$$

We are far above the Fredericksz threshold, i.e. in a regime of deformed director configuration,

since the applied filed is $B_{\rm cr} = \frac{\pi}{H}\sqrt{\frac{K}{\chi_a}} \simeq 10^{-2}$ T , where $K \simeq 7 \cdot 10^{-12}$ N is the elastic modulus, $\chi_a \simeq 10^{-7}$ is the diamagnetic anisotropy in cgs units[6] and $2H = 1.6$ mm is the sample thickness. The angle θ between the z-axis and the director $\mathbf{n} = \sin\theta\,\mathbf{e_x} + \cos\theta\,\mathbf{e_z}$ varies along the thickness of the sample as [24]:

$$\theta(\zeta) = \arcsin\left(\frac{Ae^{2\zeta} - 1}{Ae^{2\zeta} + 1}\right), \qquad A = \frac{1+\mu}{1-\mu}. \tag{6.2}$$

A is determined by μ which corresponds to the energy cost for the deviation of $\mathbf{n}$ from its preferred orientation along the normal to the surface and is given by $\mu = \frac{\sqrt{K\chi_a B^2}}{W_a}$, with W_a the anchoring strength. The dimensionless coordinate $\zeta = \frac{1-z/H}{\epsilon_\theta}$ measures the distance from the glass surface in the z-direction in units of the coherence length $\epsilon_\theta H = \sqrt{\frac{K}{\chi_a B^2}} \simeq 0.45\mu$m.

Smectic phases have a layer structure which is built on top of the bent nematic director configuration described by equation 6.1. We assume equidistant layer separation and thus smectic surfaces described by a scaler level set function ϕ are determined by solving $\nabla\phi - \mathbf{n}$, which is our ansatz.

For 8CB confined within two glass surfaces the associated Landau–deGennes free energy is [6]:

$$\mathcal{F}_{\rm sm} = \int dV \left\{ \frac{C}{2}\left(\lambda^2|\nabla\rho|^2 + \rho^2|\nabla\phi - n|^2\right) + \frac{r}{2}\rho^2 + \frac{g}{4}\rho^4 \right\}. \tag{6.3}$$

For 8CB the compression modulus $C \simeq 10^6$ J/m^3 and the interlayer spacing $\lambda \simeq 3.2$ nm [11]. The coefficients r and g are regular Landau coefficients, where only r depends on temperature, while $g > 0$. We assume that the spatial variations of ρ are negligible, because they occur within the characteristic lengthscale $\lambda \ll \epsilon_\theta H$ and prior to the change of orientation due to the rapid cooling. Then $\rho = \sqrt{-\frac{r}{g}} \propto \sqrt{T_c - T}$ and the second term in(6.3) is minimised if

$$\nabla\phi = \mathbf{n} \quad \rightarrow \quad \frac{\mathbf{dx}}{\mathbf{dz}} = \cot\theta, \tag{6.4}$$

yielding the formation of equidistant smectic layers ($|\nabla\phi| = 1$) on top of the distorted nematic phase. Substituting θ from (6.2) and integrating (6.4) we find:

$$\zeta_0(\xi) = \frac{1}{2}\log\left(\frac{\coth(\xi/2)}{A}\right). \tag{6.5}$$

This important and new result parameterizes the bending of the smectic layers in terms of the dimensionless coordinate $\xi = x/(\epsilon_\theta H)$ along the sample surface as shown in Fig.6.12 (red curve). To obtain a space-filling structure of equidistant layers we perform a parallel transport of $\zeta_0(\xi)$ along the normal $\nu = \nu_x\mathbf{e}_x + \nu_z\mathbf{e}_z$ (see Fig.6.12)), in which the jth layer is described by:

$$\mathbf{x}_j = (\xi + j\alpha\nu_x)\mathbf{e}_x + (\zeta + j\alpha\nu_z)\mathbf{e}_z, \quad j = 0, \pm1, \pm2\ldots \tag{6.6}$$

$\alpha = \frac{\lambda}{\epsilon_\theta H}$ is the dimensionless interlayer distance. In the bulk ($\zeta \rightarrow \infty$) we obtain a set of flat parallel layers perpendicular to the x-axis. The homeotropic surface alignment now creates curved smectic layers (green layers in Fig.6.12), which cannot completely fill space, without topological defects shown in Fig.6.12 as curvature walls by the dashed-blue and grey regions. The resulting structure consists of stripes parallel to the y axis with period L_x in the x direction, along the magnetic field. L_x is determined by two contributions:

$$L_x \simeq 2\frac{W_a - 2\rho\sqrt{KC}(1 - \frac{\pi}{4}}{\chi_a B^2} + 2\frac{\epsilon_\theta H}{max|k|}. \tag{6.7}$$

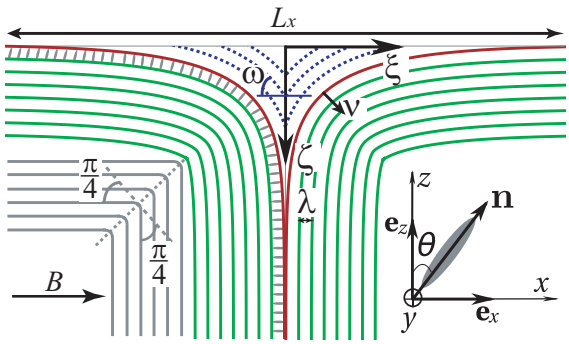

Figure 6.12: The space-filling structure of equidistant smectic layers resulting from the parallel transport of zero-level layer (red curve $A \simeq 1.1$) over a distance $\lambda = \text{const}$ along the normal ν according to (6.6). The director $\mathbf{n} = \sin\theta\mathbf{e}_x + \cos\theta\mathbf{e}_z$ coincides with the normal to the zero-level layer ν. Due to the non-zero curvature κ curvature walls are formed in the vicinity of the glass surface (dashed region) and a $\pi/2$-wall in the bulk (region at bottom corner left).

The first term corresponds to the competition between the anchoring energy (green region in figure 6.12) and the energy of the curvature wall (gray region), given by $f_\omega = \rho\sqrt{KC}(\tan\omega - \omega)\cos\omega$ [25] ($\omega = \pi/4$)) per unit area. The second term originates from a non zero curvature of the generating curve (see equation 6.5) given by $k = \partial_\xi\zeta_0/(1 + (\partial_\xi\zeta_0)^2)^{3/2}$. The first term in 6.7 is non negative only if $W_a \gtrsim \rho x 10^{-3} J/m^2$, yielding $L_x \simeq (9 \pm 4)$ μm for a strong surface anchoring ($W_a \simeq (3 \pm 1) x 10^{-4} J/m^2$) and a smectic order parameter $\rho \simeq 0.1$ in the vicinity of the N-SmA transition, which is compatible with our experimental observations. Within this model indeed no stripes defect patterns are expected for planar and small homeotropic surface anchoring.

When one of the two external forces -in our case the surface anchoring- is kept constant and the other - the magnetic field- is varied we have measured the growth speed of the line defects. The observed slower growth rate of the defects in high fields is consistent with the progressive overcoming of the magnetic force on the surface anchoring, and the consequent shrinking of the interface region where the equilibrium condition is produced by defects.

The finer structure observed at higher magnification, which shows a well defined periodicity of about 1μm, is the result of an additional frustration in the smectic layers. The irregular highly birefringent lines going across the line defects corresponds to the layers undulation on an untreated surface. On the other hand a controlled surface coating inducing homeotropic molecular alignment gives a regular undulation of the inner pattern. This is another way of relaxing stress without altering the interlayer spacing, typical of smectic structures. As calculated by Manyuhina [26], this result is an additional frustration at the surface.

6.10 Conclusion

We observed the formation of a striated defect pattern in 8CB during the N-SmA phase transition. By polarized microscopy in a background magnetic field stripes form close to the Smectic-A / Nematic transition, as a result of the competition of two antagonistic orienting forces acting in the LC cell. The planar field-induced orientation is dominant in the bulk, while a homeotropic alignment is given by the surface. In between this two regions the smectic structure is frustrated and relaxes the constrains by bending to form a stripe-like pattern. Therefore the observed defects do not perturb the system

order, but instead are responsible for the establishment of a stable smectic phase. We find that defects form in the plane of the surface, initially in a random direction and subsequently they readjust by breaking and rotating to the field induced direction. Once oriented in the field direction, defects can can develop much faster compared to the growth rate in another planar direction. The growth speed is found to strongly decrease in higher magnetic fields, where less defects are observed, since the planar orientation becomes dominant. Moreover the inner structure of the defects pattern on homogeneously hydrophobic surfaces shows a highly regular undulation. We explain the observed defect by the bending of the smectic layers, as calculated by Manyuhina. The homeotropic surface alignment creates curved smectic layers which cannot completely fill space, and give rise to topological defects as curvature walls.

The microscopic molecular structure of the stripe-like defects is compatible with the half tube-shaped defect structure observed in a X-ray study on ultrathin 8CB films [8]. The thickness and spacing of our half cylinders depend on the balance of the competing forces [27].

After a sudden rotation of the liquid crystal cell in a background magnetic field of 7 Tesla we observed for the first time the reorientation of the stripe-like pattern. By increasing the amplitude of the rotation angle the stripes reorient by breaking in small parts, each rotating towards the field induced direction. At high angles the stripes disappear and new stripes form already oriented in the direction favored by the new energy balance.

References

[1] J. Langer, Rev. Mod. Phys. 52, 1 (1980).

[2] *Solids far from equilibrium*, C. Godrèche ed., Cambridge Universiy Press (2011).

[3] H. Muller-Krumbhaar, *Theory of dendritic crystal growth* in Morphology of crystals, I. Sunagawa ed., Terra Scientific Publishing Company, Tokyo (1987).

[4] O. Shochet, K. Kassner, E. Ben-Jacob, S.G. Lipson and H. Miiller- Krumbhaar, Physica A 181, 136 (1992).

[5] O Penrose and P.C. Fife, Physica D, 43, 44 (1990).

[6] P. G. de Gennes and J. Prost, *The Physics of Liquid Crystals*, Clarendon Press, Oxford (1993).

[7] I. W. Stewart, *The Static and Dynamic Continuum Theory of Liquid Crystals*,Taylor & Francis, London and New York (2004).

[8] J.P. Michel, E. Lacaze, M. Goldmann, M. Gailhanou, M. de Boissieu and M. Alba, Phys. Rev. Lett. 96, 027803 (2006).

[9] B. I. Senyuk, I. I. Smalyukh and O. D. Lavrentovich, Phys. Rev. E 74, 011712 (2006).

[10] L. Z. Ruan, J. R. Sambles and I. W. Stewart, Phys. Rev. Lett. 91, 033901 (2003).

[11] M. Kleman, *Points, lines and walls*, John Wiley & Sons, New York (1983).

[12] C. Blanc and M. Kleman, Eur. Phys. J. B, 10, 53 (1999).

[13] E. Rubinstein and M. Glicksman, J. of Crystal Growth 112, 97 (1991).

[14] K. Mckloud and J. Maher, Phys. Rep. 260, 139 (1995).

[15] D, Grier, E. Ben-Jacob, R. Clarke and L. M. Sander, Phys. Rev. Lett. 56, 1264 (1986).

[16] A. Buka and L. Kramer, *Pattern Formation in Liquid Crystals*, Springer, New York (1996).

[17] O.D. Levrentovich and Z. Li, Phys. Rev. Lett. 73, 280 (1994).

[18] T. Ishikawa and O. D. Levrentovich, Phys. Rev. E, 63, 030501 (2001).

[19] P. E. Cladis and S. Torza, J. Appl. Phys. 46, 584 (1975).

[20] J.P. Michel, E. Lacaze, M. Alba, M. de Boissieu, M. Gailhanou and M. Goldmann, Phys. Rev. E 70, 01709 (2004).

[21] J.P. Hurault, J. Chem. Phys. 59, 4 (1973).

[22] O.V. Manyuhina, A.-M. Cazabat and M. Ben Amar, Europhys. Lett. 92 ,16005 (2010).

[23] O.V. Manyuhina and M. Ben Amar, Phys. Lett. A 377, 1003 (2013).

[24] O. V. Manyuhina, J. Phys.: Condens. Matter 24, 195102 (2012).

[25] C. Blanc and M. Kleman, Eur. Phys. J. B, 10, 53 (1999)

[26] O. V. Manyuhina, G. Tordini, W. Bras, J.C. Maan and P.C.M. Christianen, Phys. Rev. E 87, 050501 (2013)

[27] B.A. DiDonna and Randall D. Kamine, Phys. Rev. Lett. 89, 215504 (2002).

Summary

Liquid crystals (LCs) constitute an intermediate phase of matter that combines two seemingly opposing properties, such as fluidity (as in liquids) and long range periodic order (as in crystalline solids). The complex behaviour of LCs permits the (experimental) investigation of delicate equilibria at the border of two different phase-states. The fundamental relevance of the study of phase transition dynamics is, however, not restricted to liquid crystals: it is also relevant to the understanding of how matter evolves, in material science (magnetism and superconductivity), self-assembled molecular systems in supramolecular chemistry and biology and the large spatial patterns in cosmology.

Liquid crystals are ideal model systems, because their behaviour near phase transitions can easily be studied near room temperature using optical microscopy. For example, the transition from the isotropic (liquid) state to the nematic phase (liquid with orientational order) is often a weak first order phase transition. During such a transition, the system either absorbs or releases a fixed amount of energy (latent heat). Because energy cannot be transferred instantaneously between the system and its environment, first-order transitions are often accompanied by mixed-phase regimes in which some parts of the system have completed the transition and others have not. The key to investigate these extraordinary mixed-phase regimes is birefringence microscopy, because usually the different phases show different optical polarization properties.

An additional important experimental tool is the application of an external magnetic field, exploiting the diamagnetic properties of LC molecules. A diamagnetic material exhibits an increasing (magnetic) energy with increasing external magnetic field. In an inhomogeneous field, a diamagnetic object is, therefore, driven toward regions of low field strength. A spectacular application of this effect is the stable magnetic levitation of diamagnetic objects, like water droplets, strawberries or even living animals, such as a frog, a grasshopper or a caterpillar. Alternatively, diamagnetic materials can be aligned in a homogeneous magnetic field. When a molecule is anisotropic, which is often the case for LC materials, its magnetic energy depends on its orientation relative to the magnetic field direction. This leads to an orientational force, which tends to minimize the magnetic energy by aligning the molecule with its axes of smallest diamagnetic susceptibility parallel to the field direction. Due to the collective behaviour of molecules in a LC phase, this phase can be relatively easy aligned by a magnetic field, which results in enhanced macroscopic properties, such us the formation of large LC domains with a large birefringence and a high optical transparency. In this thesis we use birefringence microscopy in high magnetic fields to study the dynamics of liquid crystals in the vicinity of a phase transition. As a model system we use the material octyl-4-biphenylcarbonitrile (8CB), which shows, apart from the isotropic phase (I), two liquid crystalline phases, the nematic phase (N), with only orientational order and the smectic phase (Sm-A) with both orientational and positional order.

In chapter 2 the basic physical properties of liquid crystals are described, including a short introduction of the physics of phase transitions and the effects of an applied magnetic field.

In chapter 3 the details of our experimental techniques are given, focusing on birefringence microscopy and the corresponding image treatment and analysis.

Chapter 4 discusses the effect of a static magnetic field on the dynamics of the isotropic-nematic (I-N) phase transition. Birefringence microscopy permits to observe the nucleation and growth of nematic

domains out of the isotropic phase. We find that the nucleation of the nematic domains tends to be suppressed by the presence of a magnetic field. However, after nucleation the overall phase transition proceeds faster in an applied magnetic field, as measured by the volume fraction of the nematic phase (the nematic coverage factor), which increases faster in time. Due to the applied magnetic field the nematic clusters are all aligned in the same direction. As a result, the domains merge more easily, within a relatively short coarsening period, to form a final nematic monodomain. On the level of a single growing domain, no effect of a magnetic field was observed. The radius R of a growing domain always scales with time as $R(t) \sim t^{1/2}$, in accord with a growth mechanism that is dominated by volume diffusion.

In chapter 5 the reorientation dynamics of a SmA phase is studied by time-resolved birefringence microscopy. First a uniformly aligned SmA monodomain is prepared in a constant magnetic field and then rapidly rotated over a certain angle. Immediately after the rotation the SmA monodomain is preserved, but oriented at an energetically unfavourable angle with respect to the magnetic field direction. This results in the reorientation of the SmA phase to recover its equilibrium situation, driven by the magnetic force on the diamagnetic LC molecules. These experiments were performed within a constant magnetic field (up to 20 T), for several temperatures below the $NSmA$ phase transition temperature (T_{N-A}) and for several rotation angles ϕ. In all cases we first observe an induction time, during which the SmA phase remains fixed at its initial orientation. This induction time increases with lowering the temperature further below T_{N-A}. After this induction time the system relaxes back to the new equilibrium state. It is found to reorient via complex, transient local structures, where local deviations are dominant. The precise trajectory depends on the rotation angle. In particular, for rotation angles larger than $\phi > 45^{\circ}$, a series of fluctuations occur, forming elongated patterns that are oriented perpendicularly to the smectic layers, propagating through the system. Overall, we find that the equilibrium state is achieved faster with increasing rotation angles and increasing magnetic field strengths. From these observations we conclude that the SmA phase does not reorient as a simple monodomain, but that nevertheless this phase has the ability to withstand large deformations in order to survive non-equilibrium situations.

In chapter 6 we report the observation of a double periodic, surface defect-pattern, formed during the NSmA phase transition in a magnetic field. The pattern results from the conflicting alignment imposed to the LC molecules, i.e. homeotropic at the sample surface and planar in the sample bulk due to the magnetic field. Stripes are formed at the cell walls, which are perpendicularly oriented to the field direction. Surprisingly, within the inner structure of the stripes a second structure emerges with lines parallel to the magnetic field. We find that the stripe formation velocity decreases with increasing magnetic field strength. When the field direction is changed, the stripes break and rotate to reorient towards the new field direction. Using the continuum Landau-de Gennes theory the double periodicity of the pattern is explained. The long period ($\approx$ 10 μm) is given by the balance of the surface anchoring and the elastic bending within the defect curvature walls. The short term period ($\approx$ 1 μ m) is attributed to the effect of the saddle-splay term in the elastic energy of a SmA liquid crystal, causing the curvature walls to break up.

Samenvatting

Vloeibare kristallen (LCs) representeren een opmerkelijke vorm van materie die twee ogenschijnlijk tegenstrijdige eigenschappen combineert: vloeibaarheid (zoals in vloeistoffen) en periodiciteit (zoals in kristallijne vaste stoffen). Het complexe gedrag van LCs stelt ons in staat om het delicate evenwicht tussen verschillende (vloeibaar kristallijne) fases te onderzoeken in de buurt van faseovergangen. Het fundamentele belang van de studie naar de dynamica in de buurt van faseovergangen beperkt zich niet tot LC materialen: het is ook relevant voor het begrip van het ontstaan van complexe morfologien in andere vakgebieden, zoals de materiaalfysica (magnetisme, supergeleiding), moleculaire structuren in de supramoleculaire chemie en biologie en grote ruimtelijke patronen in de kosmologie.

Vloeibare kristallen zijn perfecte modelsystemen voor experimentele studies, omdat hun gedrag in de buurt van faseovergangen redelijk eenvoudig bekeken kan worden met behulp van optische polarisatie microscopie bij kamertemperatuur. Bijvoorbeeld, de overgang van de isotrope (homogene vloeistof) fase naar de nematische fase (vloeistof met regelmaat in orintatie) is vaak een zwakke eerste orde faseovergang. Tijdens zo een overgang wordt er energie opgenomen dan wel afgestaan (latente warmte). Omdat deze energie niet instantaan uitgewisseld kan worden gaan eerste orde faseovergangen vaak gepaard met een regime waarin twee verschillende fases naast elkaar bestaan (gemengde fases): sommige delen van het system hebben de overgang reeds doorlopen en andere delen nog niet. Deze gemengde fases kunnen bestudeerd worden met optische polarisatie microscopie, gebruikmakend van dubbelbreking, omdat de verschillende fases vaak een andere optische respons hebben.

Binnen het vloeibare kristal onderzoek is het aanleggen van een extern magneetveld een belangrijk experimenteel hulpmiddel, hierbij gebruik makend van de diamagnetische eigenschappen van de LC moleculen. De energie van een diamagnetisch materiaal neemt toe met een toenemende magnetische veldsterkte. Dit betekent dat in een ruimtelijk inhomogeen magneetveld een diamagnetisch voorwerp in die richting wordt geduwd waarin het magneetveld afneemt. Een spectaculaire demonstratie van dit effect is de magnetische levitatie van diamagnetische objecten, zoals water druppels, aardbeien of zelfs levende dieren, zoals een kikker, een sprinkhaan of een rups. Een alternatieve toepassing van een magneetveld is het uitlijnen van materialen. Wanneer een molecuul anisotroop is, wat vaak het geval is voor vloeibaar kristallijne materialen, hangt hun magnetische energie af van hun orintatie ten opzichte van de richting van het veld. Dit leidt tot een magnetische kracht die het molecuul dusdanig tracht te richten in het veld zodat haar energie minimaal is. Vanwege het collectieve gedrag van moleculen in een vloeibaar kristallijne fase, is het magnetisch uitlijnen van zon fase relatief eenvoudig. Dit leidt vaak tot verbeterde macroscopische eigenschapen van het material, zoals de formatie van grote LC domeinen met een grote optische dubbelbreking of een hoge transparantie.

In dit proefschrift wordt polarisatie microscopie, gecombineerd met magnetische velden, gebruikt om de dynamica rond faseovergangen in een vloeibaar kristal te onderzoeken. Als modelsysteem gebruiken we het LC materiaal octyl-4-biphenylcarbonitrile (8CB) dat, naast de isotrope fase (I), ook twee andere vloeibaar kristallijne fases heeft: een nematische fase (N), met alleen orintationele regelmaat en een smectische fase (SmA) met zowel orintationele en positionele orde.

In hoofdstuk 2 worden de basiseigenschappen van vloeibare kristallen behandeld, met speciale

aandacht voor de fysica van faseovergangen en het effect van een aangelegd magneetveld.

Hoofdstuk 3 geeft een overzicht van de details van de gebruikte experimentele technieken, met name polarisatie microscopie en de bijbehorende beeldverwerking en analyse.

Hoofdstuk 4 bespreekt het effect van een statisch magneetveld op de dynamica van de overgang van de isotrope naar de nematische fase (I-N). Met behulp van polarisatie microscopie is het mogelijk om de nucleatie en groei van nematische domeinen vanuit een isotrope achtergrond te volgen. Uit de experimenten blijkt dat de nucleatie van de nematische domeinen onderdrukt wordt door een magneetveld. Na de nucleatie verloopt de faseovergang echter juist sneller in een aangelegd veld: de volumefractie van de nematische fase neemt sneller toe in een magneetveld dan zonder een veld. Omdat in een veld de nematische clusters uitgelijnd zijn smelten ze gemakkelijker, en dus sneller, samen tot de algehele nematisch fase (een LC monodomein). Op het niveau van een individueel groeiend domein maakt het aanleggen van een magneetveld niets uit. De straal R van een domein neemt in alle gevallen toe met de tijd t als $R(t) \sim t^{1/2}$, in overeenstemming met een groeimechanisme dat wordt bepaald door een volume diffusie proces.

In hoofdstuk 5 wordt de reorintatie dynamica van een SmA fase bestudeerd met behulp van tijdsopgeloste polarisatie microscopie. In dit experiment wordt eerst een uniform uitgelijnd SmA monodomein geprepareerd in een constant magneetveld. Daarna wordt het domein snel geroteerd over een hoek, dusdanig dat het SmA domein intact blijft, maar onder een energetisch ongunstige hoek staat ten opzichte van de veldrichting. Hierdoor wordt het SmA domein gedwongen zich te draaien naar een nieuwe evenwichtshoek onder invloed van de magnetische kracht op de diamagnetische LC moleculen. Deze experimenten zijn uitgevoerd in een constant magnetisch veld (tot 20 T), voor verschillende temperaturen net onder de $NSmA$ faseovergang (T_{N-A}) en voor verschillende rotatie hoeken ϕ. In alle gevallen zien we dat de orintatie van het SmA domein eerst een bepaalde tijd stabiel blijft. Deze zogenaamde inductie tijd wordt langer met afnemende temperatuur, net onder T_{N-A}. Na deze inductie periode relaxeert het system naar de nieuwe evenwichtstoestand, via een zeer complex proces dat gepaard gaat met de vorming van tijdelijke, locale structuren, waarbij grote fluctuaties optreden in de LC fase. Het precieze proces hangt sterk af van de rotatiehoek ϕ. Voor hoeken groter dan $\phi > 45^{\circ}$, wordt een aaneenschakeling van locale fluctuaties waargenomen, gekarakteriseerd door langwerpige patronen, loodrecht georienteerd op de smectische lagen, die zich als een schokgolf voortplanten door het materiaal. Uiteindelijk zien we dat de evenwichtssituatie sneller wordt bereikt met toenemende rotatiehoek en toenemende magnetische veldsterkte. Deze observaties laten zien dat de smectische fase zich niet reorinteert als een simpel monodomein, maar dat desondanks de smectische fase in stand gehouden wordt zelfs ver buiten evenwicht.

In hoofdstuk 6 rapporteren we de observatie van een dubbel-periodiek oppervlakte-defect patroon, dat onstaat tijdens de $NSmA$ faseovergang in een aangelegd magneetveld. Het patroon is het resultaat van twee tegengestelde uitlijnkrachten die worden uitgeoefend op de LC moleculen: homeotropisch aan het preparaat oppervlak en planair in de bulk van het preparaat. Dit leidt er toe dat een streep-patroon wordt gevormd aan het oppervlak van de cel, waarbij de strepen loodrecht staan op de veldrichting. Tussen de strepen wordt een tweede patroon gevormd met lijnen parallel aan het veld. De formatie van het patroon wordt versneld met een toenemende veldsterkte. Wanneer de richting van het veld wordt gedraaid, breekt het patroon zich op om zich vervolgens te herorinteren in de richting die compatibel is met de nieuwe veldrichting. Het dubbel-periodiek patroon kan verklaard worden met behulp van de continuum Landau-de Gennes theorie. De lange periode ($\approx$ 10 μm) is bepaald door de balans tussen de oppervlakte verankering en de elastische deformatie van de defect structuur. De korte periode ($\approx$ 1 μm) wordt toegeschreven aan het effect van de saddle-splay term in de elastische energie van een SmA vloeibaar kristal.

List of publications

1. O.V Manyuhina, G. Tordini, W. Bras, J.C. Maan and P.C.M. Christianen *Double-periodic instability pattern in a smectic A liquid crystal*, Physical Review E **87**, 050501 (2013).

2. G. Tordini *Illumination system, luminaire, collimator and display device*, International Patent **US2014268641**, (2011).

3. G. Tordini *Illumination system and luminaire*, International Patent **TW201213730**, (2010).

4. M.C.J. Vissenberg, G. Tordini *Light emitting device*, International Patent **KR201213730**, (2010).

5. P.A.J. Holten, G. Tordini *A lighting device and a lens suitable for such a lighting device*, International Patent **KR2014036494**, (2009).

6. P.A.J. Holten, G. Tordini, V. Fabrik *Light emitting device comprising a light guide plate with reflective shielding with glare reduction*, International Patent **US2012176813**, (2009).

7. M.C.J. Vissenberg, M. Knoop-Velds,A.P.M. Dingemans, J. G. Benes, A.J.H. van der Wiel, G. Tordini *Modular Luminaire and lighting system*, International Patent **WO2011039690**, (2009).

8. P.A.J. Holten, G. Tordini *Luminaire and illumination system*, International Patent **US2014036494**, (2008).

9. P.A.J. Holten, G. Tordini *LED based light source*, International Patent **TW201000823**, (2008).

10. G. Tordini, P.C.M. Christianen and J.C. Maan, *Dynamics of liquid crystalline domains in magnetic field*, Molecular Crystals and Liquid Crystals **435**, 915 (2005).

Curriculum Vitae

Giorgia Tordini
born in Rome (Italy) on 11 April 1974

August 2012 - now	Benchmark and Technology manager at Philips Lighting, Miribel, France
September 2009 - July 2012	Optical System Designer at Philips Lighting, Miribel, France
January 2007 - August 2009	Optical System Designer at Philips Lighting, Winterswijk, The Netherlands
January 2002 - September 2006	Onderzoeker in opleiding (Junior scientist) at High Field Magnet Laboratory , Radboud University Njmegen, The Netherlands
1992-2001	Private teacher of Latin, Greek, English, Mathematics and Physics at ”Apogeo Ambiente” in Rome, Italy
1994-2001	Physics studies at “Roma Tre” university in Rome, Italy
1988-1993	Secondary school at “Liceo Classico E. Montale” in Rome, Italy

The fundamental relevance of the study of phase transition dynamics is linked to the need of understand and predict how matter evolves.